SKYLAB PROGRAM

EARTH RESOURCES EXPERIMENT PACKAGE

SENSOR PERFORMANCE EVALUATION
FINAL REPORT
VOLUME V (S193 ALT)

JANUARY 2, 1975

CONTRACT NAS8-24000

AMENDMENT JSC-14S

National Aeronautics and Space Administration

LYNDON B. JOHNSON SPACE CENTER

Houston, Texas

MSC-05546

EARTH RESOURCES EXPERIMENT PACKAGE

SENSOR PERFORMANCE REPORT
VOL. V (S193 ALT)

(SL2, SL3 AND SL4 EVALUATIONS)

January 2, 1975
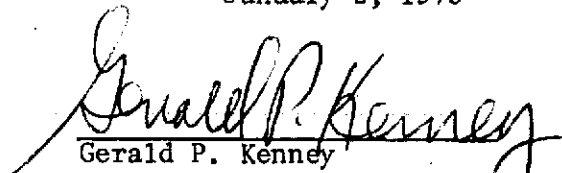
Submitted by: _Gerald P. Kenney_
Gerald P. Kenney
Skylab/EREP Sensor Performance
Evaluation Manager, JSC/HC

Technical
Review By: _N. M. Hatcher_
N. M. Hatcher
S193 Alt Project Scientist, JSC/TF
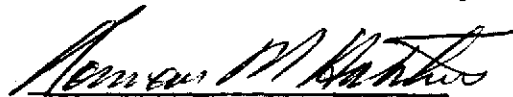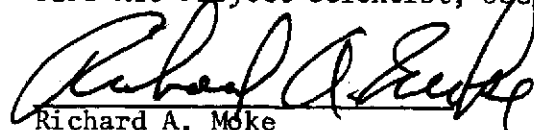
Approved: _Richard A. Moke_
Richard A. Moke
Manager, Systems Analysis and
Integration Office, JSC/HC

Contract NAS8-24000
Amendment JSC-14S

Skylab Program
Lyndon B. Johnson Space Center

FOREWORD

This volume is Section V of six sections of document
MSC-05546, submitted by Martin Marietta Corporation, in
accordance with the requirements of Annex I to Exhibit A,
Statement of Work, Part I, Data Requirements List, of Contract
NAS8-24000, Amendment JSC-14S, Line Item 295, and was prepared
under WBS 02216.

CONTENTS

Figures

1. INTRODUCTION

   1.1 Purpose

   This document reports the final results of the sensor performance evaluation of the Skylab Earth Resources Experiment Package (EREP) S193 altimeter and is based on data and evaluations reported in the interim performance evaluation report (MSC-05528, Volume V, dated September 6, 1974).

   1.2 Scope

   This document summarizes the results of S193 altimeter sensor performance evaluation based on data presented by Martin Marietta and NASA Wallops Flight Center to the sensor performance evaluation interim reports, provides the results of additional analyses of S193 altimeter performance, and describes techniques used in sensor performance evaluation (Appendix A). The summarization includes significant performance degradation identified during the Skylab missions and the performance achieved, in terms of pertinent S193 altimeter parameters. The additional analyses include final performance analyses completed after submittal of the SL4 interim sensor performance evaluation reports, including completion of detailed analyses of basic performance parameters initiated during the interim report periods.

   1.3 Usage Guide

   The basic task outline for the EREP sensor performance evaluation was specified EREP Mission Data Evaluation Requirements, JSC-05529, August 31, 1973. The results of these evaluations were subsequently reported in MSC-05528, Earth Resources Experiment Package, Sensor Performance Report, Volumes I through VII, as follows:

Volume I (S190A)	Multispectral Photographic Camera
Volume II (S191)	IR Spectrometer
Volume III (S192)	Multispectral Scanner
Volume IV (S193 R/S)	Radiometer/Scatterometer
Volume V (S193 Alt.)	Altimeter
Volume VI (S194)	L-Band Radiometer
Volume VII (S190B)	Earth Terrain Camera

These volumes were issued after prelaunch testing at KSC and updated after each mission. The single exception is Volume VII (S190B), which was originally issued after SL3, with a single update after SL4.

This document is based on the data and analyses in the first six volumes of the sensor performance report, MSC-05528. Volume VII, S190B, is not included. The same volume designation used for MSC-05528 has been retained for the individual sensor volumes, with the individual volumes bound in a single cover and identified as MSC-05546. The individual volumes are designed so they can be used independently of the full six-volume report, if desired.

1.4 Abstract

This report presents the results of thé sensor performance evaluation (SPE) of the S193 K_u-band radar altimeter, which was part of the Earth Resources Experiment Package (EREP) on Skylab. Agencies participating in the evaluation were NASA Wallops Flight Center and the Denver Division of the Martin Marietta Corporation. Findings are presented in the areas of housekeeping parameters, system stability, performance capability as reflected in the output flight data, computer simulation studies, achieved antenna scan and pointing performance, operation in the various modes, and preliminary review of the major altimeter experiments. Supplementary analyses covering antenna pattern characteristics and the usefulness of the pulse compression operation for sensing sea state are reported.

The results show that the instrument generally performed within expectations and that it provided useful design information. However, the data exceeded the original objectives of providing technological information and have been reduced sufficiently to indicate that significant scientific contributions have been provided by the S193 altimeter operation. Degradation of the sensor capability was observed as a result of two major anomalies--failure to obtain compressed pulse operation during SL2 and SL3 and a reduction of the signal-to-noise ratio during SL4, with the subsequent loss of short-pulse measurement data. Conclusions are drawn from the evaluation results and recommendations for improving the effectiveness of future programs are offered. An addendum describes the special evaluation techniques applied to the sensor performance evaluation tasks.

2. APPLICABLE DOCUMENTS

MSC-05528

Earth Resources Experiment Package, Sensor Performance Report, Volume V (S193 Alt), Lyndon B. Johnson Space Center, Houston, Texas, September 6, 1974.

72SD4234

S193 Historical Log Book, Volume 1A, Rev. A, S193 Vehicle 001, General Electric - SSO, 27 October 1972.

Alternate Designation: Document No. 72SD4207, Rev. C, S193 Calibration Data Report, Flight Hardware - Prime Unit 1A, Volumes 1A and 1B, General Electric - SSO, Contract NAS9-11195, 27 October 1972 and Volumes 1A and 1B, Rev. D, 22 March 1973.

MSC-05528

Earth Resources Experiment Package, Sensor Performance Report, Volume IV (S193 R/S), Lyndon B. Johnson Space Center, Houston, Texas, October 30, 1974.

72SD4234

S193 Historical Log Book, Volume 2, S193 Vehicle 001, General Electric - SSO, VFSC, 8 August 1972.

Alternate Designation: Specification No. SVS7846, Rev. C, Flight Hardware Configuration Specification, Contract NAS9-11195, 27 April 1972.

E. L. Hofmeister and B. N. Keeney: Final Report, Radar Altimeter Waveform Sampling Study, General Electric, Utica, New York for NASA, Wallops Station, W. I. Virginia, Contract NAS6-1823, October 1971.

S193 Microwave Radiometer/Scatterometer Altimeter Preliminary Design Review Technical Reports, Volume V, Books 1 and 2, General Electric - SSO, Contract NAS9-11195 and 6, 7 October 1970.

MSC-05489

Earth Resources Experiment Package Test Data Analysis Report, All-Up EREP System Test (St. Louis) FIV, SFIV, SSFIV, SDPV, Martin Marietta Corporation, Denver, Colorado, February 20, 1973.

72SD4207

S193 Calibration Data Report, Flight Hardware, Volume II, Rev. B, General Electric - SSO, Contract NAS9-11195, 31 July 1972.

73SD4226

S193 Calibration Data Report, Flight Backup Hardware, Volume II, General Electric - SSO, Contract NAS9-11195, 27 March 1973.

MSC-07744

Skylab Instrumentation Calibration Data Book, Volume IV (EREP), Section 5, Skylab Mission SL1, Rev. B, Lyndon B. Johnson Space Center, Houston, Texas, August 1973, Change Notice 3, November 1974.

Interface Specification, Martin Marietta Corporation, SKYBET Tape Format - Program TD322, 26 February 1973.

3.   SUMMARY OF SENSOR PERFORMANCE EVALUATION INTERIM REPORT

After preflight testing of the EREP experiments at Kennedy
Space Center and after each Skylab mission, raw data were reduced
to provide performance data for each EREP sensor. These data were
presented by mission in interim sensor performance evaluation
reports entitled EREP Sensor Performance Report (Engineering
Baseline, SL2, SL3, and SL4 Evaluation), MSC-05528, Volumes I
through VII. Preflight test data and selected qualification test
data were the engineering baseline, and flight data were added
after each Skylab mission. This section summarizes Volume V (S193
Alt), Change 3, September 6, 1974 of the sensor performance report,
paragraph by paragraph. However, sections of the interim report
that were similar or contained redundant evaluation data have been
combined. To provide traceability, applicable interim report
paragraphs are referenced in the summary.

3.1   Function/Limit Verification (SPE-S193-001)

The general integrity of the S193 altimeter was evaluated by
an analysis of data on mode sequencing, engineering parameters,
internal science, sample-and-hold gate internal calibration,
malfunction diagnostic data, and a review of the comments made by
the EREP control and display (C&D) panel operator during the
Skylab missions.

3.1.1 Malfunctions

There were several diagnostic monitors provided on the EREP
C&D panel to allow the EREP operator to quickly analyze the
operation of S193. These monitors also appeared as bilevel (on-
off) indicators in the S193 data. These diagnostic monitors were:

1)   Radiometer ready;

2)   Scatterometer ready;

3)   Altimeter ready;

4)   Transmitter overheat;

5)   Transmitter malfunction;

6)   Receiver overheat;

7)   Receiver malfunction;

8)   Gimbal malfunction;

9)   Altimeter unlock.

The diagnostic monitors visually indicated to the operator
that the S193 was ready to take data or that there was a problem
with the instrument. For instance, the ready lights would light
up when the power switch(s) were placed in the ON position for
the particular mode of operation desired (Rad, Scat, Rad/Scat,
or Alt) and the appropriate time delays in the S193 had elapsed.
The malfunction, overheat, and unlock lights would light up if
there were abnormal operation. A malfunction was defined as an
unexpected indication on one of these monitors. Therefore, if a
ready indicator did not light up when the proper power switch was
turned on or a malfunction or overheat|indicator did light up, a
malfunction was indicated. In addition to the malfunctions de-
fined here, the S193 experienced anomalous operation in which
the data indicated performance that did not agree with expecta-
tions. Anomalous operation is considered separately from malfunc-
tion indications in this report.

In addition to the light displays, several S193 voltages
were displayed on C&D panel meters for performance verification.

All the diagnostic monitors gave the indications that were
expected as a result of switch operation and altimeter operation
throughout the Skylab missions, with one exception. During EREP
pass 96, which was the next-to-last altimeter data pass, the
altimeter ready light failed to illuminate. No data were obtained
from this run and the reason for the failure of the ready light
to come on was not determined. As expected, the unlock indicator
lighted up frequently due to loss of lock by the altimeter. This
resulted from rapid altitude changes in targets during all missions,
the effect of the beam being offset from nadir on some passes, and
the lower antenna gain during SL4. The S193 anomaly that occurred
during EREP pass 40, when a short occurred in the pitch gimbal
potentiometer, was not indicated by the malfunction lights on the
S193 altimeter operation due to the malfunction light logic, but was
indicated by the transmitter malfunction light and receiver mal-
function light during Rad/Scat operation. S193 malfunction light
logic was summarized by GE.*

---

* S193 Historical Logbook, S193 Vehicle 001, Vol 1A, Document
No. 72 SD4234 Rev. A, 27 October 1972, General Electric
Company, p 1-29.

Alternate Designation: S193 Calibration Data Report, Flight
Hardware, Doc. No. 72SD4207 Rev. D, 22 March 1973, Prime
Unit 1A Volume 1A, SSO Contract NAS9-11195, General Electric.

3.1.2 Sequencing

Altimeter mode sequencing was verified by comparing the number and sequence of each frame for each altimeter mode with the sequencing requirements specified in the Cal Data Report*. This included checking the status word indications along with the frame and subframe count to ensure that each mode and its subsequent submode, sub^2 mode, and sub^3 mode of operation were preperly sequenced. Modes 1, 2, 5, and nadir align were verified to be in complete accordance with the sequencing requirements specified in the Cal Data Report* throughout all missions. Mode 3 met all requirements except that there was a consistent loss of two frames of data in all mode 3 operations throughout all missions. This sequencing error always occurred at the same spot and was the loss of the two frames of data in submode 4 (DAS2), sub^2 mode 0, sub^3 mode 0. This error in sequencing did not occur at KSC, but a review of GE thermal vacuum testing data revealed that the same problem had occurred in that test.

During several altimeter operations, the instrument was turned off or to standby before all specified sequencing for the particular mode had been completed. This occurred when intermittent losses of lock caused the mode to exceed the preassigned time for the mode or when the mode had to be terminated early because of time-allocation constraints. Data were also lost for a short period whenever the EREP tape recorder speed was changed to accommodate S192 operation. This short (up to 6-second) data loss should not be construed as anomalous S193 sequencing.

3.1.3 Engineering Parameters

An altimeter engineering parameter limit verification was performed for all altimeter operations during SL2, SL3, and SL4 by analyzing each individual parameter to determine its minimum and maximum value for each run, determining if these minimum and maximum values were within established limit criteria, noting the operational characteristics of each parameter and (where applicable) performing a comparative analysis with other associated parameters.

---

*   S193 Historical Logbook, S193 Vehicle 001, Vol 1A, Document
    No. 72 SD4234 Rev. A, 27 October 1972, General Electric
    Company, p 5-7.

    Alternate Designation: S193 Calibration Data Report, Flight
    Hardware, Doc. No. 72 SD4207 Rev. D, 22 March 1973, Prime
    Unit 1A Volume 1A, SSO Contract NAS9-11195, General Electric.

All engineering parameters showed a marked repeatability in their respective minimum and maximum readings in meeting the flight criteria from pass to pass throughout all missions, with the following exceptions:

1) Measurements A050-293 00A, pitch bias, and A058-293 00A, roll bias, changed to maximum negative readings when the short occurred on the -10-volt reference power supply during EREP pass 40 and remained there throughout the remainder of the SL3 mission.

2) Measurements A053-293, antenna feed temperature, A054-293, input waveguide temperature, and A056-293, driver TWTA temperature, gave higher temperature indications late in SL4 than previously seen in SL2, SL3 or earlier SL4 passes. They exceeded the flight criteria in EREP passes 88 through 93, but returned to nominal values in EREP pass 94, then returned to the higher-than-normal temperature readings in EREP pass 95 and remained there to the end of the mission (EREP pass 98). A review of these same parameters during Rad/Scat operation in these same passes shows concurring data. Although these three parameters exceeded the limits specified for flight criteria in the EREP passes mentioned, no degradation of altimeter data or abnormal operation of the altimeter was indicated.

A more detailed analysis of the engineering parameters, including tables containing the minimum and maximum values and flight evaluation criteria, is in MSC-05528, Volume V, paragraph 3.3, September 6, 1974.

3.1.4 Gimbal Operation

The nadir align mode was the only altimeter mode of operation that caused movement of both the roll and pitch gimbals. The roll gimbal was locked throughout operation of modes 1, 2, 3, and 5. The pitch gimbal was commanded to step forward to 0.43 and back to 0.0 degrees in mode 1 and to step through pointing angles of 0.43, 15.6, 7.56, 2.65, and 1.3 degrees and return to 0.0 degrees in mode 2.* There was no gimbal movement associated with modes 3 and 5.

---

* As of November 1974, JSC data do not account for these pitch offsets in the field-of-view.

The gimbal limit criterion for modes 1 and 2 was the summation of the target nadir (OOA bias parameters), commanded angle value, and a tolerance of ±1.2 degrees in roll and ±0.8 degrees in pitch.*

Gimbal performance for all altimeter operations was satisfactory and within limits for SL2 and SL3 before the S193 anomaly that occurred in EREP pass 40. During SL4, the pitch gimbal was pinned at the 0-degree position. Therefore, there was no movement of the gimbals throughout SL4 in altimeter modes.

3.1.5 Internal Calibration

SL2, SL3, and SL4 data were assessed to determine the internal time delay of the altimeter RF path and whether it changed during the Skylab missions. It was determined that the internal time delay was 100.2 ns for SL2, 99.8 ns for SL3, and varied from 96.3 to 101.7 ns during SL4.

During altimeter mode 2 operations, the relative change in AGC level was used to evaluate relative surface reflectivity changes. In this mode, the antenna was pointed at a different pitch angle from 0.0 to 15.6 degrees for each submode to measure reflectivity changes with beam incidence angle. Internal AGC-level drift was checked during CDS submodes. In CDS-1 and -2, an additional 10.6 dB compared with CDS-3 was inserted to provide a two-level calibration. In all CDS submodes, the transmitter pulse was coupled to the receiver to provide a self-contained internal AGC calibration. The AGC levels were set by peak pulse power levels in an AGC gate.

The average relative AGC level attained for each of the three submodes for each Skylab mission converted to output power at the transmitter was:

Mission	CDS-1 (dBm)	CDS-2 (dBm)	CDS-3 (dBm)
SL2	59.2	60.8	60.2
SL3	61.4	62.9	60.8
SL4	61.8	63.0	60.9

---

* S193 Historical Logbook, S193 Vehicle 001, Vol 1A, Document No. 72 SD4234 Rev. A, 27 October 1972, General Electric Company, p 5-33a.

Alternate Designation: S193 Calibration Data Report, Flight Hardware, Doc. No. 72 SD4207 Rev. D, 22 March 1973, Prime Unit 1A Volume 1A, SSO Contract NAS9-11195, General Electric.

An altimeter transmitter power limit verification was performed for all missions based on the fact that the AGC output was a function of the received-pulse power. In CDS submodes, the transmitter power level was sampled by the altimeter receiver for an internal calibration of the transmitter power. Transmitter power was related to the radiated output power by a preflight calibrated path attenuation (118.5 dB). The AGC output in altimeter mode 1 CDS-1 was compared to preflight test data to indicate any change in output power from the altimeter transmitter. Path attenuation from the transmitter to the antenna was assumed to remain constant so that output transmitted power could be calculated from the AGC level.

Data from SL2, SL3, and SL4 revealed that transmitter power did not vary significantly from the preflight test measured value of 61.0 ±0.4 dBm. The power actually appeared to be higher in SL3 and SL4 than in SL2 by a small amount, but this was attributed to measurement readability using the AGC curves in the Cal Data Report*. The AGC curves themselves were estimated to be no better than ±1 dB in absolute value.

Another subtask of the function/limit verification task was altimeter system noise limit verification, which employed the fact that the noise gate output was the integrated voltage from the altimeter receiver during the period preceding the return pulse. Thus, it provided a measure of the noise output of the system with little or no return energy.

Parameter A017-293, noise gate integrated voltage, was analyzed throughout all missions to determine altimeter system noise. No significant change in the noise level was detected in any of the flights. The comparative standard was 129 bit counts equalling 0 volts of noise, and the following results were obtained:

Mission	Average 100-MHz BW (PCM counts)	Average 10-MHz BW (PCM counts)	Average of all Samples (PCM counts)
SL2	129.0	128.8	128.9
SL3	128.9	128.9	128.9
SL4	128.25	128.25	128.25

* S193 Historical Logbook, S193 Vehicle 001, Vol 1A, Doc. No. 72 SD4234 Rev. A, 27 October 1972, General Electric Company.

Alternate Designation: S193 Calibration Data Report, Flight Hardware, Doc. No. 72 SD4207 Rev. D, 22 March 1973, Prime Unit 1A Volume 1A, SSO Contract NAS9-11195, General Electric.

3.1.6 Sample-and-Hold Outputs

The altimeter sample-and-hold (S/H) outputs from the internal
calibration data submodes (CDS) taken during operation of modes 1,
2, 3, and 5 were evaluated for each mission. These data were created
by routing the transmitted signal directly to the receiver system
via an 118.5-dB attenuator (mode 2 CDS-1 and -2 used 129.1 dB) that
represented a typical space loss and bypassed the antenna system.
These data provided an inflight power level and pulse shape
calibration and, in the case of the S/H gate circuitry, an
indication of performance. The S/H data were also evaluated in
conjunction with the AGC level to assure that a proper pulse was
transmitted and that the transmitter and receiving operation was
normal. Pulse shape output consistency with the desired transmitter
and receiver operation was used to verify that the S/H gate data were
were faithfully reproducing the internal pulse characteristics.
The transmitter pulse shapes were independently verified by the use
of a ground-based pulse-shape measurement. (See STAPE discussion
in Section 1 of Appendix A to this volume.)

The design characteristics defining the mode 1 CDS-1, -2, and -3
S/H gate operation were:

1) Pulse width = 100 ns

2) Receiver BW = 100 MHz (CDS-1)
                   10 MHz (CDS-2, -3)

3) Single pulses (100 pulses sampled per second)

4) Two sample positions (8 gates per position)

5) Gate spacing and gate width = 25 ns

6) Samples per mean value (plotted point) = 728 (CDS-1)
                                             520 (CDS-2, -3)

The mode 1, CDS-1, -2, and -3 output waveforms displayed no
significant changes throughout all missions. Examples of S/H
waveform construction for mode 1, CDS-1, -2, and -3 operations
are shown in Figures 3.1-1 through 3.1-3, respectively. These pulse
waveforms show three curves for each pulse. The middle curve is
the mean-value waveform for an entire submode set of S/H outputs.
The outside curves are plots of the mean value plus and minus the
1σ values for the entire submode set of S/H outputs.
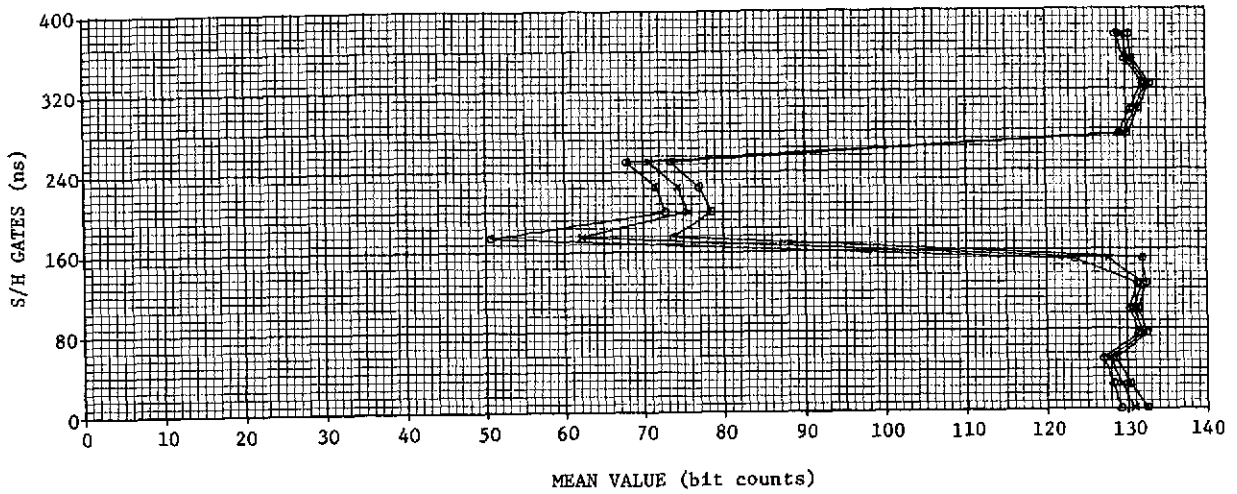
Figure 3.1-1 Typical Mode 1 CDS-1 Sample and Hold Waveform
Construction
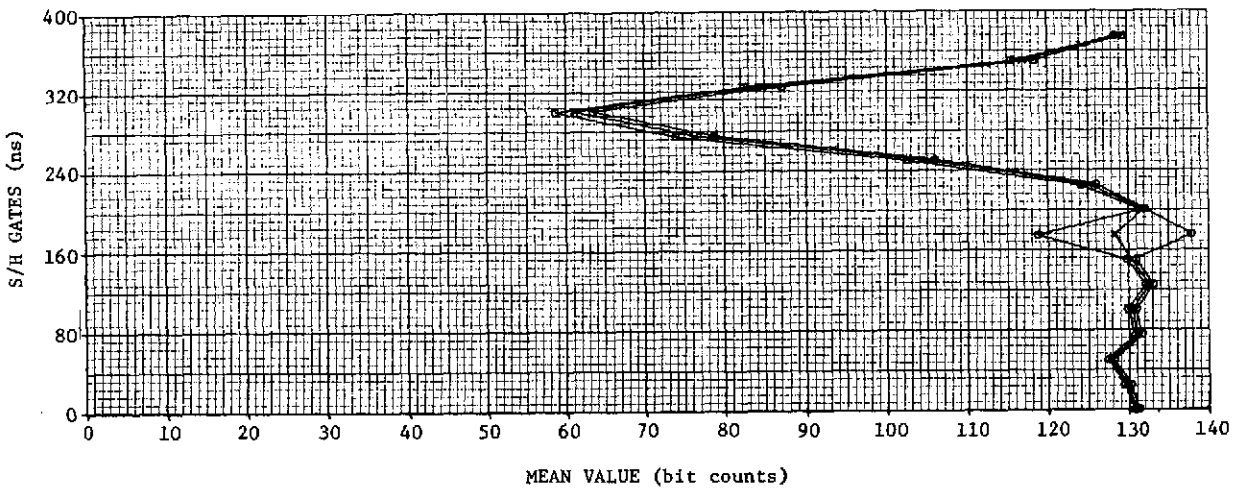
Figure 3.1-2 Typical Mode 1 CDS-2 Sample and Hold Waveform
Construction
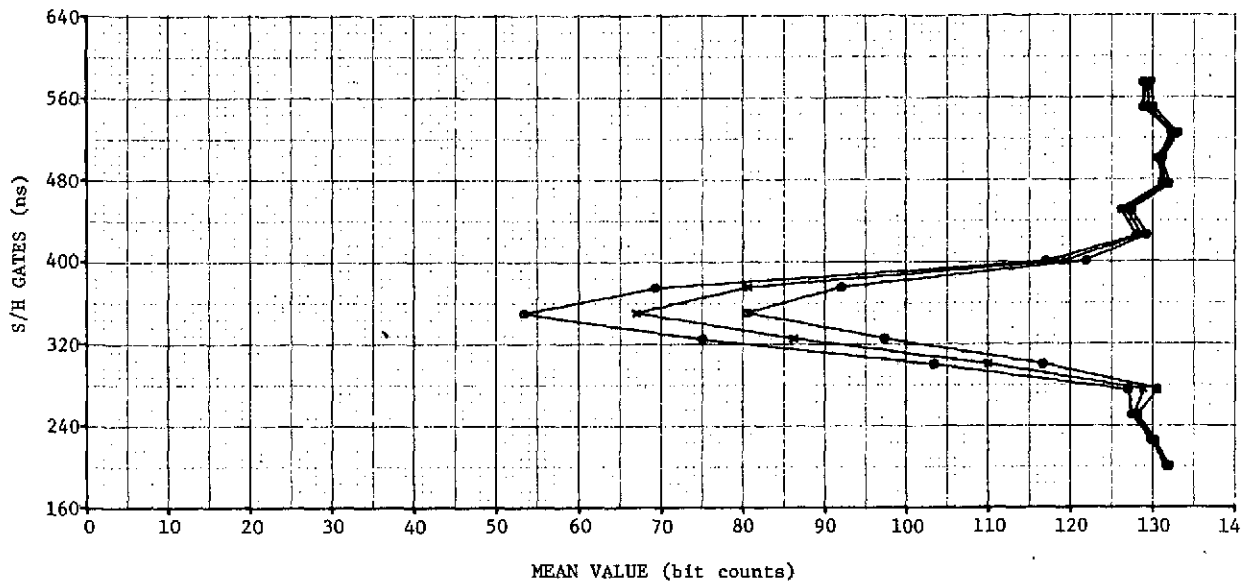
Figure 3.1-3 Typical Mode 1 CDS-3 Sample and Hold Waveform
Construction

The characteristics defining the mode 2, CDS-1, -2, -3 S/H
gate operation were:

1) Pulse width = 100 ns

2) Receiver BW =   10 MHz (CDS-1)
                  100 MHz (CDS-2, -3)

3) Single pulse (100 pulses sampled per second)

4) Two sample positions (8 gates per position for CDS-1)
   Three sample positions (8 gates per position for CDS-2, -3)

5) Gate spacing and width = 25 ns (CDS-1)
                            10 ns (CDS-2, -3)

6) Samples per mean value (plotted point) = 728

The waveforms plotted for mode 2, CDS-1, -2, -3 operations
showed little variation throughout all missions. Examples of
mode 2 waveforms for CDS-1, -2, and -3 are shown in Figures 3.1-4
through 3.1-6, respectively. The three-pulse waveform curves
represent the mean and the mean plus and minus 1σ values for the
entire submode set of S/H outputs.
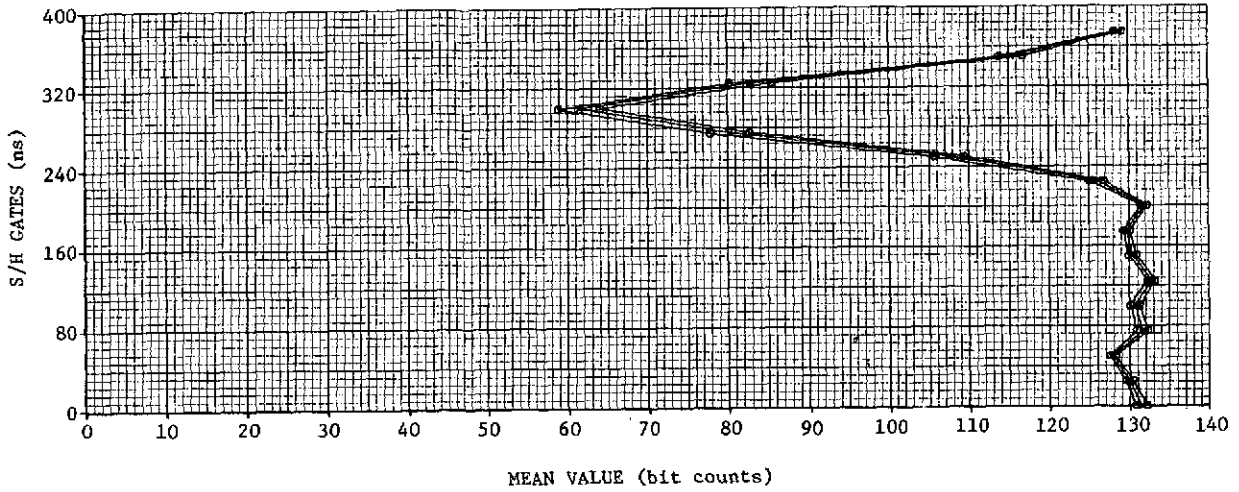
Figure 3.1-4   Typical Mode 2 CDS-1
              Sample and Hold Waveform Construction
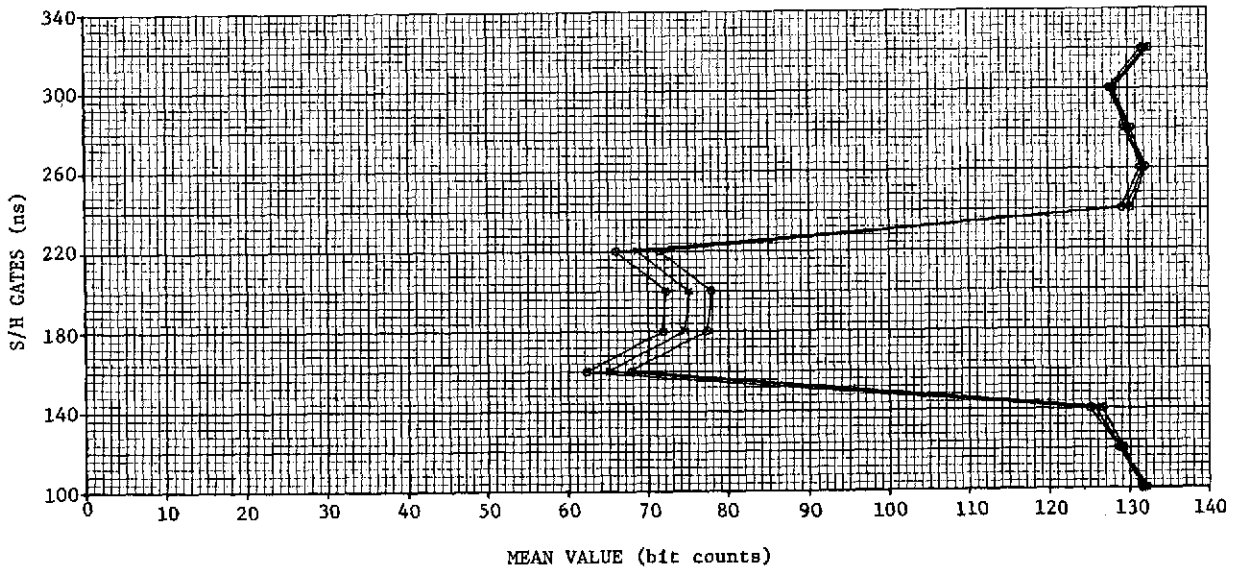
Figure 3.1-5   Typical Mode 2 CDS-2
              Sample and Hold Waveform Construction
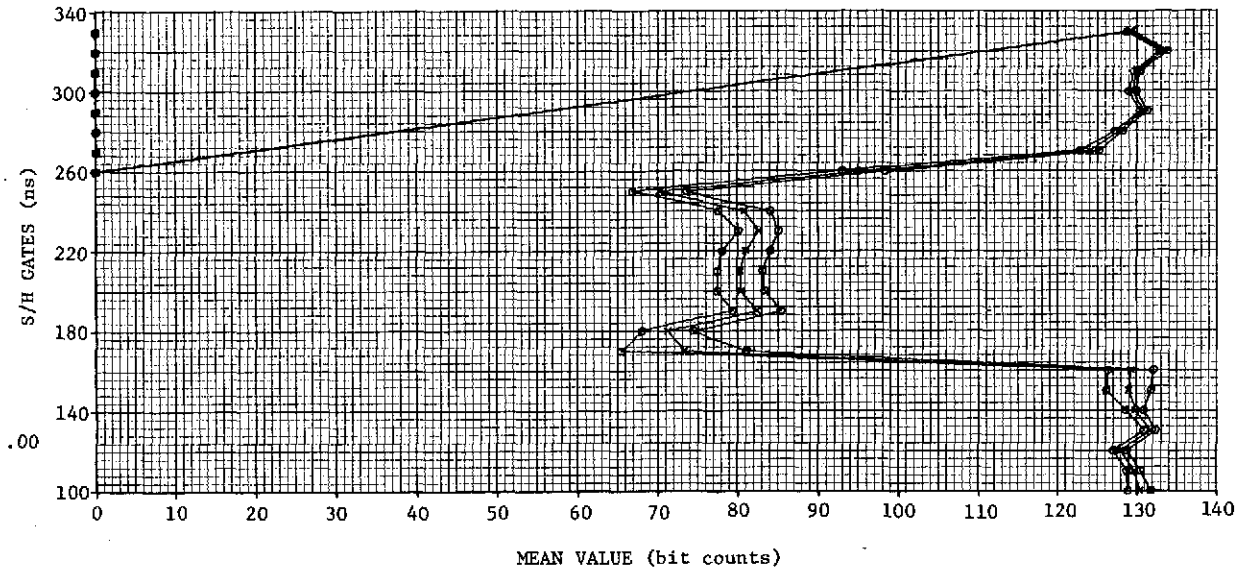
Figure 3.1-6   Typical Mode 2 CDS-3
             Sample and Hold Waveform Construction

The characteristics defining the mode 3 CDS-1, -2, -3, -4, and
-5 S/H gate operation were:

1)   Pulse width = 100 ns (CDS-1, -3, -4)
                    18 ns (CDS-2, -5)

2)   Receiver BW = 100 MHz (CDS-1, -2, -4, -5)
                    10 MHz (CDS-3)

3)   Double pulses (CDS-1, -2, -4, -5)
     Single pulse (CDS-3)

4)   Six sample positions - 3 per pulse (CDS-1, -4)
     Eight sample positions - 4 per pulse (CDS-2, -5)
     Two sample positions (CDS-3)

5)   Gate spacing and width = 25 ns (CDS-1, -3, -4)
                              10 ns (CDS-2, -5)

6)   Samples per mean value (plotted point) = 2392 (CDS-1)
                                               2600 (CDS-2)
                                                312 (CDS-3)
                                               2080 (CDS-4)
                                               2600 (CDS-5)

Mode 3 was known as the dual-pulse experiment, and there were
two pulses per repetition period in CDS-1, -2, -4, and -5, spaced
at varying distances for this pulse correlation experiment. The
S/H gates were grouped so that gates 5 through 8 corresponded to
the second pulse. The preflight status of the system was such
that the first pulse was sampled entirely by the first four gates

in four positions. The second pulse was sampled partially in CDS-1
and -4 and not at all in CDS-2 and -5. Examples of mode 3 S/H
waveforms are shown in Figures 3.1-7 through 3.1-15 for CDS-1
through -5, respectively. Just as for modes 1 and 2, there are
three curves shown, with the middle curve representing the mean and
other two representing the mean plus and minus 1σ values for the
entire submode set of S/H outputs.
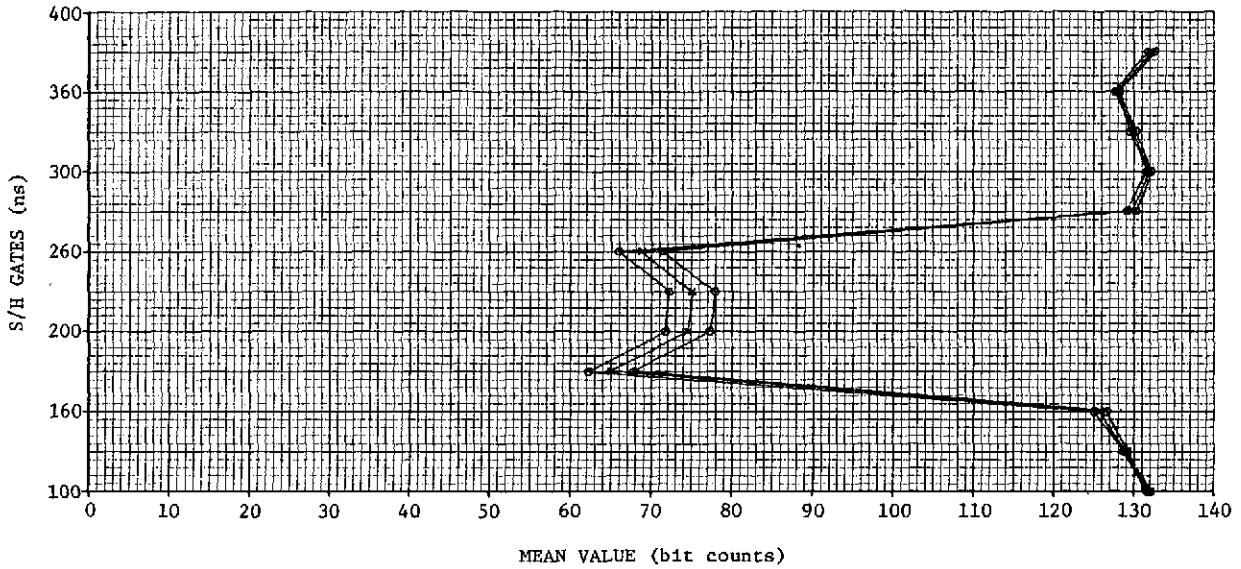
Figure 3.1-7 Typical Mode 3 CDS-1 First-Pulse
Sample and Hold Waveform Construction
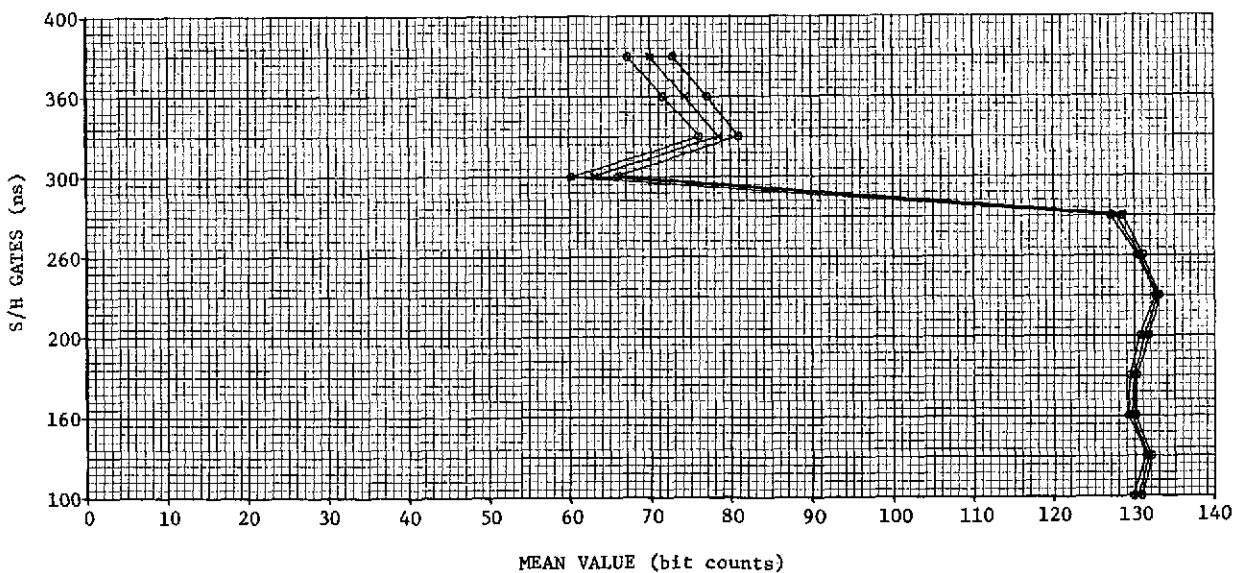
Figure 3.1-8 Typical Mode 3 CDS-1 Second-Pulse
Sample and Hold Waveform Construction
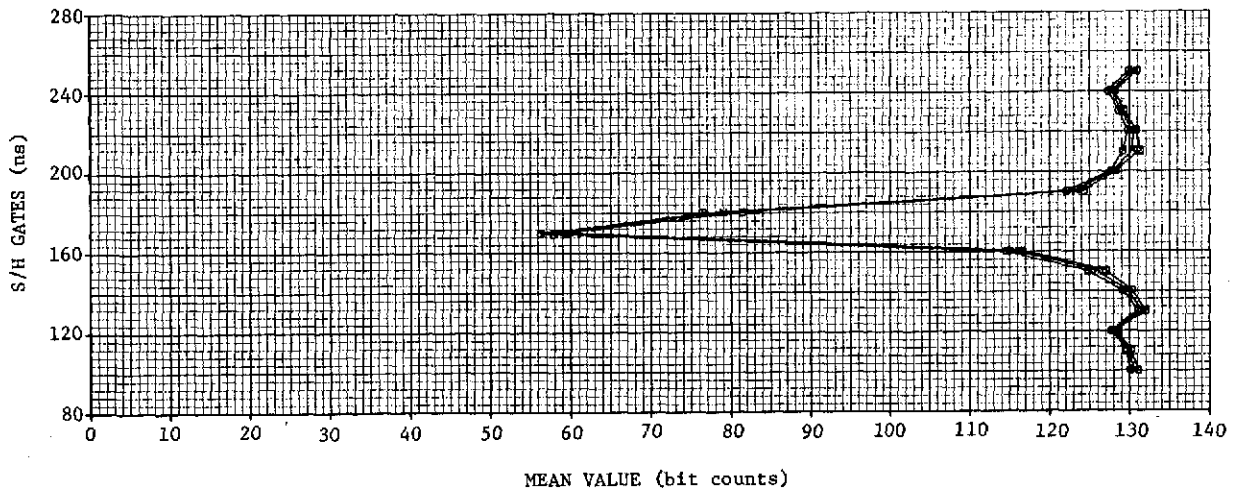
Figure 3.1-9   Typical Mode 3 CDS-2 First-Pulse
Sample and Hold Waveform Construction
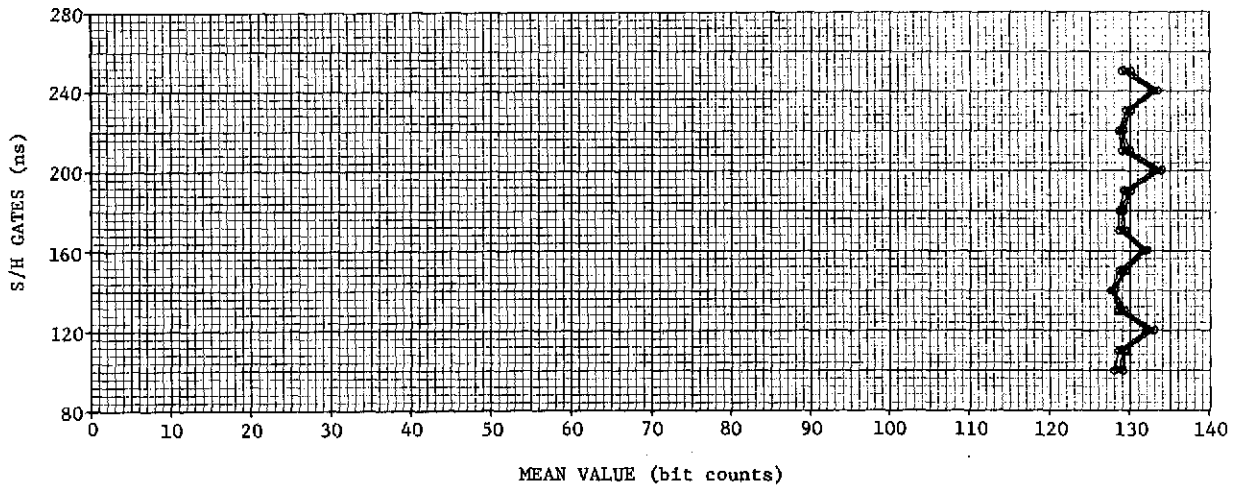
Figure 3.1-10   Typical Mode 3 CDS-2 Second-Pulse
Sample and Hold Waveform Construction
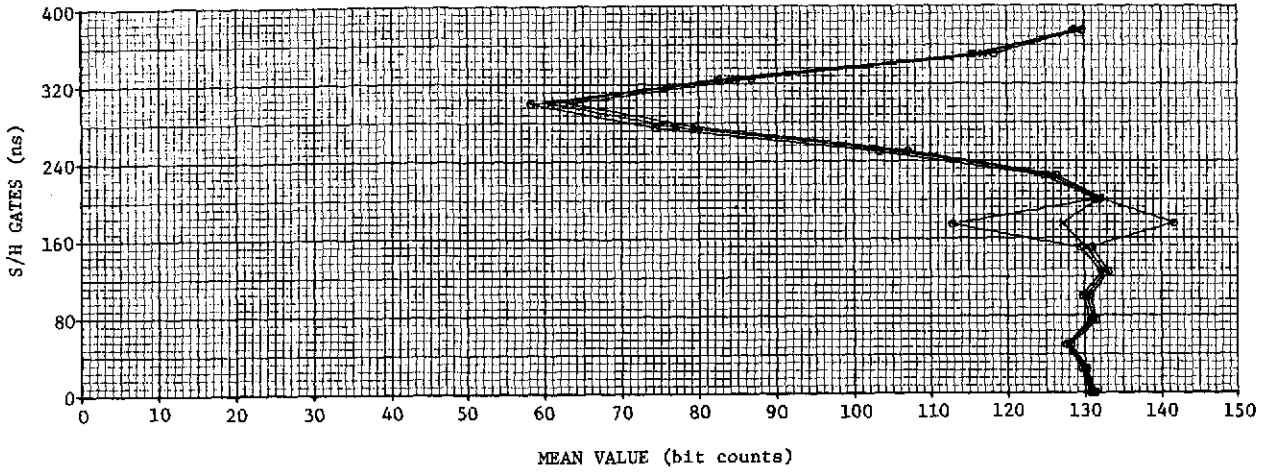
Figure 3.1-11   Typical Mode 3 CDS-3
Sample and Hold Waveform Construction
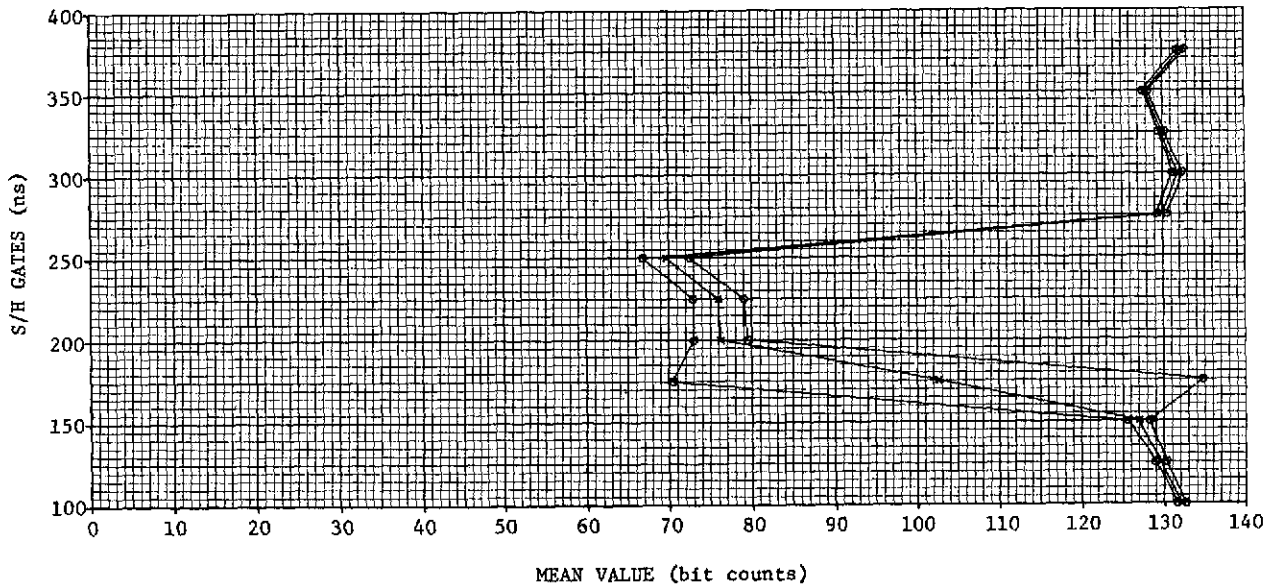
Figure 3.1-12   Typical Mode 3 CDS-4 First-Pulse
Sample and Hold Waveform Construction
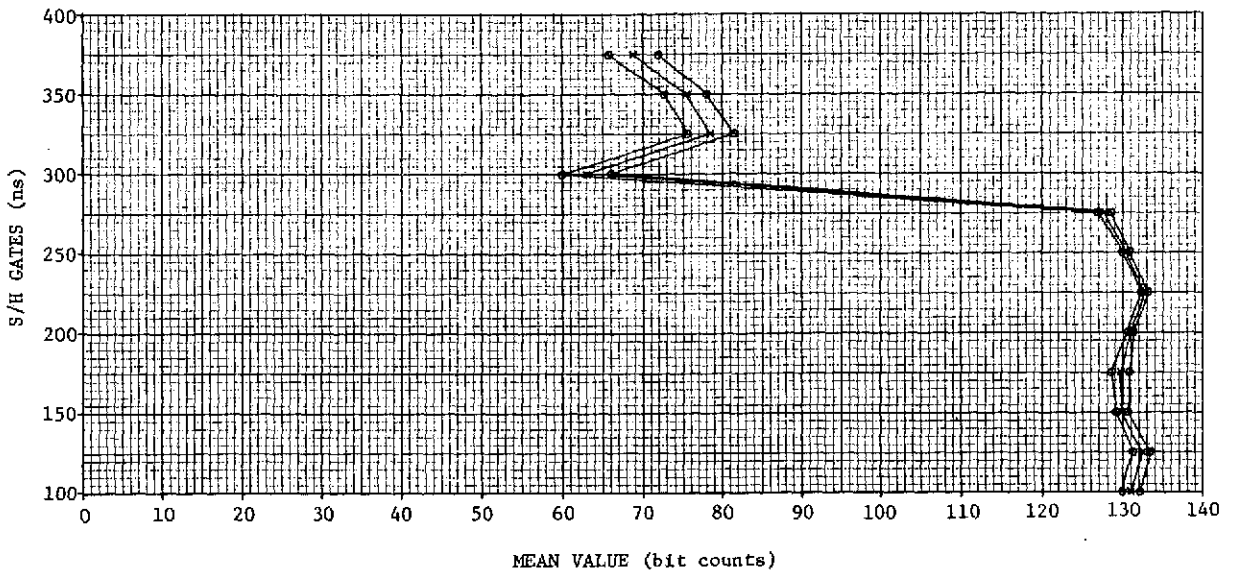
Figure 3.1-13   Typical Mode 3 CDS-4 Second-Pulse
Sample and Hold Waveform Construction
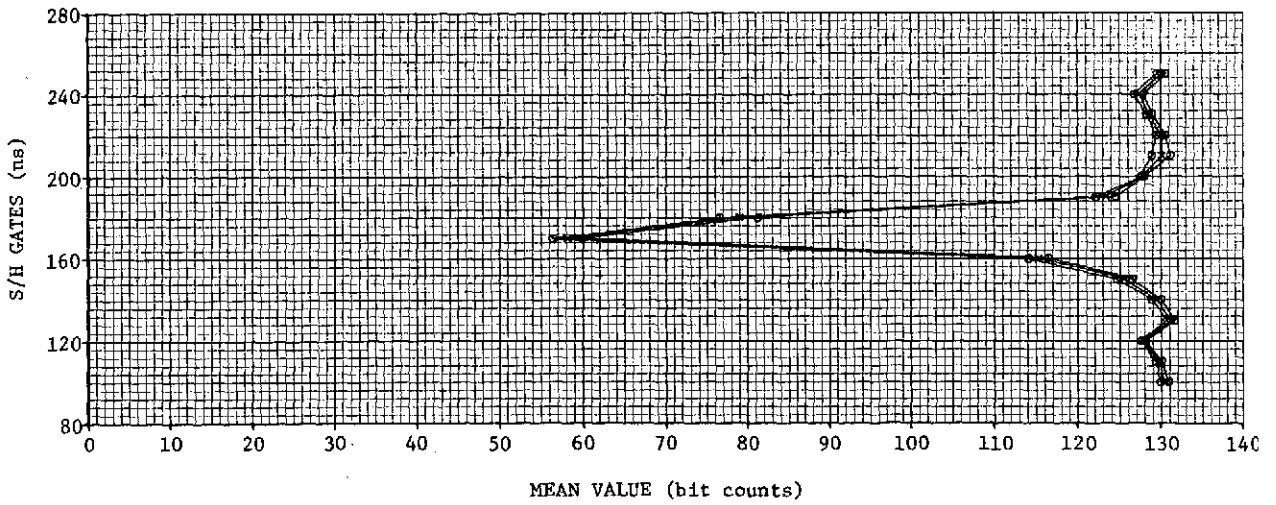
Figure 3.1-14   Typical Mode 3 CDS-5 First-Pulse
Sample and Hold Waveform Construction
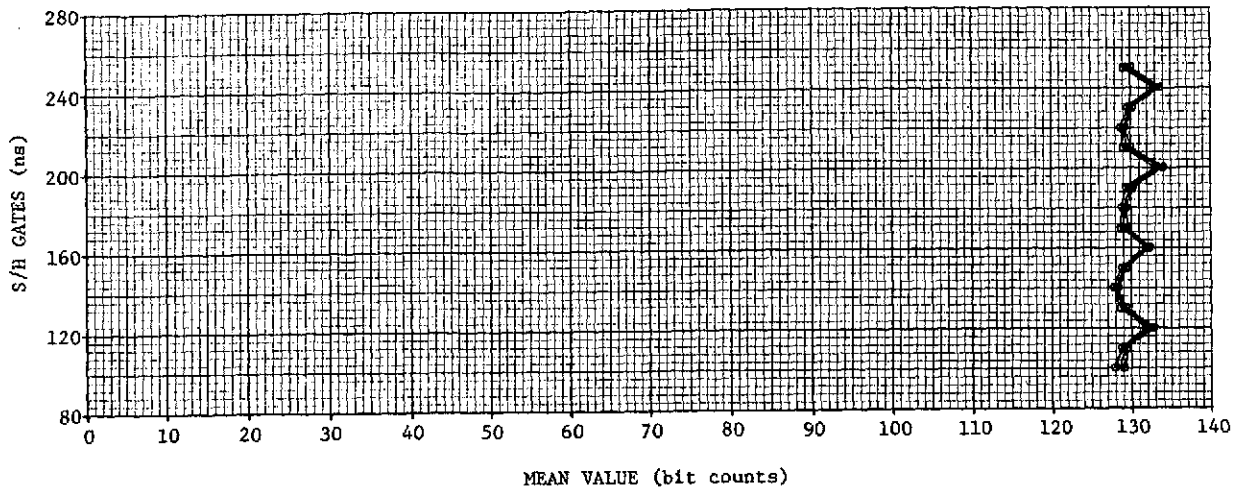
Figure 3.1-15 Typical Mode 3 CDS-5 Second-Pulse
Sample and Hold Waveform Construction

The characteristics defining the mode 5, CDS-1, -2, -3 S/H gate operation were as follows:

1) Pulse width = 18 ns (CDS-1)
   130 ns PC to 10 ns (CDS-2)
   100 ns (CDS-3)

2) Receiver BW = 100 MHz (CDS-1, -2)
   10 MHz (CDS-3)

3) Single Pulses

4) Two sample positions (CDS-1, -3)
   Three sample positions (CDS-2)

5) Gate spacing and width - 10 ns (CDS-1, -2)
   25 ns (CDS-3)

6) Samples per mean value (plotted point) - 728 (CDS-1 -2)
   520 (CDS-3)

The waveforms plotted for mode 5, CDS-1 and -3 showed little variation throughout all missions. However, mode 5, CDS-2, which is the pulse compression submode, did not function properly during SL2 or SL3 until EREP pass 39. Mode 5, CDS-2 did function properly during SL4. Figures 3.1-16 through 3.1-19 are examples of the S/H waveforms for mode 5, CDS-1, CDS-2 (pulse compression network not operating), CDS-2 (pulse compression network operating) and CDS-3, respectively. Again, as in the previous modes, there are three curves representing the mean and the mean $\pm 1\sigma$ values for the entire submode set of S/H outputs.
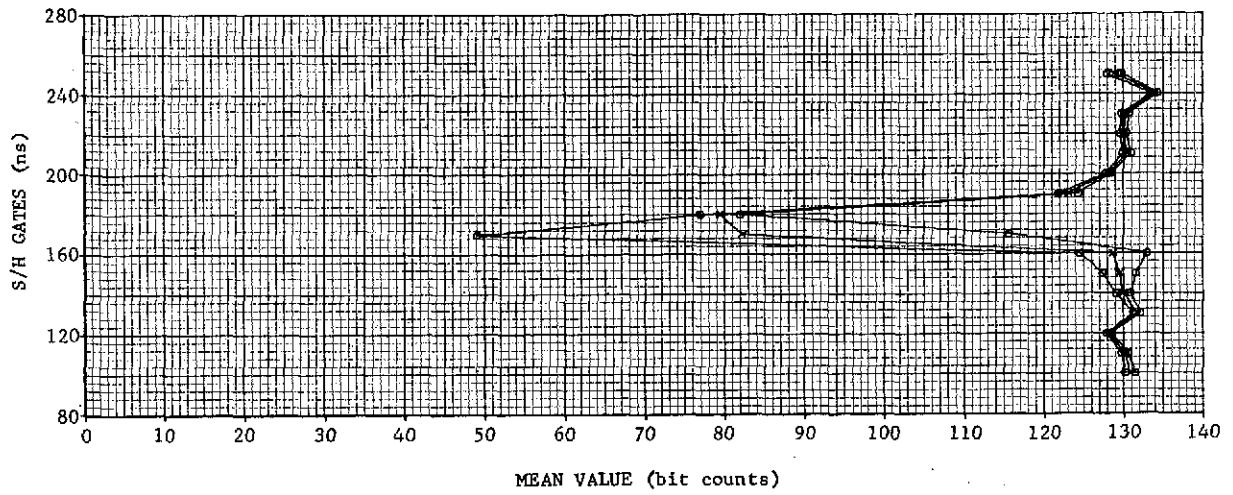
Figure 3.1-16 Typical Mode 5 CDS-1
Sample and Hold Waveform Construction
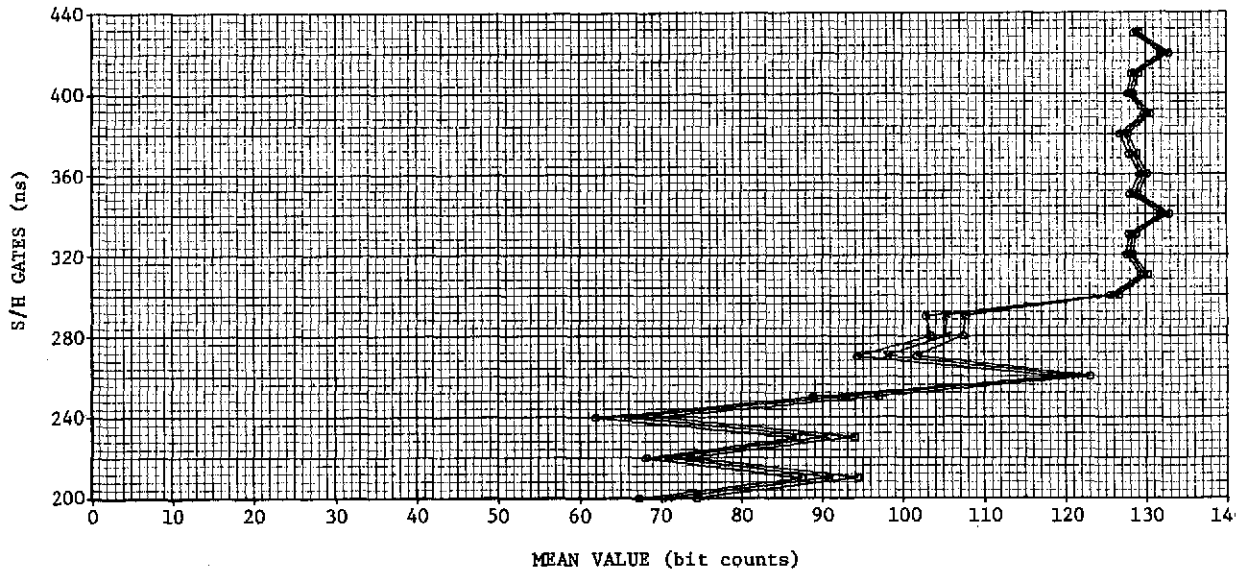
Figure 3.1-17 Typical Mode 5 CDS-2 Sample and Hold
Waveform Construction (Pulse-Compression
Network Not Operating)
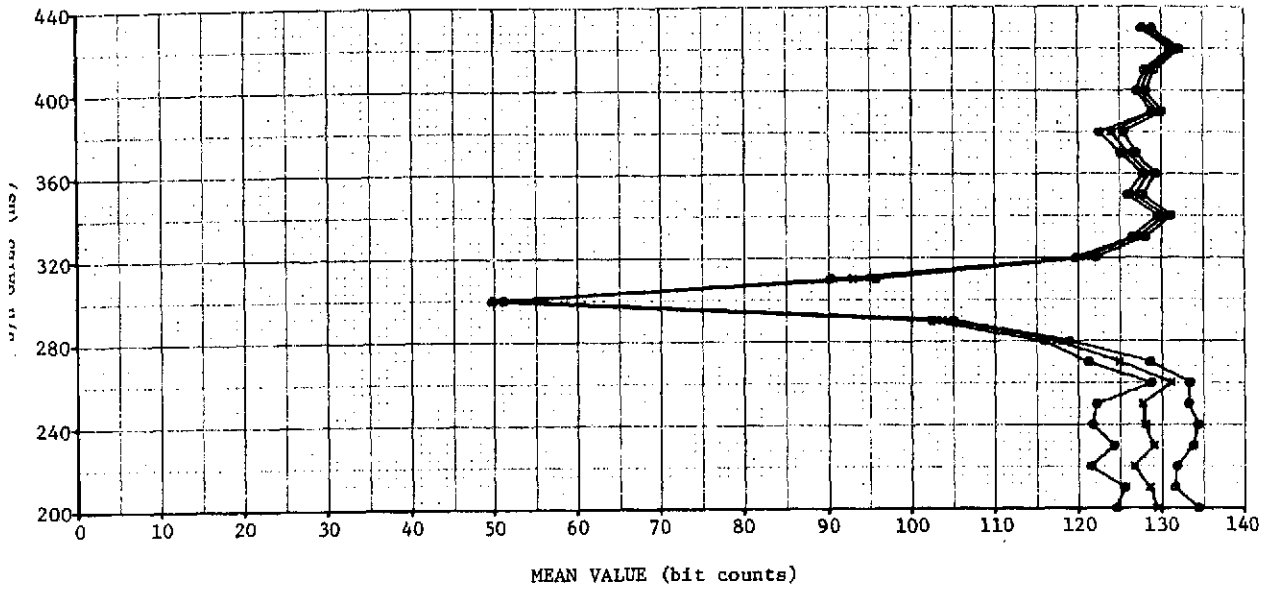
Figure 3.1-18   Typical Mode 5 CDS-2 Sample and Hold
                Waveform Construction (Pulse-Compression
                Network Operating)
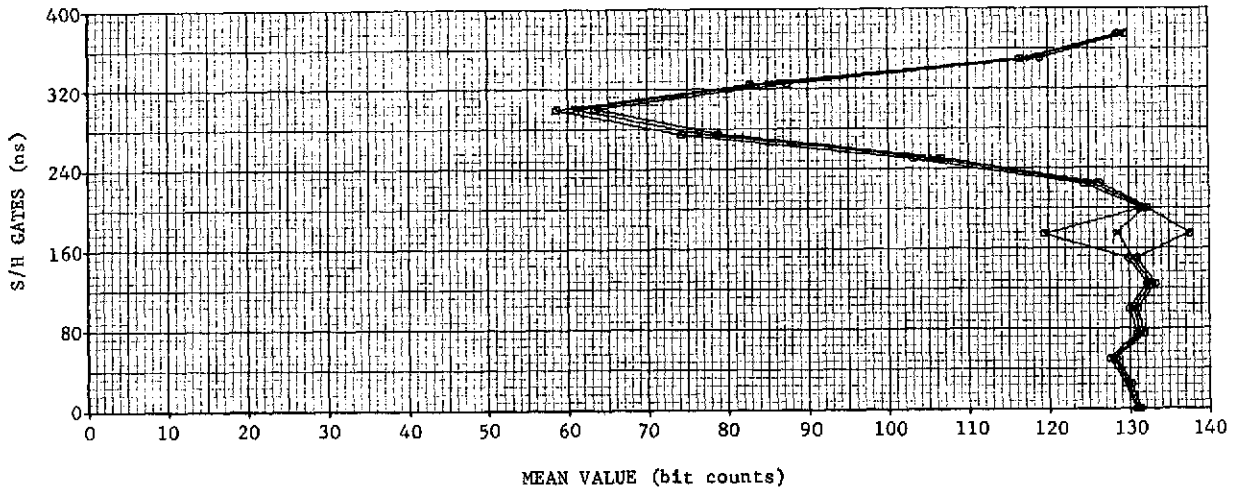
Figure 3.1-19   Typical Mode 5 CDS-3
                Sample and Hold Waveform Construction

3.1.7 Interference

Electrical interference was checked for all missions. There were no indications in any of the altimeter data of any perturbations caused by electromagnetic or radio frequency interference (EMI/RFI). However, some data were lost at S192 turn-on and turn-off times due to the change in tape speeds required to accomodate S192 operation.

3.1.8 Antenna Pattern

Though not a specific sensor performance evaluation task, some discussion of the antenna pattern was included in the interim sensor performance evaluation report, paragraph 4, MSC-05528, Volume V. The S193 antenna was common to both R/S and Alt operation. A parabolic reflector with a feed similar to a Cutler type was flown*. References for the antenna patterns include antenna patterns in the calibration data report** and those from the last measurements made at JSC.†

The antenna half-power beam width was nominally 1.6 degrees for SL2 and SL3. The half-power beam width for SL4 was estimated to have been between 2 (VV polarization) and 4 degrees (HH polarization). The feed cup was determined to have been missing during SL4 and, thus, the gain dropped by approximately 12 dB‡, and the sidelobes greatly increased. New patterns were measured at JSC to simulate SL4 conditions.

---

* Jasik, Henry: _Antenna Engineering Handbook_, McGraw-Hill Book Company, 1961, p 25.

** _S193 Calibration Data Report, Flight Hardware_, Vol II, Document No. 72SD4207, Rev. B, General Electric-SSO, Contract NAS9-11195, 31 July 1972.

S193 Calibration Data Report, Flight Backup Hardware, Vol II, Document No. 73SD4226, General Electric-SSO, Contract NAS9-11195, 27 March 1973.

† _Skylab S193 Radiometer/Scatterometer/Altimeter Sensor Antenna Testing Results_, Lockheed Electronics Co., Contract Number 9-1220 for NASA/JSC Tracking and Communications Development Division, Report LEC-4502 Skylab, Houston, Texas, September, 1974.

‡ Based on APEX data from the University of Kansas.

For some altimeter evaluations (See paragraph 11.2.2 of MSC-05528, Volume V.), the antenna pattern for SL2 and SL3 was approximated by

$$P(\theta) = \exp\left(\frac{-2\ \sin^2(\theta)}{5.5\ \times\ 10^{-4}}\right) \qquad [3.1\text{-}1]$$

The antenna gain (GE calibration data report, page 8-155*) for SL2 and SL3 was assumed to have been approximately +41.2 dB.

3.2 Altimeter Receiver Stability (SPE-S193-015)

The altimeter system provided measurements of AGC voltage (which indicated received signal level and was related to the target scattering cross-section), altitude word (which could be converted to altitude), and S/H gate voltage (which indicated received pulse shape and could be related to beam incidence angle and sea state).

3.2.1 AGC Voltage

The "peak" value of the transmitted waveform (average power during the pulse) was measured as 61.0 ± 0.4 dBm during the ground test program at KSC (paragraph 3.4.3.2 of MSC-05528, Volume V). This value was compared to AGC readings taken during test submodes on all three missions. The AGC voltage was corrected for temperature and related to transmitted power by using calibration curves and the measured value of attenuation between the transmitter and AGC test point in the receiver. Variances of about 1.5 dB were noted for these AGC measurements over the total preflight and mission evaluations, indicating a system stability near that value for the calibration submodes. If this AGC measurement were converted to radar cross-section (RCS) variance, other factors must be taken into account. There was considerable difference between the dependence of the AGC itself on the return pulse shape and the dependence of the RCS data values (derived in part from the AGC data) on the return pulse shape. Beam incidence angle varied with spacecraft attitude, causing changes in received waveform and thus the calculated RCS.

---

* S193 Calibration Data Report, Flight Hardware, Vol II, Document No. 72SD4207, Rev. B, General Electric-SSO, Contract NAS9-11195, 31 July 1972.

   S193 Calibration Data Report, Flight Backup Hardware, Vol II, Document No. 73SD4226, General Electric-SSO, Contract NAS9-11195, 27 March 1973.

A correction for this effect was derived by simulation (paragraph 7.1.2 of MSC-05528, Volume V). A heavy rain could cause an error in RCS of as much as 3 dB, but normal clear-air errors due to propagation were on the order of 0.1 or 0.2 dB. Corrections also had to be considered for spacecraft altitude, but this was known to sufficient accuracy to reduce this source of error to negligible values (less than 0.1 dB).

3.2.2 Altitude Word

Internal stability of the altitude-word measurement was indicated by mode 1 CDS-3 measurements taken during KSC tests and in flight for the three missions. This calibration submode measured internal delay. The mean value for internal delay for all three flights was 100 ns with a standard deviation of less than 1 bit count for SL2 and SL3 and approximately 1 bit count (2 ns) for SL4. This converted to a 0.3-meter altitude error. In evaluating total altitude error, external factors were also considered. Beam incidence angle changes the shape of received waveforms and a correction for this factor was derived from simulation. Terrain features and spacecraft altitude stability also affected the accuracy of the altitude measurement. However, for large off-normal spacecraft angles, oscillations occurred in altitude word readings. For beam incidence angles less than about 0.3 degrees from the vertical, altitude oscillations appeared to be of little consequence. Terrain features caused dynamic tracking errors. Contour plots were made for various types of terrain to illustrate the order of magnitude of these errors as a function of terrain type (paragraph 6 of MSC-05528, Volume V).

3.2.3 S/H Gate Voltages

The means of the S/H gate voltages were plotted for calibration submodes (CDS) and these were close to simulated values. Wave shape variations appeared to be no greater than those produced from computer simulation. Thus, it was estimated that the gate position instability was less than the resolution of the simulation, 2 ns.

Plots of S/H voltages for DAS submodes showed variations in waveshape expected by changes in terrain shape and beam incidence angle and were within expected limits compared to simulations. Generally, the rise time of short pulses (16 ns or compressed Barker code) increased with an increase in sea state. Fall time on all pulses increased with increasing beam incidence angle (beam pointing angle off normal increasing). When the beam

incidence angle increased to above half beam width (0.8 degrees), pulse rise time increased with further increases in beam incidence angle.

3.2.4 Tracker Acquisition

One subtask requested under this sensor performance evaluation task was a review of the types of terrain over which the S193 altimeter tracker would maintain lock, reported in paragraph 5.2 of MSC-05528, Volume V. In general, during SL2 and SL3, the altimeter tracker successfully acquired and maintained lock over water and flat or rolling terrain targets, but had difficulty acquiring and/ or maintaining lock over mountainous terrain. At discontinuities in target backscatter such as at land—sea interfaces, there was often a momentary loss of lock. There was much difficulty in acquiring and/or maintaining lock over any type of terrain during SL4 due to a combination of spacecraft attitude and the altimeter beam position being offset from nadir and/or the loss of return power by the altimeter due to the loss of the feed cup. No data were obtained during SL4 from the low—energy mode 5 DAS-3 short-pulse operation.

3.3 Altimeter Altitude Precision (SPE-S193-016)

For the sensor performance evaluation, the term "precision" was defined as the standard deviation of the altitude word. However, under this task, all possible sources of altitude measurement error were discussed. These included stability, resolution, servo response, tracker dynamics, and ground averaging effects over the illuminated ground coverage path. The true altitude defined as the height of the satellite above the subsatellite point was not always the standard for comparison. Skylab altitude over the subsatellite point as measured by S193 was the altitude to some averaged terrain height over the illuminated area (covered by the antenna main beam, neglecting sidelobes) when the spacecraft was in a normal attitude (z axis aligned with the gravity vector). Thus, comparisons were made to average topographical contours. A table of system errors was developed by NASA, WFC, (Table 3.3-1) which shows upper bounds on errors derived from system simulations with beam reflections from sea surfaces.

Review of the mode 1 CDS-3 data, which measured internal altimeter delay, indicated that the h_0 error in the first line of Table 3.3-1 (zero set, discrimination drift, servo unbalance, operating parameter change), which contributes most of the "systematic instrument error" was actually much better than the worst case values shown and was approximately 1 meter.

Table 3.3-1 Typical System Error Model and Residuals

	ERROR TERM AND FORM	UNCORRECTED MAGNITUDE	ERROR SOURCE	CORRECT DATA RESIDUALS (THEORETICAL)
1. INSTRUMENT ERRORS Systematic in total	h_σ = constant	<50 m	Zero set error, discriminator drift, servo unbalance, operating parameter changes	<10 m (correcting operating for parameters only)
	$h_t = \Delta t \dot{h} + \Delta t \ddot{h} + \cdots$	≈1 cm	Timing errors	≈1 cm (no correction suggested)
	$h_{tt} = -\left[\frac{1}{c} h\dot{h} + \frac{1}{c} h\ddot{h} + \cdots\right]$	≈30 cm	Transit time error	<1 cm
	$h_{dl} = \frac{\dot{h}}{K_v} + \frac{\ddot{h}}{K_a} + \cdots$	<40 cm	Dynamic lag error K_a = Servo acceleration constant (276 per s) K_v = Servo velocity constant (35 per s)	<10 cm (using waveform analysis during high dynamic conditions)
Random	$\sigma h = \sqrt{\sigma h_t^2 + \sigma h_q^2}$	<70 cm	σh_t = Height thermal noise $\sigma h_t = \dfrac{T\sqrt{7/6 + \frac{6}{s/n} + \frac{8}{(s/n)^2}}}{\sqrt{\frac{prf}{\pi b}}}$	≈30 cm (where features permit, more averaging can be applied)
		Approximately 5 cm	σh_t = quantizing error = $\dfrac{bit\ weight}{\sqrt{12}}$	
2. POINTING	h_p = f (pointing angle, antenna pattern, surface scattering vs angle tracking technique, etc)	<30 m	Off-nadir pointing	<1 m (if trailing edge is used to generate off-nadir position) (Based on SL data)
3. SEA SURFACE EFFECTS	h_{ss} = Constant for given waveheight	<0.75 m	Electromagnetic MSL vs MSL	<10 cm (if waveheight is known to 25%)
4. ATMOSPHERE	h_{at} = Constant for given total moisture content	<2 m	Atmospheric refraction path delay	<10 cm (if temperature, pressure, and humidity are known)

The table shows sea "sea surface effects" (line 3). If the beam illuminated a terrain surface, the effect of the terrain-produced errors could be much greater than those from sea surfaces. Rough mountainous terrain could cause unlocks, which produce unreliable data. Rolling terrain over which locks are maintained could cause dynamic tracking errors of as much as tens of meters. Observations of relatively smooth sea areas (2-meter significant wave height or less) showed that altitude oscillations of up to 50 meters could occur if the beam incidence angle was of the order of a beam width, but tended to be less than 1 meter for beam incidence angles of less than 1/4 beam width (0.4 degree). This oscillation was believed to be caused by spacecraft attitude instability.

These error sources are discussed in some detail in MSC-05528, Volume V, paragraph 6, with terrain plots derived from the altimeter data compared to topographical maps, geoidal and bathymetric charts.

3.4 Altimeter Receiver Dynamic Range/Linearity, Resolution (SPE-S193-017)

Martin Marietta developed a comprehensive computer model for the entire altimeter system, including reflections from ground targets. Separate programs covered the CDS and the DAS submodes and all transmitted waveshapes were handled. The DAS model reported in MSC-05528, Volume V, paragraph 7, was designed only for reflections over sea water, but a revised program is available to cover four different target models, with one or more types of terrain making up the reflection zone. These altimeter system models (See Appendix A, Section II, of this volume) were used to determine the relationships between S/H waveforms, altitude word, AGC voltage, and several system variables. The system variables were beam incidence angle, wave height (for sea water) or terrain type, transmitted waveform, receiver bandwidth, and sample interval.

In addition, a program was developed to calculate radar cross-section (RCS) from JSC computer-compatible tape data and the beam incidence angle. Plots were derived from the program of RCS versus time as well as tabulations of RCS, time, average altitude per frame, and mode status.

The program and results are in paragraph 7.7 of MSC-05528, Volume V. Additional discussions of such items as the link calculation and pulse shape correction of the AGC were also prepared. The backscatter calculation examples showed a correlation of the sea reflectivity with wind speed and the fluctuation of reflectivity of land targets. S193 sea reflectivity data agreed well with a theoretical model used for comparison.

Correction curves were derived from S193 system computer models to correct RCS and altitude for errors caused by beam incidence angle off of the normal. The models were also useful for comparison with S/H waveshapes to show waveform stability and the effects on the waveforms of terrain and beam incidence angle. Contributions to the measured waveform of various parts of the system could also be observed, because waveforms were available from several points in the system and for all possible combinations of transmitted waveforms, receiver bandwidths, and receiver sampling intervals.

3.5 Altimeter Pulse Compression Verification (SPE-S193-018)

The pulse compression submode (DAS-2) for mode 5 operated as a 130-ns pulse, but compression did not occur in the receiver during SL2 and most of SL3. This was evident from inspection of the CDS waveforms, altitude word discontinuities, and AGC bias errors. This submode spontaneously began to operate properly after EREP pass 39 of SL3 and continued to do so throughout SL4. Data from DAS-2 operation with the pulse compression network (PCN) compared very favorably with the 16-ns submode (DAS-3) except for the higher AGC voltage in DAS-2. PCN operation in DAS-2 increased the peak detected level by about 9 dB, as expected.

Failure of the PCN to properly switch into the receiver did not prohibit operation of the mode for obtaining good altitude data. Thus, many mode 5 operations were run to obtain both good altitude and short-pulse (mode 5, DAS-3) data. Altitude data when the PCN was not operating required an additional time-delay correction factor corresponding to approximately 15 meters. (See paragraphs 6.1.2 and 8.4 of MSC-05528, Volume V.)

Also under this task, measurements of the mode 5 waveforms received on the ground (STAPE) with a broad band receiver were reported. They indicated that the DAS-1 submode was transmitting properly after the gimbal anomaly in SL3 because 100-ns pulses were received on the ground. The half-amplitude pulse width was 82 ns, which was within 2 ns of the value obtained from the 10-MHz simulation and the S/H plots.

3.6 Altimeter Measurement Time (SPE-S193-019)

The altimeter's ability to measure pulse return time was fundamental to several tasks. Considerable discussion of the errors affecting and the procedures required for computing the altitude evaluation from S193 altitude data was presented in paragraph 6 of MSC-05528, Volume V. Based on preflight tests, the internal

calibration of the instrument time delay (mode 1 CDS-3) was expected to have a variation of ±8 ns (or ±1.3 m). However, the altitude precision on smooth sea targets with good Skylab orientation was typically 0.6 meters and the variation of the in-flight internal time delay was equivalent to less than 0.3 meters.

3.7 Nadir Align Precision/Accuracy (SPE-S193-020)

The specified pointing accuracy of the nadir align seeking mode of altimeter operation was ±0.75° from nadir. An inspection of received waveforms and pitch gimbal readouts confirmed that this was achieved in practice. However, spacecraft attitude instabilities during and after nadir align operations were such that the nadir pointing established for the S193 was not maintained during the entire flight periods between nadir alignment modes. The nadir seeker operation was designed to point the antenna toward the maximum return signal over sea targets by following a prescribed homing motion. The proper gimbal motion was verified. However, total operation time was long enough to allow the Skylab attitude to change during nadir seeking. Thus, on some occasions, the apparent target pointing position drifted during the alignment operation.

3.8 Additional Evaluations (SPE-S193-YYY)

A number of additional evaluations that did not logically apply to other tasks were included in this section, as follows.

3.8.1 Wallops Flight Center Statistical Models

Statistical models were developed and used to show the theoretical relationship between received pulse rise time and sea state for flights over ocean areas. Sample waveforms were given (See paragraph 11.1.1 in MSC-05528, Volume V.) that show an increase in pulse rise time with an increase in significant wave height. A tracker model was discussed (paragraph 11.1.2.1 of MSC-05528, Volume V) to illustrate the effects of tracking jitter, tracker averaging and quantization, and output-time granularity. Typical altitude outputs were shown as a function of the number of frames of data processed in the altimeter for the simulation and for actual Skylab data. A procedure for interpolating S193 altitude data output was presented (paragraph 11.1.3 of MSC-05528, Volume V), which used a third-order polynomial fit. The altimeter altitude bit weight was 2.5 ns. The average quantization error for the altimeter was determined to be 0.72 ns. The averaged altitude samples measured by S193 were output only every 1/8 of a

second. For instantaneous altitude estimates, it was determined
that a weighted linear combination of altitude averages within
approximately a 2.1-second span centered on the time of interest
was required. The jitter of the tracker gate was determined to be
less than 22 ns, worst-case, for the 100-ns pulse operation and
was generally considered negligible.

3.8.2 Sample-and-Hold Correction Rationale

Sample-and-hold (S/H) gates were positioned by the tracker
gate on the return pulses measured. Thus, their position in time
fluctuated with the return pulse. The instantaneous gate position
in time was not outputted in the data stream; only the average
position was available through the altitude-word data. Therefore,
in some average pulse shape reproduction from the S/H data, the
instantaneous altitude or gate position had to be determined as
described above in order to properly weight the contributions to
the S/H output from a given gate position.

The S/H gates were subject to a direct-current bias offset
drift, which was assumed to be linear in time. A technique for
correcting the gate outputs for this bias was presented with some
examples of both its need for incorporation and illustrations of
the success of its application in paragraphs 3.5, 3.5.1, and 11.1.3
of MSC-05528, Volume V.

3.8.3 STAPE Description and Evaluation

A description of the STAPE ground-based test setup was
presented in the interim sensor performance evaluation report, MSC-
05528, Volume V. STAPE was used in the receive mode so that an
estimate of the transmitted waveform for the 100-ns pulse was
obtained. Using STAPE, the transmitted pulse operation for the S19:
altimeter was confirmed during flight. Additional information is
presented in Appendix A, Sections I and III of this volume.

3.8.4 Off-Nadir Angle Position (Beam Incidence Angle)

A method for determining the beam incidence angle by observing
the fall time on the received pulse was developed. Curves from the
WFC simulation were given, showing a comparison between some Skylab
data and computed values. Based on the limited SL2 comparisons
completed, it was estimated that antenna pointing angles between
0.25 and 0.75 degrees to nadir could be determined to within ± 0.05
degrees. This estimate may have been overly optimistic, as
indicated in paragraph 4.3. Discussions of pointing-angle
determination from the pulse shape were given in paragraphs 11.2.2.:
and 7.1.2 of MSC-05528, Volume V.

3.8.5 AGC Corrections for Returned Wave Shape

Some corrections for AGC values as a function of the wave shape change caused by the beam incidence angle were discussed in paragraphs 7.6 and 11.2.7 of MSC-05528, Volume V. A term known as the r-factor was defined to relate the "peak of the mean waveform" (the quantity required for determining the absolute return power level) to the "mean of the peak (individual) waveform value" (the quantity that set the AGC voltage values). Values of the r-factor for some specific pulse shapes were tabulated in the interim sensor performance evaluation report.

3.8.6 Pulse-to-Pulse Correlation Study

A study of the correlation between pulses in the pulse pairs of mode 3 operation as a function of the pulse separation was started and reported in paragraph 11.3 of MSC-05528, Volume V. Plots of the sample-and-hold waveforms for each of the two separated pulses in a pulse pair, together with a plot of pulse-to-pulse correlation, were included. Roughly 111 µs were required for decorrelation between pulses for mode 3, DAS-2 (100-ns pulse). This corresponded to the value predicted from the Van Cittert-Zernike theorem. There was a seemingly premature rise of the correlation before the mean return signal, which was considered due to smearing resulting from the jitter of the S/H gates.

In the CDS submodes, the S/H gates did not show the second of the two transmitted pulses due to mispositioning of the gates. Thus, the time between the transmitter pulses of a pulse pair during the flight was not measurable, and preflight separation values had to be used. A summary of the mode 3 correlation investigation will be in the WFC sensor technology final report expected in the spring of 1975. One investigation from which results should be available is of the interesting possibility that the direction of the beam pointing off-nadir might be determined from the pulse-to-pulse correlation coefficients.

4.   SUPPLEMENTARY ANALYSES

This section presents the results of analyses conducted
to supplement the basic evaluation summarized in Section 3.
These include further results from the antenna pattern evaluation,
comparison of the measured pulse shape data with computer
simulations to verify that S193 pulse shape rise times provided
a measure of sea state, and an example of the pulse shape
degradation resulting from the long time required to obtain the
pulse shape data.

4.1   STAPE Evaluation

The S193 altimeter mode 1 pulse shape experiment transmitted
single 100-ns pulses at a rate of 250 pulses per second.   The
pulse width and rate were fixed for all DAS and CDS submodes.
Waveforms of the transmitted pulses were received by the STAPE
system operating in the configuration shown in Appendix A,
Section I.   A STAPE pulse shape was measured during SL3 EREP
pass 36, on track 43, September 12, 1973, at approximately
17:09:30 GMT and during SL4 EREP pass 74, on track 57,
January 6, 1974, at approximately 18:00:00 GMT.   The shapes of
the received pulses were recorded on film during STAPE system
operation and the photographs from SL3 are shown in Figure 4.1-1
and from SL4 in Figure 4.1-2.   The pulses photographed were
received through the horizontally polarized receiver channel,
and the waveform was the output of a crystal detector that fed
directly into a low-impedance high-frequency wide-bandwidth
oscilloscope.

The SL3 pulse shapes shown in Figure 4.1-1 A, B, C, and D
were the first representative pulses received by STAPE from the
S193 altimeter.   Figures 4.1-1 A and C were the original
photographs taken, and Figures 4.1-1 B and D are copies
reworked to enhance the wave shapes.   Different amplitudes were
the result of receiving signals through different antenna
sidelobes as a function of time, action of the automatic
leveling circuits in the STAPE system, and the effects of
antenna pointing by the S-Band tracking system.   The parallel
lines in the picture are not calibrated time increments.   They
appear to be light sources occurring above or below the pulse
presentation area and were present on the oscilloscope used for
the tests.   Light levels for the pulses were too low to permit
enhancing the scale markings using the internal controls.
Extremely faint traces of the scale markings on several photo-
graphs were used to scale the pulses in Figures 4.1-1 B and D.

MSC-05546
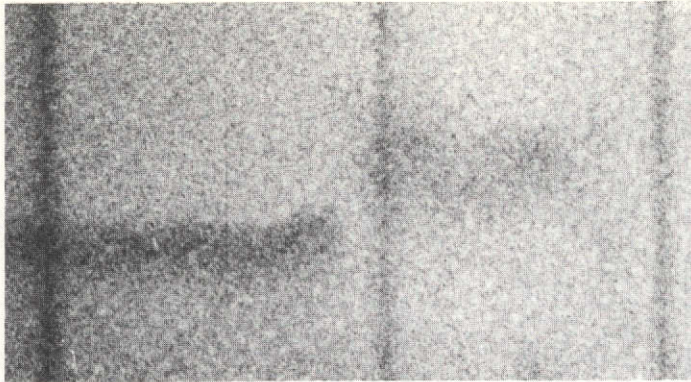
A. Original photograph
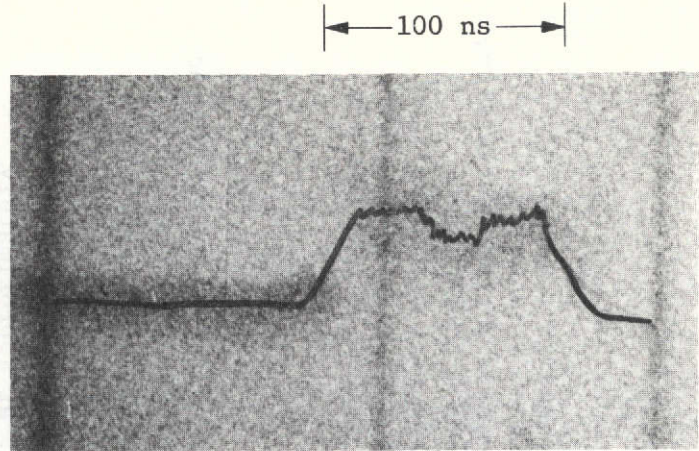
B. Photograph A with pulse outlines enhanced
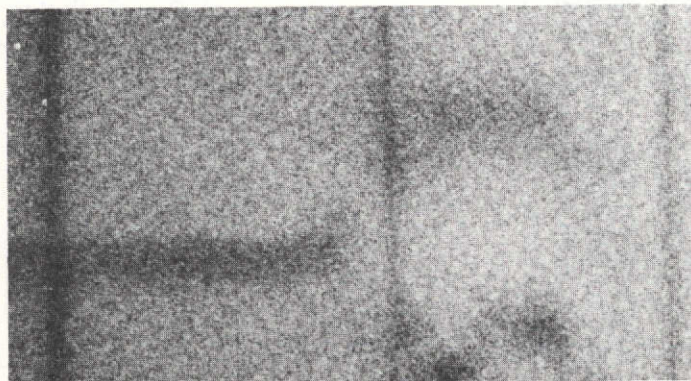
C. Original photograph
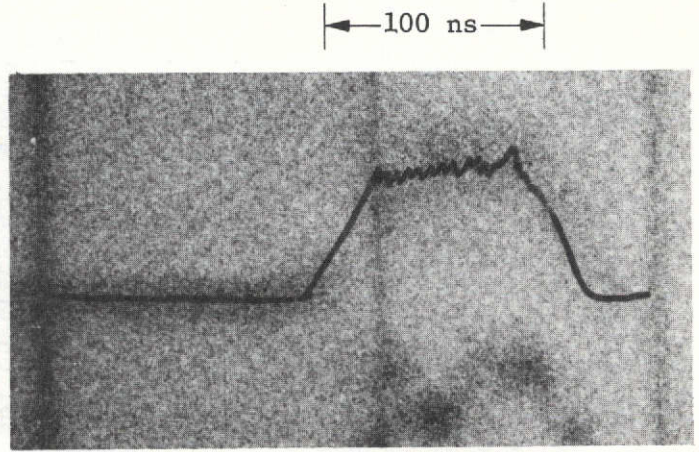
D. Photograph C with pulse outlines enhanced

Figure 4.1-1   SL3 Transmitter Output Waveforms for Mode 1

← 100 ns →   ← 100 ns →

A.   B.

C.   D.

← 100 ns →   ← 100 ns →
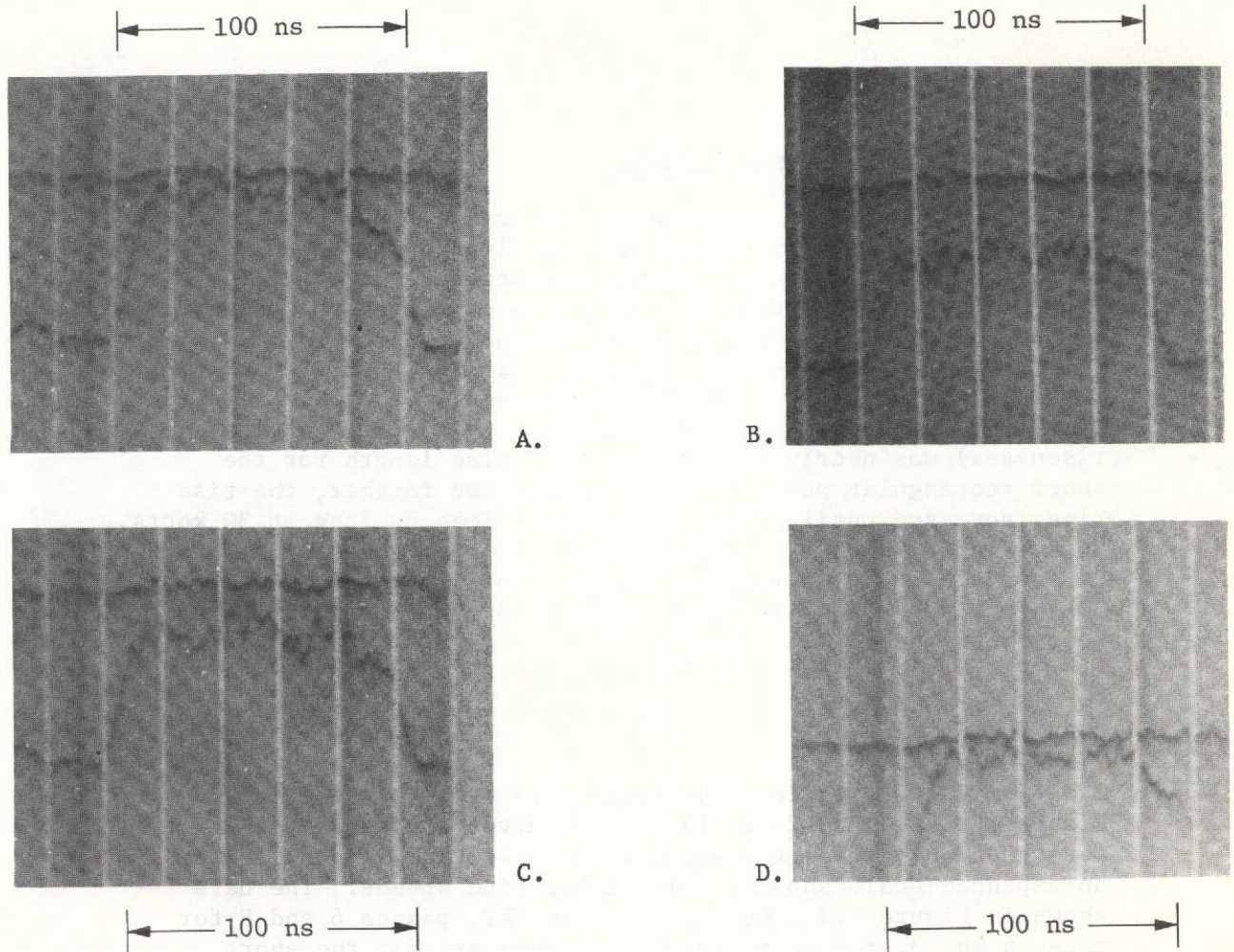
Figure 4.1-2 Original Photographs of SL4 Transmitter Output Waveforms for Mode 1

The resultant pulse width was determined to be 100 ns, measured at the trace baseline, greater than 90 ns across the top of the pulse, and 95 ns at 50% amplitude. These pulse widths correlated well with KSC baseline data for the S193 altimeter.

The SL4 pulse shapes shown in Figures 4.1-2 A, B, C, and D were the first representative pulses received by STAPE during EREP pass 74 from the S193 altimeter. The problem of defining time increments was resolved for SL4 tests by darkening the scale at the time interval markings. These show up as bright lines (no light) on the photographs and are 20 ns apart. These time scale markings were used to scale the pulses in Figures 4.1-2 A, B, C, and D. The resulting pulse width was determined to be 100 ns measured at the trace baseline, greater than 90 ns across the top of the pulse, and 97 ns at 50% amplitude. These mode 1 pulse widths show good repeatability compared to the SL3 mode 1 pulse widths and also correlate well with the KSC baseline pulse widths for the S193 altimeter.

4.2 Sea State Measurements

Simulations were conducted to determine the received waveforms to be anticipated at the sample-and-hold (S/H) gate output for both the short (16-ns) rectangular pulse and the 130-ns Barker coded pulse as a function of sea state. Reception of the 130-ns Barker encoded pulse assumed the PCN to be properly switched into the receiver. Figures 4.2-1 and 4.2-2 show the simulations for the two transmitted pulses, respectively. The rise time for smooth seas (5- to 10-knot winds for a fully risen sea) was nearly the same as the pulse length for the short rectangular pulse. As the sea became rougher, the rise time increased until it was about five times as long at 30 knots. However, for the Barker coded pulse, the rise time for smooth seas was about 30 ns (Figure 4.2-2). For rough seas (i.e., 30-knot winds) the rise times of the two types of transmitted pulses were nearly the same.

Some actual performance (S/H) data are presented in Figures 4.2-1 and 4.2-3. The solid curves in Figure 4.2-3 were reproduced from the simulation curves of Figure 4.2-2 on an expanded scale showing only higher wind speeds. The data shown in Figure 4.2-1 were taken from SL2, passes 6 and 9 for modes 5 and 3, respectively. These data are for the short (16-ns) rectangular-pulse submodes and are shown on the appropriate simulation curves. The data in Figure 4.2-1 appear to match the 20-knot curve most closely, with the pass 9 data at a windspeed interpolated to about 22 knots and pass 6 almost exactly 20 knots. Weather data in that general area show winds up to about 20 knots maximum. Figure 4.2-4 shows an average radar cross-section for pass 6, mode 5, DAS 3 of about 10.5 dB. Reference to the Barrick* model of Figure 4.2-5 indicates a radar cross-section of 10.3 dB for a 20-knot wind. This 0.2-dB difference was considerably better than the internal stability of the altimeter system (See paragraph 3.2.1.), so that other comparisons would not necessarily be expected to be as good, but this did provide at least a single-point check of the model.

---

* D. E. Barrick: "Wind Dependence of Quasi-Specular Microwave Sea Scatter," Communications Section of IEEE Transactions on Antennas and Propagation, January 1974, p 135.
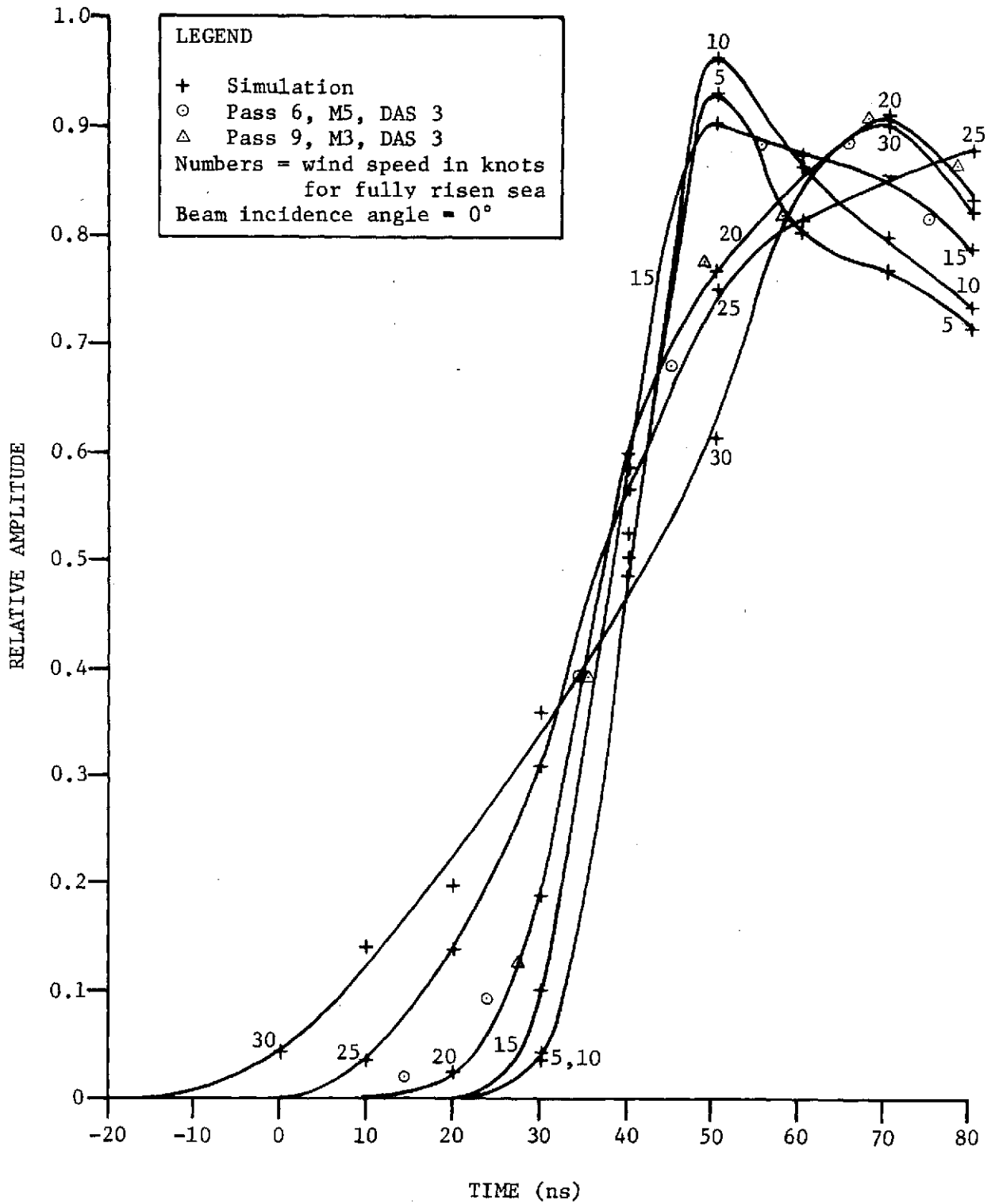
Figure 4.2-1 Leading Edge of 16-ns Pulse for Fully Risen Sea
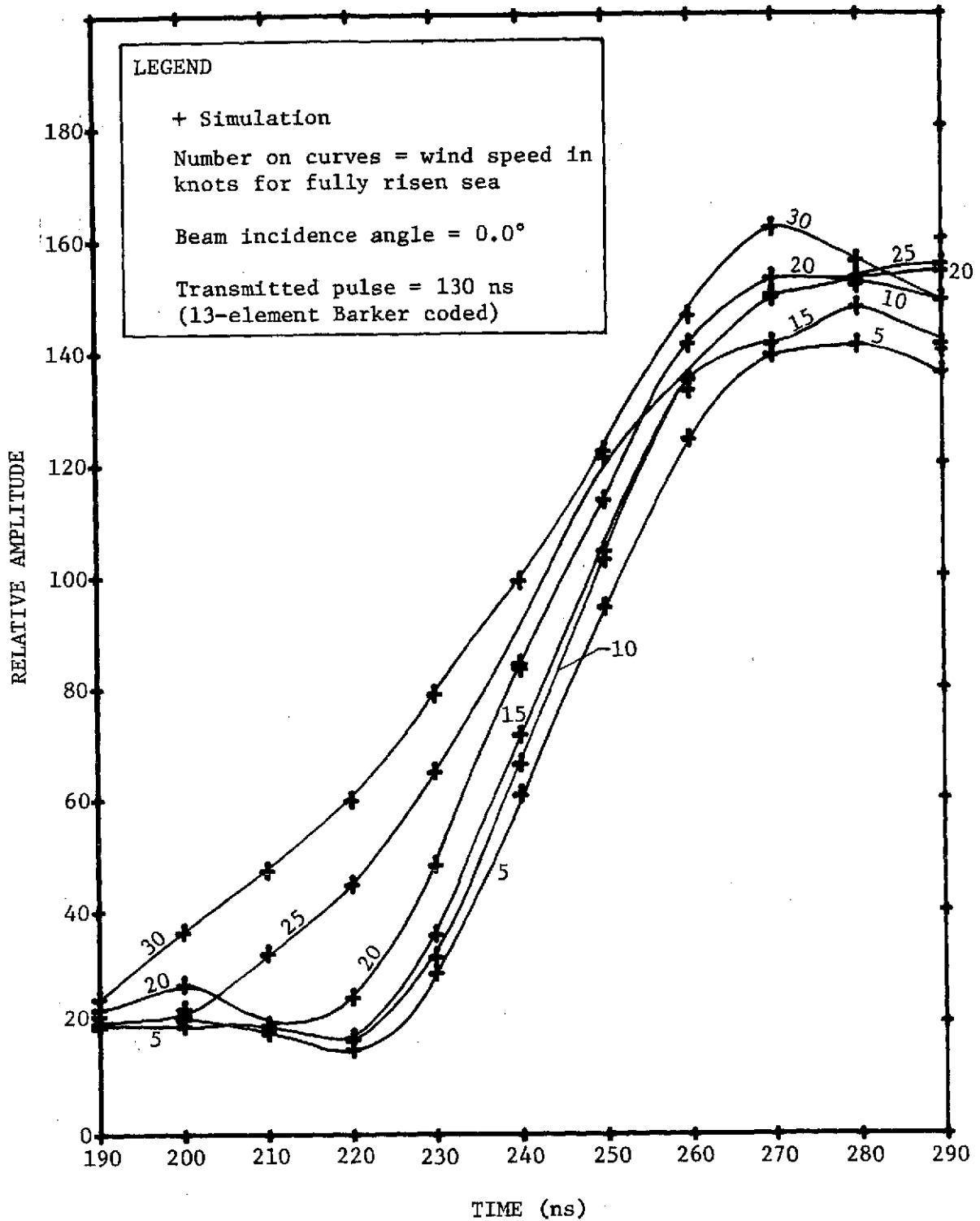
Figure 4.2-2 Simulation of Leading Edge of Barker Coded Pulse for Fully Risen
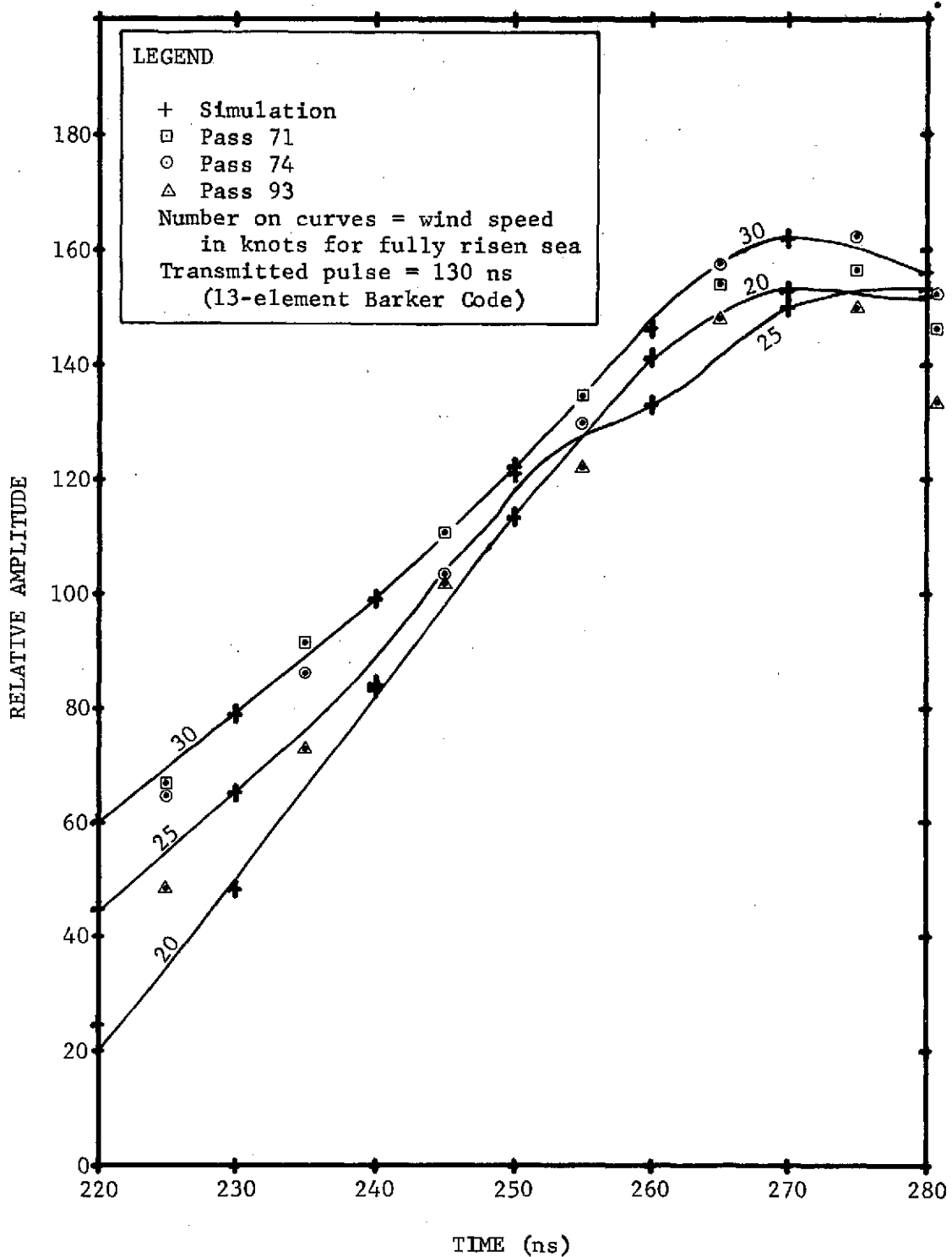
Figure 4.2-3   Leading Edge of Barker Coded Pulse, Simulation versus
Skylab Data

MSC-05546

When the same type of check for the Barker coded pulse was
attempted, the correlation between simulation and Skylab data
was not so close. Figure 4.2-3 would indicate that the wind
speed was on the order of 25 to 30 knots, but a radar cross-
section of 13 dB (Figures 4.2-5 and 4.2-6) and the weather map
(Figure 4.2-7) indicate wind speeds on the order of 10 knots.
This would suggest that the actual flight data indicated that,
as an instrument for measuring sea state, the Barker coded mode
was not performing even as well as the simulation would indicate.

In future flights such as the planned SEASAT experiment, it
would be desirable to obtain altimeter data over a wide range
of sea states, and provide direct sea measurements directly
under the satellite.
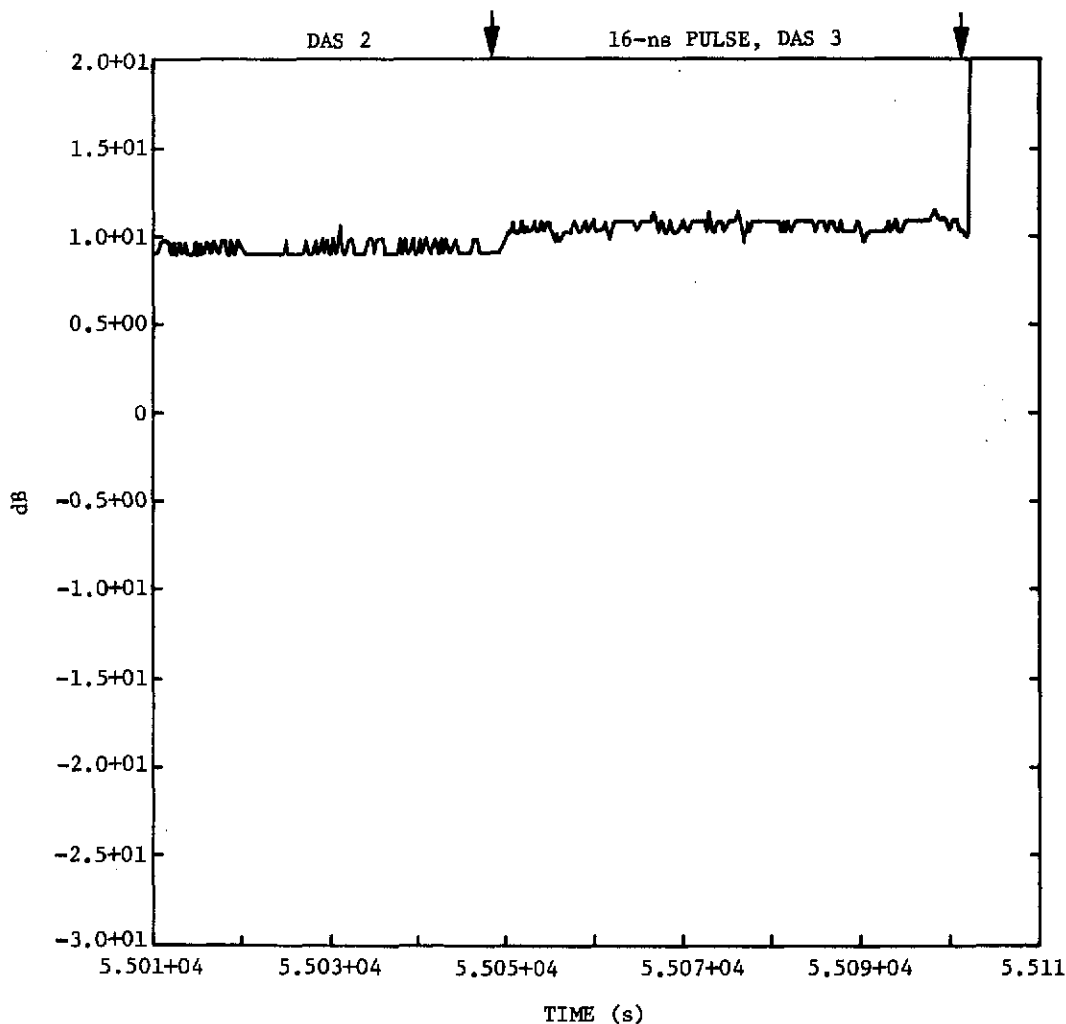
Figure 4.2-4 SL2 Radar Cross-Section, Mode 5, Pass 6

V-40
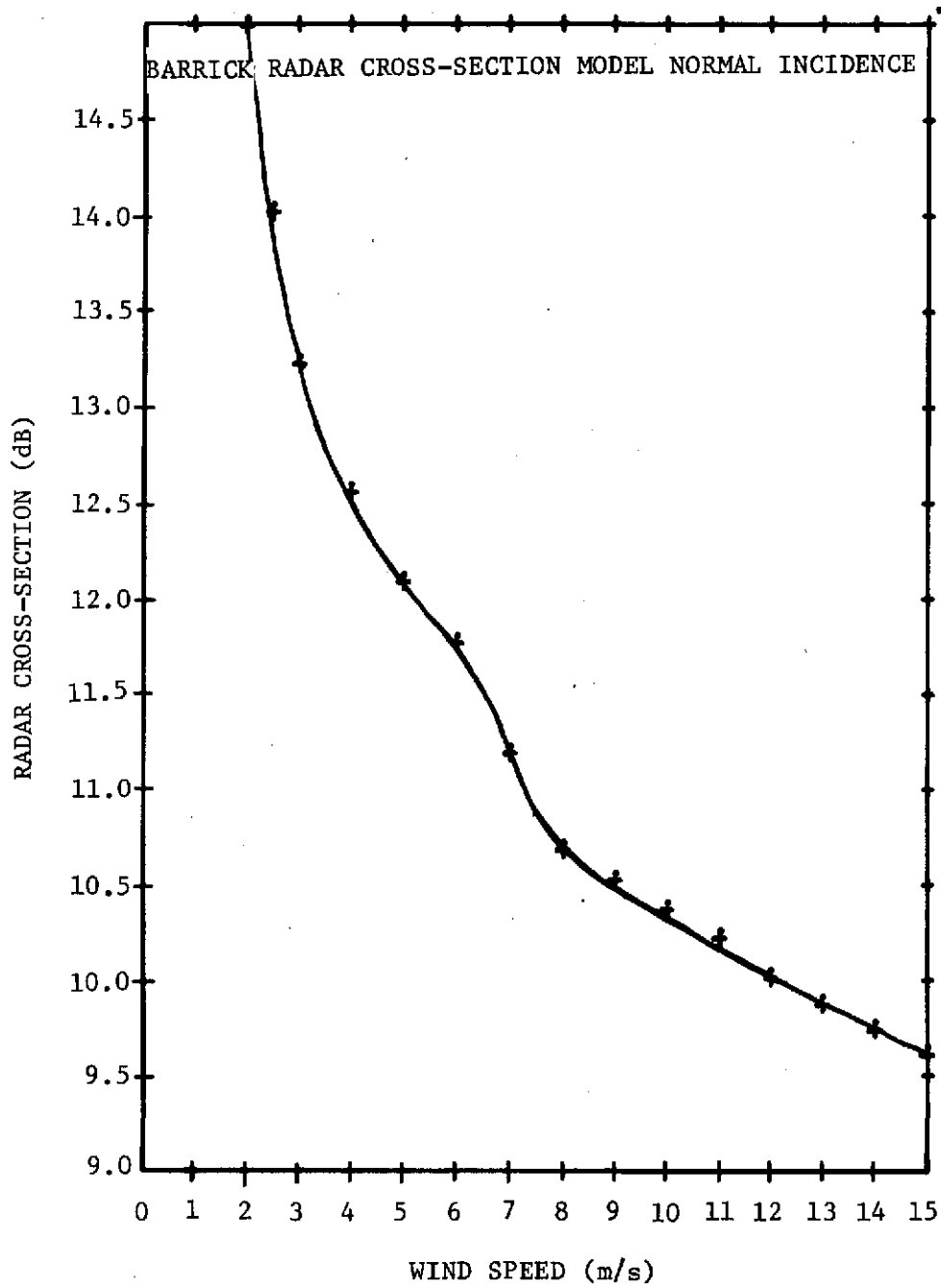
Figure 4.2-5 Wind Speed versus Radar Cross-Section

PASS 21 (74)   DOY 6   IA11 OBZ

DAS 1   DAS 2   MODE 5
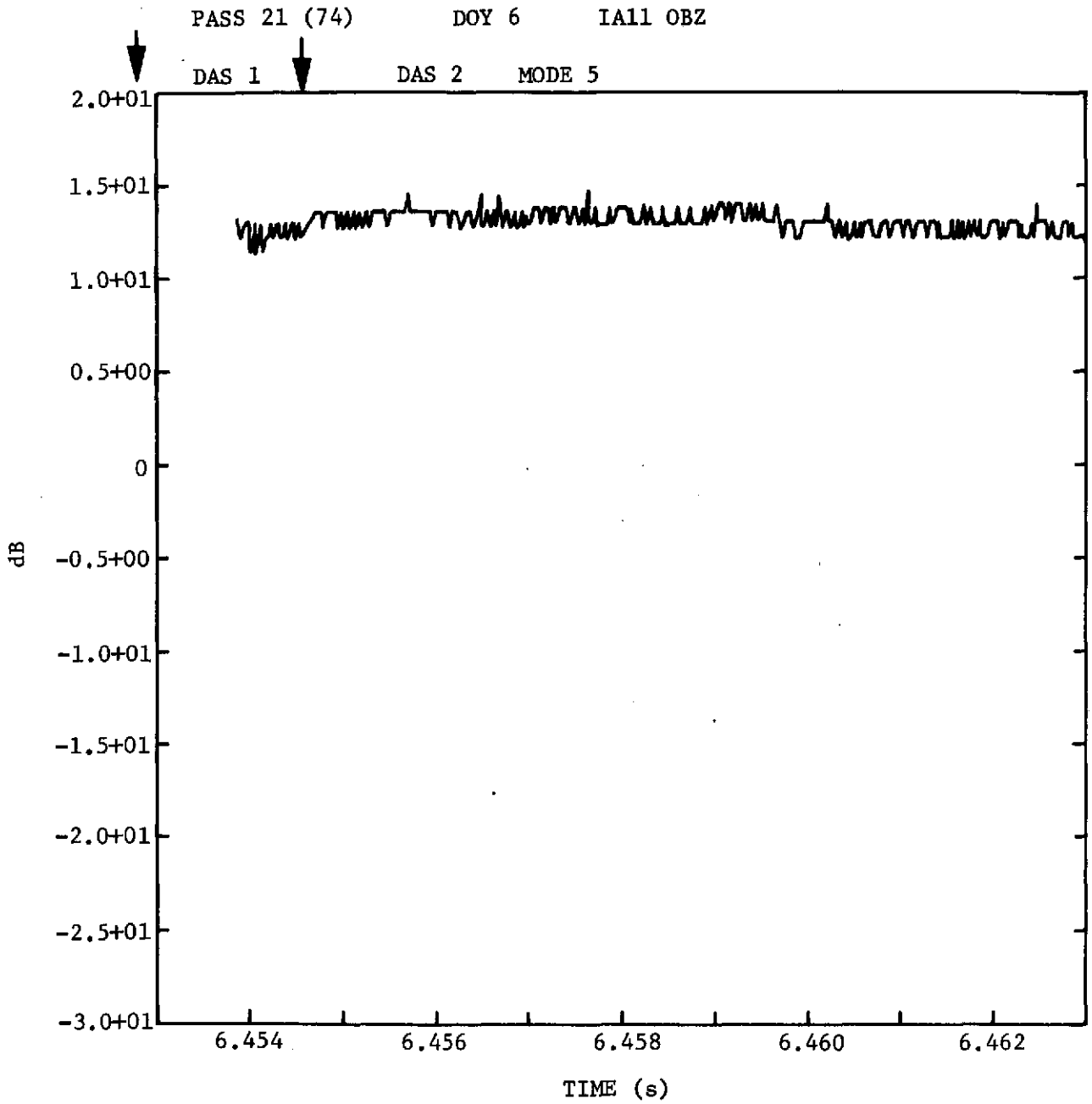
Figure 4.2-6   Radar Cross-Section
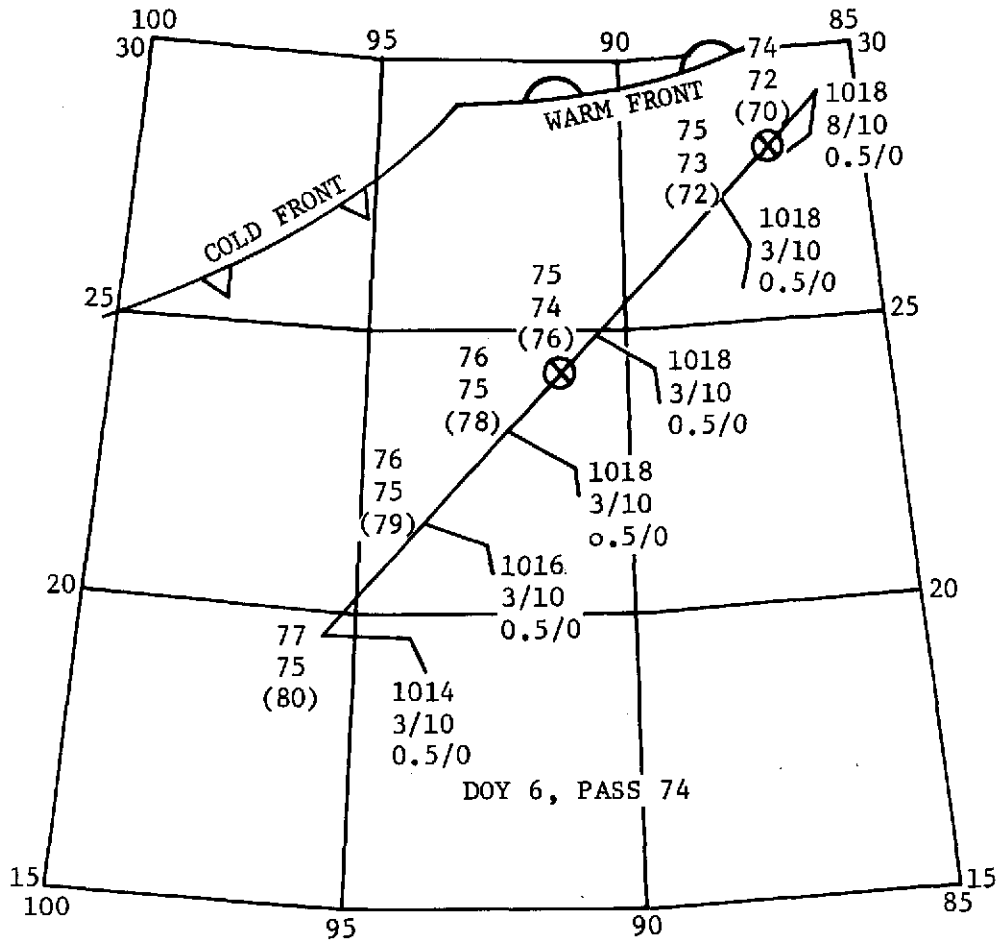
Figure 4.2-7 Weather Map and Skylab Track for 1756 GMT,
January 6, 1974

4.3   Antenna Pattern Measurements

Antenna pattern cuts were measured by G.E.* before SL2 and
by JSC after SL4, using the backup antenna. G.E. measured both
the flight and backup antennas. The JSC patterns were made
using the backup antenna adjusted to represent both the SL2 and
SL4 configurations of the flight antenna. In-flight measurements
of the antenna pattern by the University of Kansas APEX
(See MSC-05546, Volume IV, Appendix A, Section III.) were used
to guide the postflight antenna measured by JSC.

Table 4.3-1   Antenna-Pattern Principal-Axis Cuts, Vertical Feed

	G.E. (w feed cup)		JSC (w feed cup)		JSC (w/o feed cup)	
	E plane	H plane	E plane	H plane	E plane	H plane
3 dB BW	1.5	2.0	1.5	2.0	2.7	2.0
10 dB BW	2.5	3.5	2.5	3.8	4.2	4.5
1st SL	-20 dB	-27 dB	-25 dB	-28 dB	-16 dB	-16 dB
Residual Sidelobes	-38 dB	-38 dB	-37 dB	-37 dB	See plots.	

Figures 4.3-1 through 4.3-6 are 360-degree plots of the
principal-plane cuts for the G.E. and JSC measurements. There
are some differences, as shown in Table 4.3-1, which lists some
characteristics of the principle-plane cuts. The major
differences appear to be in sidelobe levels, with the main beam
shape matching closely down to the 10-dB points. For the first
sidelobe levels, a difference of about 5 dB was noted in the
E-plane cut and only about 1 dB in the H-plane cut. These
differences can be accounted for by the new feed applied to the
antenna before testing at JSC and possibly to some range
differences. To simulate antenna conditions for SL4, patterns

* S193 Microwave Radiometer/Scatterometer/Altimeter, Calibration
  Data Report, Flight Hardware, Vol II, Revision B, General
  Electric, 31 July 1972.

Skylab S193 Radiometer/Scatterometer/Altimeter Sensor Antenna
Testing Results, Job Order 16-604, Lockheed Electronics
Company, Inc. Aerospace Systems Division, Houston, Texas,
Contract NAS9-12200.
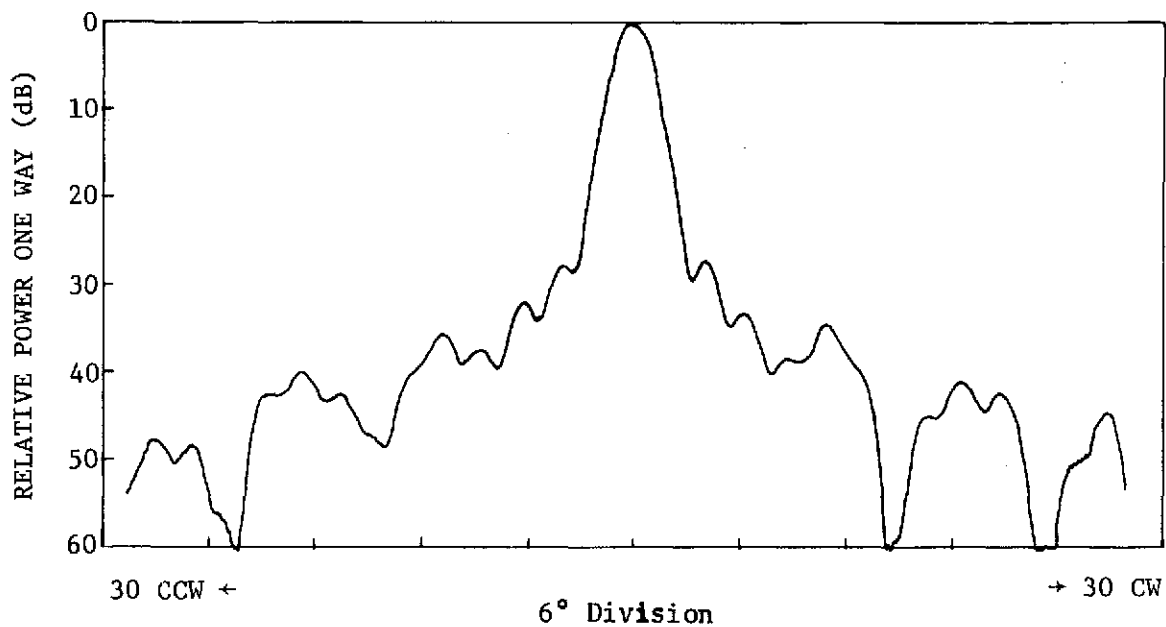
Figure 4.3-1 H-Plane Cut, GE
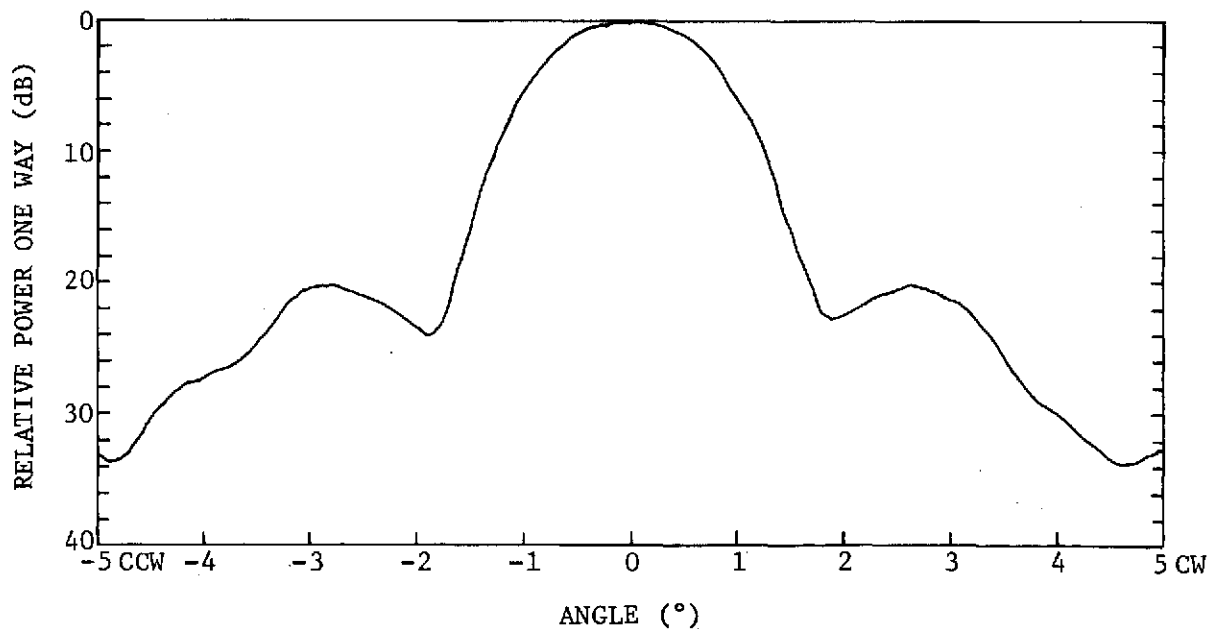
Figure 4.3-2 E-Plane Cut, GE
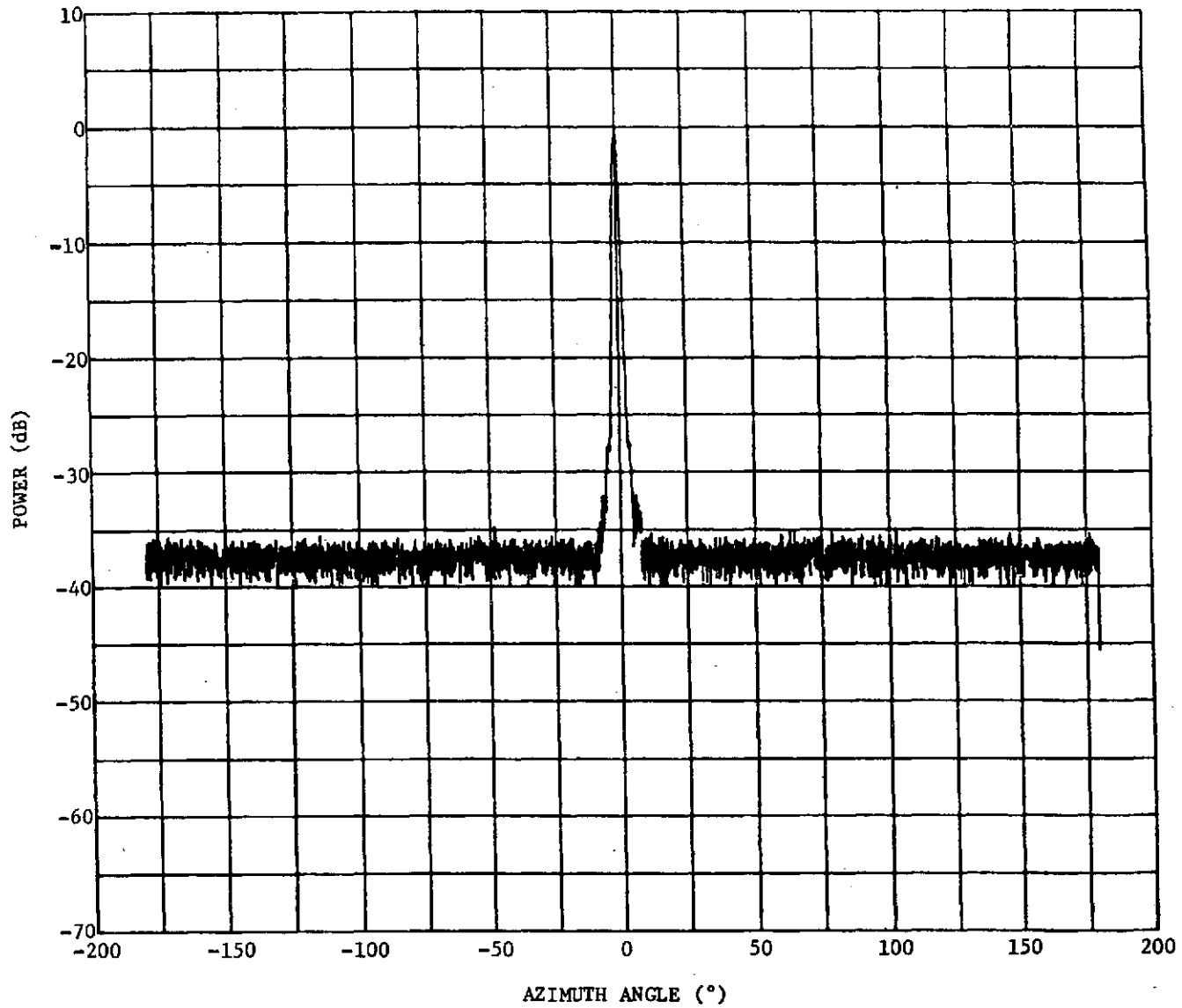
Figure 4.3-3 H-Plane Cut, JSC Feed Cup On
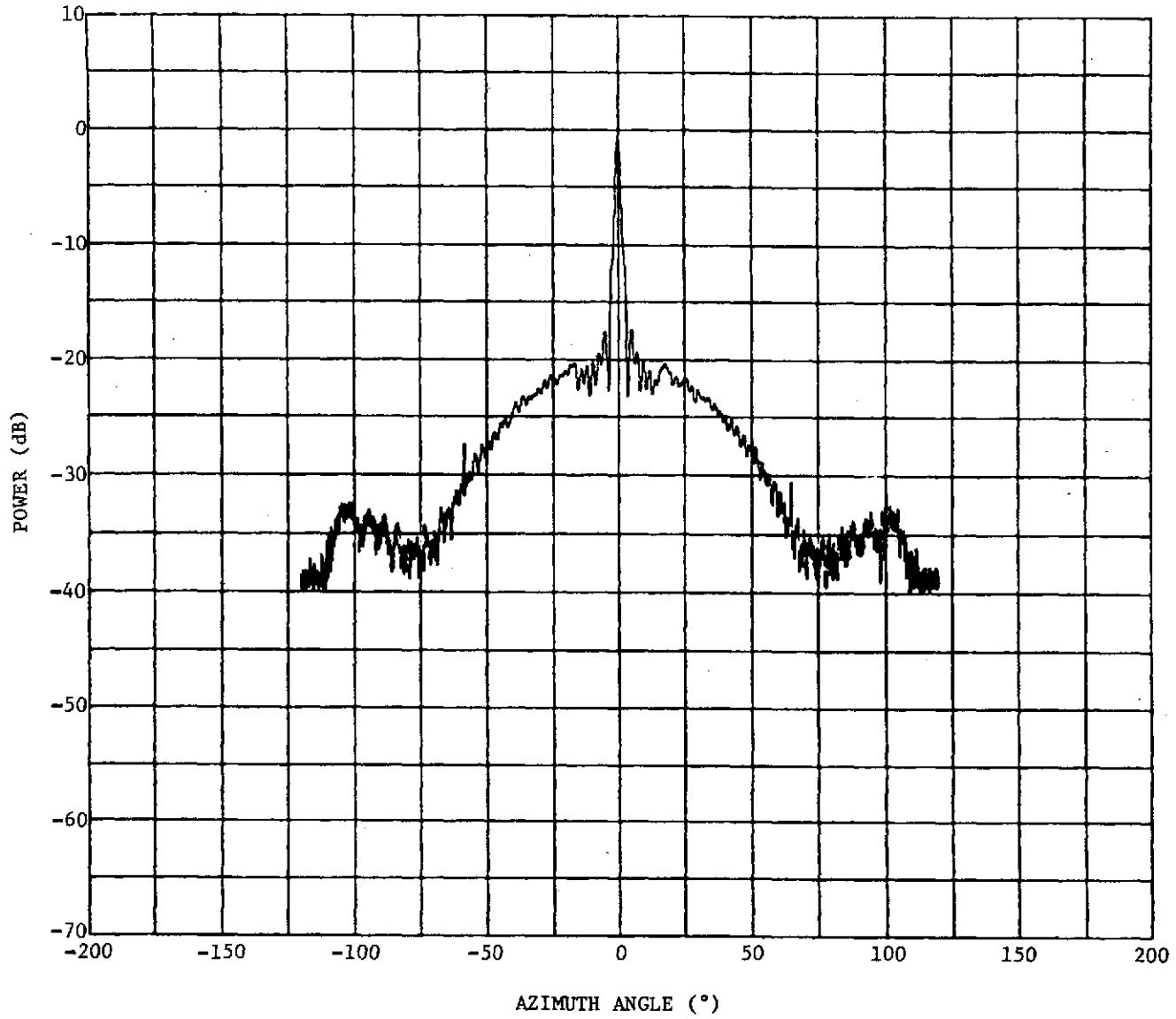
Figure 4.3-4 E-Plane Cut, JSC Feed Cup Off

ANGLE (°)

6° Division
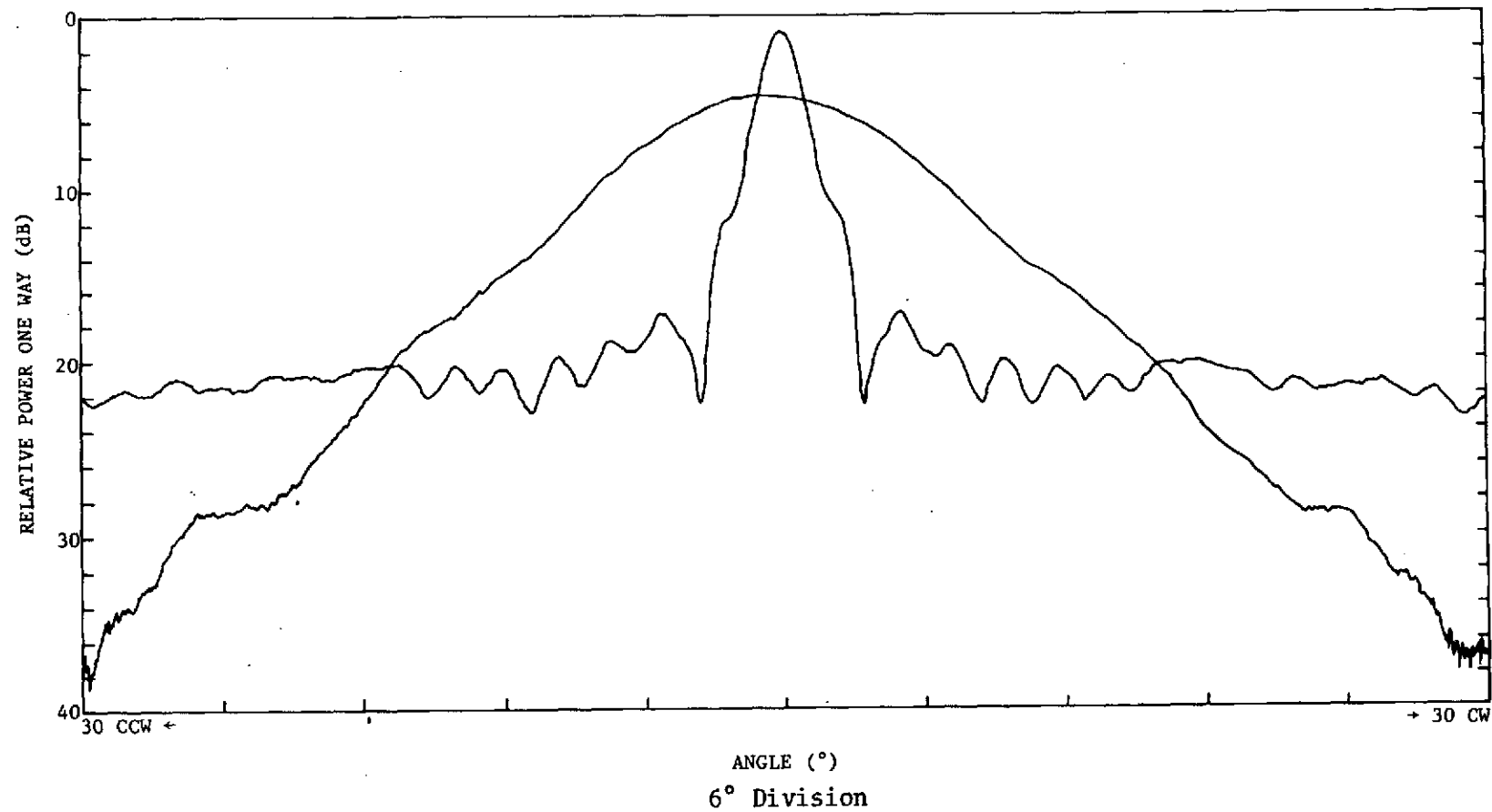
Figure 4.3-5 H-Plane Cut, JSC Comparison with Standard-Gain Horn, Feed Cup Removed

ANGLE (°)

6° Division
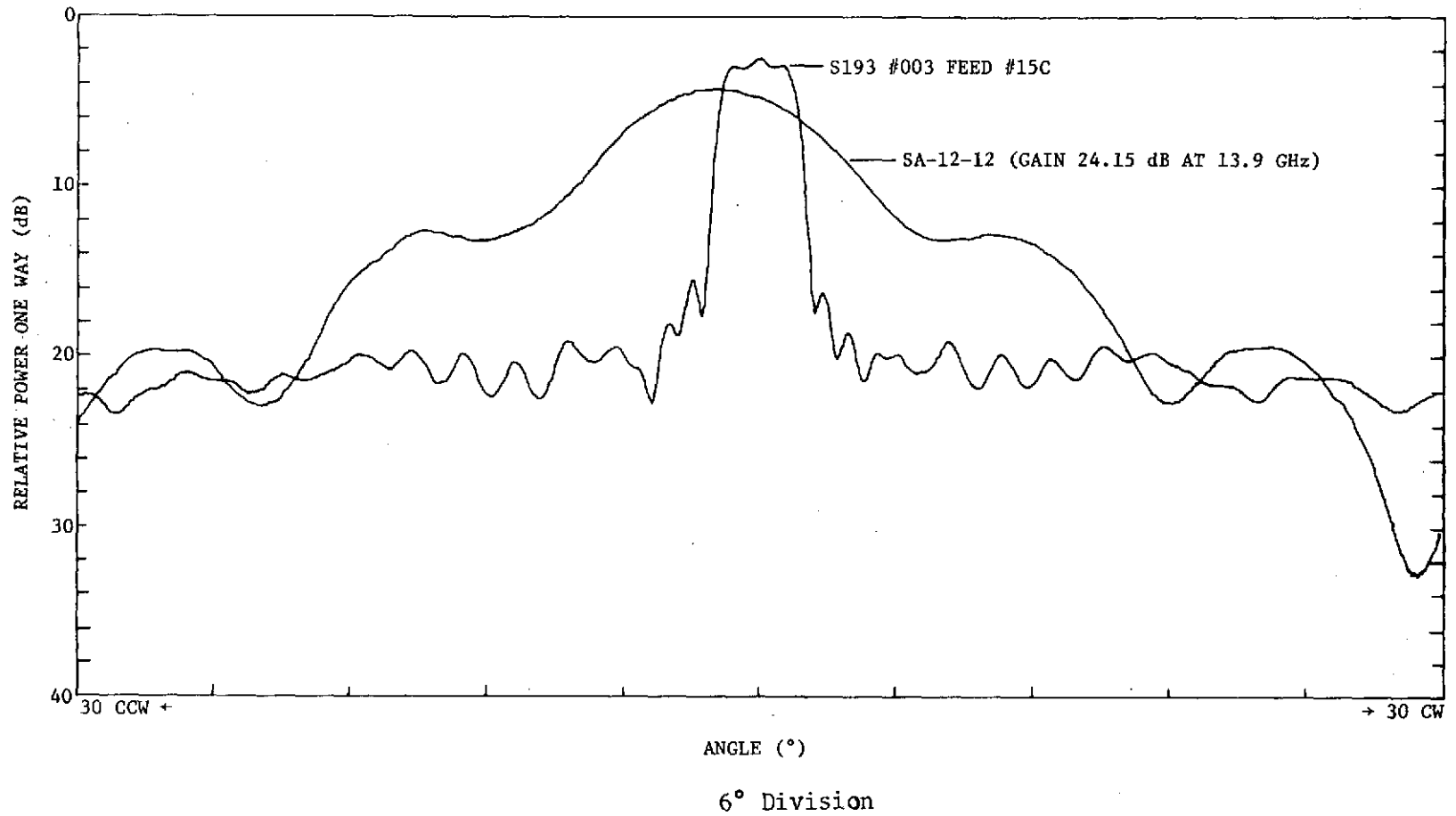
Figure 4.3-6 E-Plane Cut, JSC Comparison with Standard Gain Horn, Feed Cup Removed

were also cut at JSC with the feed cup removed. In this case,
the main beam was widened somewhat, as shown in Figure 4.3-4
compared to 4.3-3, but the major difference is again in the
higher sidelobes.

Gain measurements were taken on the antenna boresight
(pattern peak gain) by G.E. with the feed cup in place and by
JSC with the cup removed. Gain loss due to the missing feed cup
was 13.1 dB when driving the vertical port and 15.3 dB when the
horizontal port was driven (roughly comparable to the one-way gain
loss seen in the SL4 altimeter data.) (See Table 4.3-2.)
In-flight measurements with APEX had given a preliminary indication
of a gain loss on the order of 12 dB. The JSC cuts were taken
every 22.5 degrees, rotating the antenna for each cut around the
boresight axis of the antenna so that each cut ran through the
peak gain point on the antenna. G.E. cuts were taken in azimuth
for various elevation angles in elevation steps of 0.1 degree.
In both antenna tests, cross-polarization plots and dominant-
polarization plots were developed. Both vertical and horizontal
ports were driven. Complete patterns are given in the reports
cited.

Table 4.3-2 Antenna Peak Gain with and without Feed Cup

	G.E. (w feed cup) (dB)	JSC (w/o feed cup) (dB)	Gain Loss in SL4 (dB)
Vertical Feed	41.1	28.0	13.1
Horizontal Feed	41.3	26.0	15.3

4.4 Beam Incidence Angle Determination from Returned-
Pulse Waveforms

The 100-ns pulse was the favored pulse length for use in
determining beam incidence angle. Because the amplitude of the
short and long transmitted pulse was the same, the long (100-ns)
pulse contained more energy. This resulted in a higher received
pulse amplitude for the long pulse and better discrimination
against noise because the AGC reduced the gain and suppressed
noise for larger pulse-input amplitudes. Also, the pulse shape
of the longer pulses was much less affected by sea state than
the short pulses, as discussed in Section 4.2.

As previously mentioned (See paragraph 3.8.4.), the procedure for determining beam incidence angle was to match the trailing slope of the S/H output waveform with the appropriate beam incidence-angle curve from the simulation calculations. However, when doing this, it was necessary to keep the operation of the S/H circuitry in mind. In every case, a group of either four or eight gates was used sequentially in several positions. Thus, as in the case shown in Figure 4.4-1 (pass 4, mode 1, DAS 2), eight gates were used in each of three positions. The three positions were each maintained for 20 seconds for a normal run and even longer if momentary unlocks occurred. For each gate position, the spacecraft traversed at least 82 nautical miles, or a total of 246 nautical miles to reconstruct the entire waveform. Over these distances, substantial changes could occur in spacecraft attitude or the spacecraft might move from over sea water to over land. Land reflections will generally produce waveforms quite different from the sea reflections assumed by the simulation calculations so that the over-land determination of beam incidence angle would be very difficult, if possible. Figure 4.4-1 shows a sharp break between the second and third gate positions, as evidenced by the waveform slope change. It appears as though the construction of this mean waveform resulted from the S193 measuring two different mean waveform shapes separated in time. Changes in spacecraft attitude, the most likely situation in Figure 4.4-1, or departure from uniform reflectivity patterns even over sea water distorted the waveform. Therefore, any determination of beam incidence angle from the S193 S/H waveform was only an average over a relatively long period.
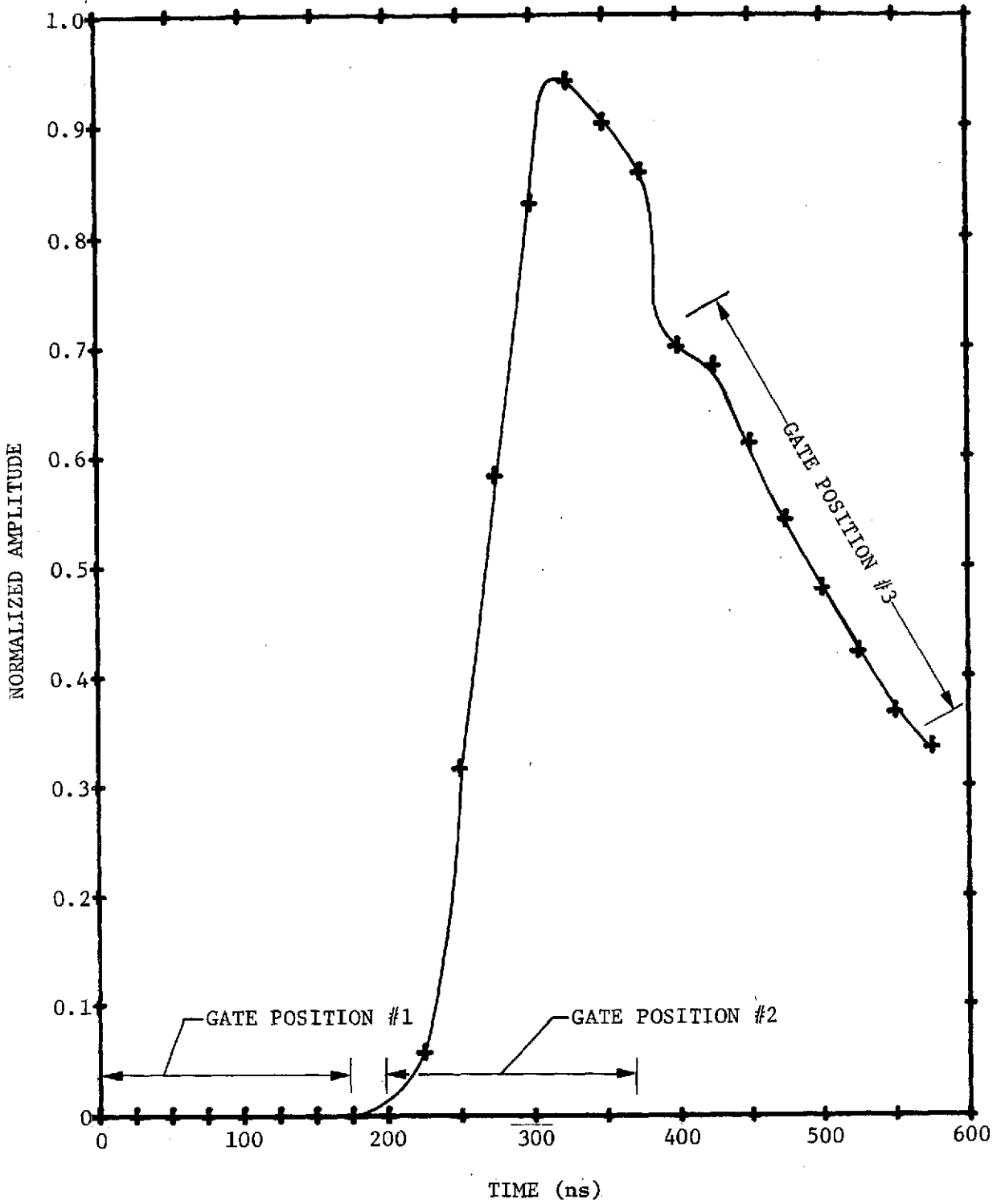
Figure 4.4-1   Waveform Distortion Caused by a Shift in Spacecraft Attitude
during a Submode

5. FINAL RESULTS

The S193 instrument was an experimental, not operational, earth resources sensor. Thus, its operation was channeled as much toward obtaining design information and demonstration of the capability of making K_u-band radar measurements from space as obtaining earth terrain measurement information.

The altimeter generally met the overall objectives successfully in four different modes, each containing a number of submodes designed to assess performance under different types of operation. Operation with short, long, and coded pulses (16-, 100-, and 130-ns coded) was obtained. The effects of instrument and target variations were observed on radar cross-section, return-pulse shape, sea-state, altitude, and attitude measurements. In a few cases, radar malfunctions and less-than-desired spacecraft attitude stability prevented obtaining the desired quality or quantity of data. However, even in these cases in which operation was not normal, a careful observation of performance versus operation conditions led to useful conclusions.

The sensor performance evaluation was aimed at in-flight verification of the operational status of the sensor. This was handicapped by delays in the data processing, which required more hand evaluation than desired and by lack of supporting ground truth and aircraft data. Thus, the evaluation was not as complete as might have been accomplished.* However, many instrument performance capabilities were identified, as presented in Section 6, and many hardware parameters were evaluated. A tabulation of some of the pertinent parameters is given in Table 5-1. In addition, several data-processing and instrument anomalies were discovered through the performance evaluation. A summary of the malfunctions and operational performance results is given below.

The first malfunction that occurred was the lack of compression (decoding) of the 130-ns Barker coded pulse. This condition lasted through all passes of SL2 and until near the end of SL3. The pulses were decoded properly for the remaining few passes of SL3 and throughout SL4. Data taken during the

---

* Also see WFC sensor technology final report to be published in the spring of 1975.

period in which decoding was not taking place could be processed
like a long uncoded pulse if the proper correction factors were
employed for radar cross-section and attitude.

During pass 40 (SL3), a short developed in a gimbal
feedback potentiometer, and pitch and roll control was erratic
until the pitch gimbal was pinned at 0.0 degrees early in SL4.
Also, the roll gimbal readings were at a misleading 59.7 degrees
during all nadir align modes and for various other modes
during the three missions, as explained in MSC-05528, Volume 5.
Nadir align modes were successful during all attempts before
the erratic gimbal operation during SL3. Successful operation
of the nadir align mode was defined as positioning the antenna
gimbals so that the antenna beam incidence angle was less than
0.75 degrees at the end of the mode. (During periods in which
altitude stability was not accurately held, the beam incidence
angle often exceeded this value.)

A third malfunction was the loss of approximately 24 dB
(possibly as much as 30 dB) of antenna gain (12-dB transmit
plus 12-dB receive), which existed throughout SL4.
This caused all short pulse submodes to abort because of the low
signal-to-noise ratio. The longer-pulse submodes, including
the Barker coded submode of mode 5, continued to operate
successfully during SL4 because of the higher energy content
in these pulses.

Simulations and performance data show that operation of
the altimeter was degraded when the beam incidence angle
exceeded about one-fourth of the beamwidth. Good alignment was
consistently obtained for only part of SL2 and for part of SL3
after changing the gyro six-pack.

Table 5-1 Performance Specifications

Parameter	Value	Note	Reference paragraph of MSC-05528, Vol V
TRANSMITTER			
Frequency	13.9 GHz	1	---
Peak power (tube output)	1.26 kW	1,2,3	3.4.4
Pulse widths	16 - 18 ns	2,5	8.2
(dependent on submode)	100 ns	2,4,5	8.2
	130 ns	2,5	8.1
Pulse repetition rate	250 pps	1	---
Pulse decorrelation time	~ 111 μs	2,6	11.1.5
ANTENNA			
Type	Parabolic dish, mechanically scanned	---	4.0
Half-power beamwidth	1.5° E plane for SL2,3	1	---
	2.0° H plane for SL2,3	1	---
	2.7° E plane for SL4	7	---
	2.0° H plane for SL4	7	---
Gain	~ 41.2 dBi for SL2,3	1	---
	~ 27 dBi for SL4	7	---
RECEIVER			
IF frequency	350.3 MHz	1	7.1
IF bandwidth	12.5 MHz	1	7.1
(dependent on submode)	115.1 MHz	1	7.1
Signal-to-noise ratio (typical)	20 - 30 dB over sea targets for SL2,3, with 100-MHz 100-ns conditions	2	11.2.5
AGC calibration	Readable to ±1.0 dB	1,8	---
PULSE COMPRESSION			
Type	Binary phase code	---	8.1
Code	13-bit Barker	---	8.1
Uncompressed pulsewidth	~ 130 ns	2	8.1
Compressed pulsewidth	~ 20 ns	2,5	8.1
ALTITUDE PROCESSOR			
Type	Digital using split gate tracker	---	11.1.2.2
Loop bandwidth	2 Hz	1	11.1.2.2
Acquisition time	<6 s	1	---
Quantization	5.0 ns internal	1	11.1.3
	2.5 ns on readout	1	
Average quantization error	0.72 ns	2	6.5.3
Tracker jitter	<22 ns	2	6.5.3
Altitude data precision	<1 m	2,6	6.4
Altitude absolute accuracy	<±38 m	2,9	6.3
Altitude relative accuracy	<±1.3 m	2,9	6.0
WAVEFORM SAMPLING PROCESSOR			
Number of S/H gates	8	---	3.5
Sample gate widths	10 ns	1,10	3.5
	25 ns		
Gate spacing	10 ns	1,10	3.5
	25 ns		
NADIR ALIGNMENT			
S193 seeker	<±0.75°	2	10.1
Skylab attitude (variable pass to pass)	<±1.0°	2.11	10.5
INTERNAL HOUSEKEEPING VALUES			
All values within tolerances except:			
A053-293, antenna feed temperature	Too high in late SL4	2	3.3.4
A054-293, input waveguide temperature	Too high in late SL4	2	3.3.4
A056-293, driver TWTA temperature	Too high in late SL4	2	3.3,4

NOTES: See next page.

Table 5-1 (concluded)

NOTES:

1. Measured before flight

2. Measured in flight

3. Measured at input to antenna

4. Measured 95 ns for mode 1, DAS-1, and 82 ns for mode 5, DAS-1
    in flight at 50% amplitude

5. One-half amplitude pulse width from CDS S/H outputs

6. Over "smooth" sea targets

7. Measured after flight

8. See paragraph 6.3 of the GE calibration data report*; AGC
    highly dependent on average return pulse shape.

9. Data with good aspect angle were as good or better than the
    ability to evaluate it.

10. Output waveforms were shown to be affected by receiver
    characteristics and sea surface.

11. Beam incidence angle determined from S/H pulse-shape readout
    for angles from 0.25 to 0.75°.

---

* S193 Historical Logbook, S193 Vehicle 001, Vol 1A, Document
  No. 72 SD4234 Rev. A, 27 October 1972, General Electric
  Company.

  Alternate Designation: S193 Calibration Data Report, Flight
  Hardware, Doc. No. 72 SD4207 Rev. D, 22 March 1973, Prime
  Unit 1A Volume 1A, SSO Contract NAS9-11195, General Electric.

6. CONCLUSIONS

The S193 altimeter was the first of a series of planned
satellite altimeters. Thus, the experiment was designed to
evaluate specific hardware design parameters for future
application. In addition to providing a hardware capability
demonstration and useful design information, the S193 has
yielded valuable scientific information. Several papers have
already been published demonstrating the significant altimetry
and geodetic data, and several others are being prepared. The
objectives of the mission were essentially met in that conclusions
can be drawn with respect to the performance of an altimeter
under the restrictions imposed by the design of the S193
altimeter and its various modes and submodes. The conclusions
are stated in the following paragraphs.

The longer pulse operation provided a better indication of
altitude because of the increased energy content. Reflection
from the sea surface caused the shape of the returned shorter
pulse to be nearly the same as that of the long pulse (except
for a shorter rise time on the short pulse) as expected for the
beam-limited operation of the S193. However, the amplitude of
the returned long pulse was greater by approximately the ratio
of the transmitted pulse lengths.

The beam incidence angle was best determined by observation
of the fall time on the long pulse up to angles large enough to
cause an increase in pulse rise time. (This occurs at greater
than about one-half the antenna beamwidth.)

Verification that the antenna pointing, a significant
variable in all of the data utilizations, could be determined
from the altimeter data itself without reliance on the vehicle
attitude readouts was one of the significant conclusions from
the S193 evaluation program. The deviation of the pointing
relative to the vehicle flight line may also be available from
the pulse-to-pulse correlation data. However, this is still
under study.

Altitude could be determined by the altimeter to precision approaching 1 meter for special situations. Accuracy of this measurement was not affected by the beam incidence angle until this angle exceeded about one-quarter beamwidth, but correction curves were effective up to about one beamwidth. The conditions under which the 1-meter accuracy could be obtained were a spacecraft attitude stability good enough to hold the beam to within one-quarter beamwidth of the vertical, slowly rolling or flat terrain or sea water with smooth to moderate seas, and good signal-to-noise ratio. In the cases shown in the sensor performance evaluation report (MSC-05528, Volume V) for typical "moderate" terrain, correlations of the S193 radar relative altitude data with topographic terrain heights averaged over the beam illuminated area were obtained to within tens of meters. Over very rough mountainous terrain, and often at sea-to-land interfaces, a measurement could not be made because of the tracker unlocks.

The absolute altitude accuracy of the S193 was never a preflight specification. However, the accuracy appeared to be as good as the means of verifying the data. Most data passes were only taken over small portions (short areas) of a complete orbit. Special short-arc computations of the Skylab orbit were used, along with geodetic models of the earth, to provide altitude comparisons. With these, it appeared at first as though an absolute altitude bias might have been present and variable from pass to pass. However, the "around-the-world" data pass late in SL4 provided data that nearly "closed" the orbit circle while still containing some bias offsets on individual short-arc sections. Thus, the model used for comparison may have been as much suspect as the altitude data.

An interesting application for altitude measurements was the conversion of these measurements into sea "topography" height contours for measurements over sea water. These contours correlated very well with geoidal measurements and bathymetrical charts. Abrupt changes in the sea floor were shown by changes in sea height contours measurable by the S193 altimeter. An idea of the degree of these correlations and the sensitivity of sea height contours to sea floor contours can be obtained by examination of the plots in MSC-05528. Volume V.*

---

* Also see the following papers:

J. T. McGoogan, et.al.; "Skylab Altimeter Applications and Scientific Experiments of Skylab," Huntsville, Alabama, AIAA Paper Number 74-1221, 30 October 1974.

J. T. McGoogan, et.al.: "The S193 Radar Altimeter Experiment", Proceedings of IEEE, Volume 62, Number 6, June 1974.

J. T. McGoogan, et.al.: "Skylab S193 Altimeter Experiment Performance Results and Applications", International Symposium on Marine Geodesy, Columbus, Ohio, June 1974.

The S193 AGC data could be converted to target radar
cross-section values to within a few decibels if corrections
were made for beam incidence angle, operating mode, AGC charac-
teristics, and altitude. Correction for beam incidence angle is
given in MSC-05528, Volume V, Section 4, for sea-water conditions.

Economy in instrument design, spectrum usage and integration
concerns resulted in the radiometer/scatterometer portion of
the S193 time-sharing operation with the altimeter. This
resulted in a reduction of the types of target samples because
operation of both the scatterometer and altimeter were desired
over some of the same targets, e.g., high wind-driven seas.
The preprogrammed altimeter operation sequences also resulted
in a scheduling requirement to adequately cover desired target
areas. However, the best scheduling was unfortunately
sometime undone by the interrupted operation resulting from
momentary "unlocks" over targets with low or widely variable
reflectivity.

The sensor was designed to include manual switching and
meter readouts by the astronauts. It was fortunate for the
S193 experiment that the astronauts were available to tend the
instrument. Examples of their assistance included reading the
gimbal position meters after the roll torquer failure in pass
79, which resulted in flying some of the last data passes with
a Skylab roll bias approximately 1 degree off nadir, visual
verification of the antenna position after the gimbal
potentiometer short during SL3, physical repair of the S193
antenna gimbal problems at the start of SL4, which permitted
operation during SL4, and maintenance of the tape recorder.
All of these operations contributed to the excellent quality
of data recorded.

The sensor performance evaluations were hindered by the
problems and delays in the postflight data processing of the
flight data. Most of these problems were overcome by the
parallel use of previously developed programs from system
integration testing. However, one item that could not be
overcome in the in-flight evaluation was the limited availability
of supporting ground truth or aircraft data. This shortage was
partially compensated with increased use of deep-space and
computer-model simulations. There was also a definite need
for better preflight antenna pattern information because it
proved difficult to adequately obtain in-flight. Postflight
reevaluation of the antennas using the backup antennas was
required.

The in-flight evaluation was successful in evaluating
many of the performance characteristics of the S193, as
indicated in Section 5. However, in doing so, many computer
models of the sensor or its subsections had to be developed
as a basis for comparison. Verification of these models was
only partially accomplished with preflight system testing data.
End-to-end "bench" system testing in parallel with simulation
model development would have been desirable, even though a high
confidence in the computer models was obtained in the postflight
data review.

7. RECOMMENDATIONS

The S193 altimeter was a multipurpose sensor designed to study various parameters such as pulse length, sampling interval, receiver bandwidth, and pulse spacing with respect to several applications. An optimum design for any particular application would require a given set of parameter values. Experience gained from studies involving an analysis of Skylab data, a study of simulation results, and observation of ground truth data leads to the following design recommendations for specific applications.

A short pulse of less than 16 ns is recommended for sea-state measurements to permit the use of the slope of the leading edge of the pulse to measure wave height. A pulse length on the order of 5 to 10 ns, with a proportionally higher peak amplitude (to preserve the pulse shape measurement capability), is recommended. Sampling interval would also have to be reduced proportionately to permit accurate pulse rise-time determination. A closer spacing of the sample-and-hold gates relative to the pulse shape than that used for S193 is recommended.

Flight-vehicle attitudes should be held to within approximately one fourth of the antenna beamwidth, so that no correction is required for either the radar cross-section or altitude evaluations. When this is not possible, an accurate on-board determination of spacecraft attitude would be desirable. Narrowing the antenna beamwidth would be desirable because it increases antenna gain and raises the energy content in the tracking gates because the peak of the received pulse is higher, and less energy is lost due to a long pulse trailing edge falling outside of the plateau gate. However, spacecraft attitude would have to be controlled to the one fourth beam width criteria in order to realize the improvement. Also, when this attitude criterion is met, significant pulse distortion due to the radiation returned from normal incidence can be avoided. In the Skylab experiments, unlocks occurred due to excessive

off-normal beam incidence angles. Also, pseudo-oscillations in altitude were observed that show up in the sea profiles as a result of spacecraft attitude variations.

Resolution of the altitude measurements can be improved by the use of shorter pulses, but consequently, the pulse energy must be maintained to ensure an adequate signal-to-noise ratio, and the IF bandwidths and gate widths must be adjusted for best results. It is also recommended that the gap between the two gates be narrowed or eliminated to avoid loss of the energy that falls in the gap. The S193 tracker was not adjusted to use the potential tracking improvement of the narrower pulses.

It is not recommended that any attempt be made to substantially improve resolution over rough terrain, due to anticipated problems with tracker following. It would be necessary to greatly increase tracking rate and substantially reduce the antenna beamwidth so that the tracker "sees" a stable attitude at any given time. Otherwise tracker hunting and increased loss of tracker locks would be experienced, as was seen over rough terrain during the Skylab flights. Terrain profile measurement is sufficiently complicated that a very complete simulation of the altimeter system is recommended, including typical terrain profiles, before future designs are attempted.

Improvements in resolution will probably be achievable (as desired for geoid measurements) for smooth seas where altitude changes slowly, allowing longer tracker measurement times (narrower tracker bandwidths).

The S193 AGC output has produced very usable backscatter values for the terrain measured. However, it is recommended that the precision scatterometer operation be planned in future altimeters. Investigations have shown that both pulse shape and backscatter values correlate with sea-state data.

Complete error analyses for the S193 altimeter have not been accomplished. It is recommended that future programs complete an error analysis investigation after acceptance testing and before launch. Verification of it can then be realized in the postflight analysis. While there were many useful computer models before the Skylab missions, several had to be generated during and after the mission to simulate the total S193 system. A high confidence level in the computer model simulations was established by users and evaluators. However, a complete computer modeling that incorporates the necessary subsystem and component parameters should be developed in parallel with the acceptance and system testing of the sensor hardware so that all parameters can be evaluated against the flight hardware during simulation model development.

For program expediency and cost, much of the system integration testing was limited to verification of performance continuity based on limited acceptance tests. In retrospect, opportunities were lost that could have been used for verification of calibration data and computer programs to be used for postflight data reduction and sensor performance evaluation.

There was a limited down-link capability for special data dumps from the instrument. This was used in the anomaly investigations. However, the primary mode of data transfer was by recording on magnetic tape, with subsequent return to earth by the astronauts. Any practical increase in down-link capability is recommended to support data quality and performance anomaly investigations.

8. NOTES

8.1 Acknowledgements

The effort covered by this report was sponsored by the Lyndon B. Johnson Space Center Earth Resources Program Office. It is based on the results of a concerted effort by numerous individuals within NASA, industry, and academic organizations. These results primarily reflect the contributions of NASA Wallops Flight Center in addition to those of the Martin Marietta Corporation.

Particular acknowledgement is due the late Mr. Charles K. Williams of the Skylab Program Office at JSC for his conception and implementation of the EREP sensor performance evaluation. His dedication and leadership were essential to the successful completion of these evaluation studies.

Acknowledgement is also made of the assistance of R. Eisenberg of the General Electric Space Systems Organization and E. L. Hofmeister of General Electric, Utica, New York, with sensor design and calibration.

This volume of the final report was prepared by R. J. Plugge, P. Norris, W. B. Cox, and D. Lamarque.

8.2 Abbreviations

Abbreviations in common usage have been used for English units of measure. International units (SI) have been abbreviated in accordance with E. A. Mechtly's NASA SP-7012, The International System of Units, 2nd Rev, National Aeronautics and Space Administration, Washington, D.C., 1973--except for steradian, which has been abbreviated to ster.

ADAS	Advanced Data Acquisition System
AGC	Automatic Gain Control
Alt	Altimeter
APEX	Antenna pattern exercise
BW	Bandwidth
Cal(s)	Calibration(s)
CDC	Control Data Computer
CDS	Calibration Data Submode (or Step)

C&D	Control and Display
DAS	Data Acquisition Submode
EMI	Electromagmetic interference
EREP	Earth Resources Experiment Package
GE	General Electric
GMT	Greenwich Mean Time
H	Horizontal
h_o	True altitude
IF	Intermediate frequency
JSC	Johnson Space Center
KU	University of Kansas
KSC	Kennedy Space Center
MSC	Manned Spacecraft Center
NASA	National Aeronautics and Space Administration
OOA	On orbit alignment
PCA	Point of closest approach
PCM	Pulse code modulation
PCN	Pulse compression network
PRF	Pulse repetition frequency
$P(\theta)$	Antenna pattern
R, RAD, Rad	Radiometer, radiometer output data
RCS	Radar cross-section
RF	Radio frequency
RFI	Radio frequency interference
R/S	Radiometer/scatterometer
Scat	Scatterometer
S/H	Sample & hold
SL	Sidelobe, Skylab
SPE	Sensor performance evaluation
STAPE	Surface Test for Altimeter Performance Evaluation

TWT	Traveling wave tube
V	Vertical
WFC	Wallops Flight Center
σ	Standard deviation

APPENDIX A

TECHNIQUES ADDENDUM

This appendix describes the techniques used to evaluate S193 Altimeter performance as presented in the Sensor Performance Evaluation Report, MSC-05528, Volume V, dated September 6, 1974. These descriptions of the techniques include both the theoretical approach and the mechanics of application.

I. USE OF A GROUND-BASED RECEIVER TO DETERMINE ALTIMETER PULSE
   CHARACTERISTICS

   The altimeter data output consisted largely of pulse shape
information from the sample-and-hold-gate digital measurements of
both the altimeter transmitted and received echo return pulses.
On-board pulse-shape measurements were undersampled and the subject
of some concern. Because pulse shape data may provide a good sea
state measurement, an alternative evaluation of the shape of the
radiated pulse as received at the earth surface was desired. The
technique used to determine altimeter pulse-shape characteristics
involved a test set up referred to as STAPE (surface test for
altimeter performance evaluation) and had multiple uses and setup
variations. A general summary is given below. Also refer to
MSC-05528, Volume IV, paragraph 5.1.2; MSC-05528, Volume V,
paragraphs 8.2.1 and 11.1.4.2; paragraph 3.3, Appendix A, Sections
III and V of Volume IV of this report; and Section 4 of this
volume for additional discussions of the STAPE setup.

   A. Concept

   STAPE used three distinct configurations to measure different
characteristics of the S193. These configurations are shown in
figures A.I-1, A.I-2, and A.I-3. The first was to measure the
antenna pattern, altimeter or scatterometer pulse shape and pulse
repetition frequency, and RF frequency. The second was used to
retransmit the encoded pulse from S193 to supplement internal
calibration evaluation of the pulse compression network operation
in flight. The third configuration was intended for use in
transmitting a known power-level pulse to the S193 to evaluate
the response of the instrument AGC.

   In general, the STAPE setup used wideband preamplifiers to
provide the detectors with an amplified pulse received from S193
in both the horizontal and vertical polarizations. To increase
system gain, the pulses were received and transmitted through a
steerable 60-foot parabolic dish antenna from the Advanced Data
Acquisition System (ADAS) at NASA's Wallops Flight Center (WFC).
The detected pulse was displayed on a wideband oscilloscope that
limited the system bandwidth to approximate 250 MHz, which was
sufficient for recording the 100- and 130-ns pulses. There was
no desire or attempt to record the 18-ns pulses from S193. The
displayed pulses were then photographed by a high-speed "framing"
camera. To stabilize the amplitude of the pulse display and
record the input pulse power, receiver gain was controlled by a
digital attenuator and a meter measuring peak pulse power, which
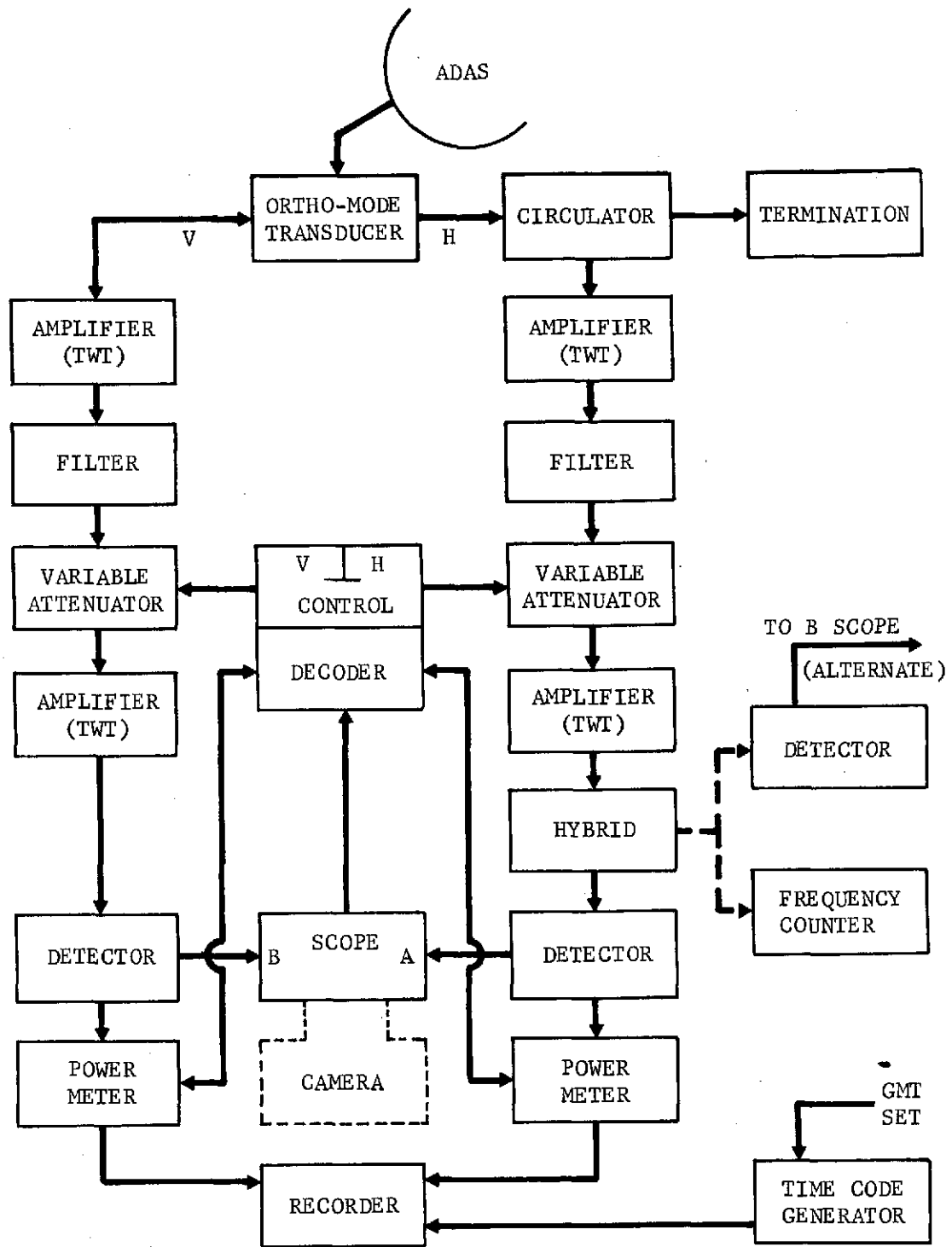
Figure A.I-1   STAPE Test Set Configuration for S193 Altimeter Antenn
                Pattern, Pulse Shape and PRF, and Frequency Tests
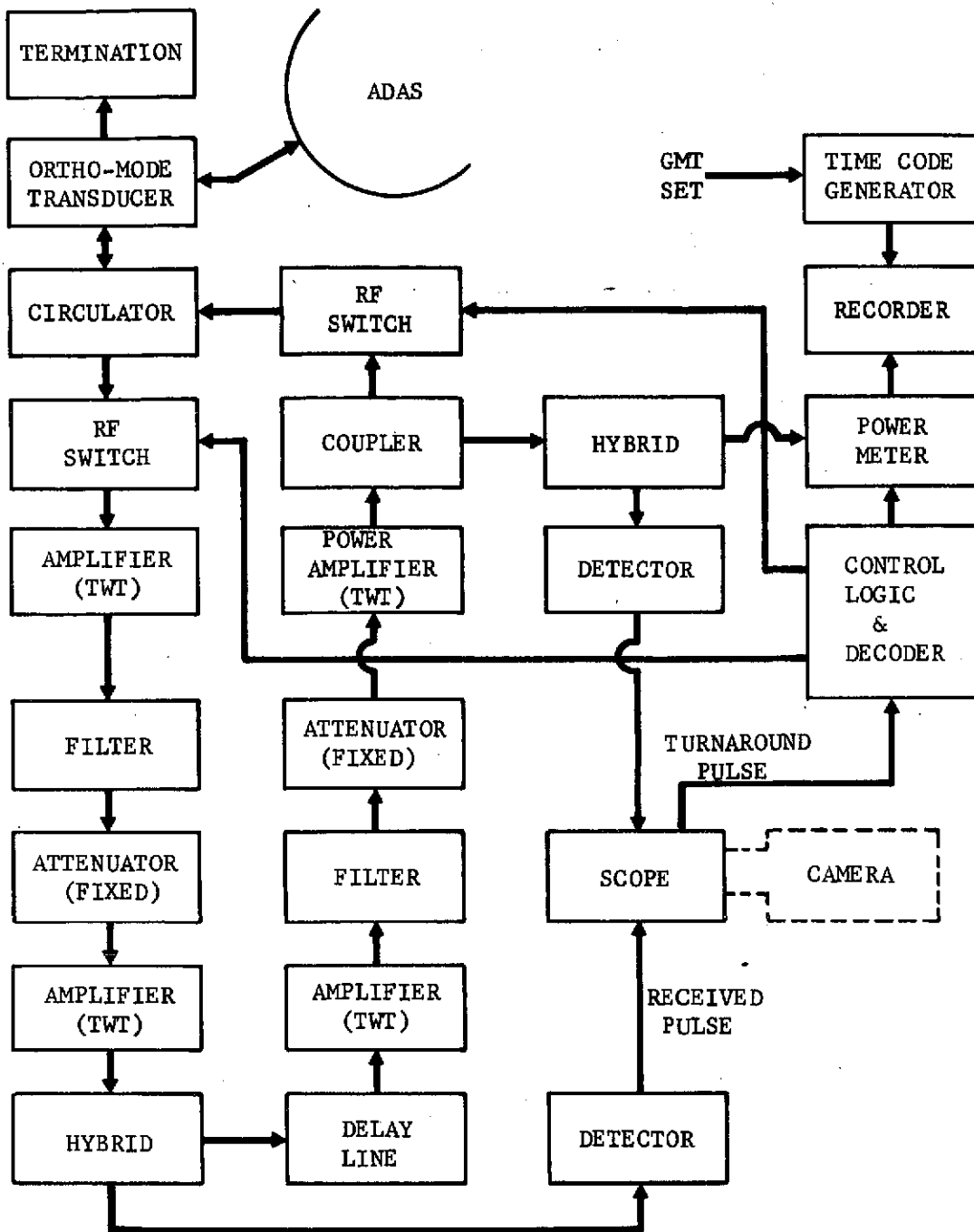
Figure A.I-2 STAPE Test Set Configuration for S193 Altimeter
Pulse Compression Network (PCN) Test
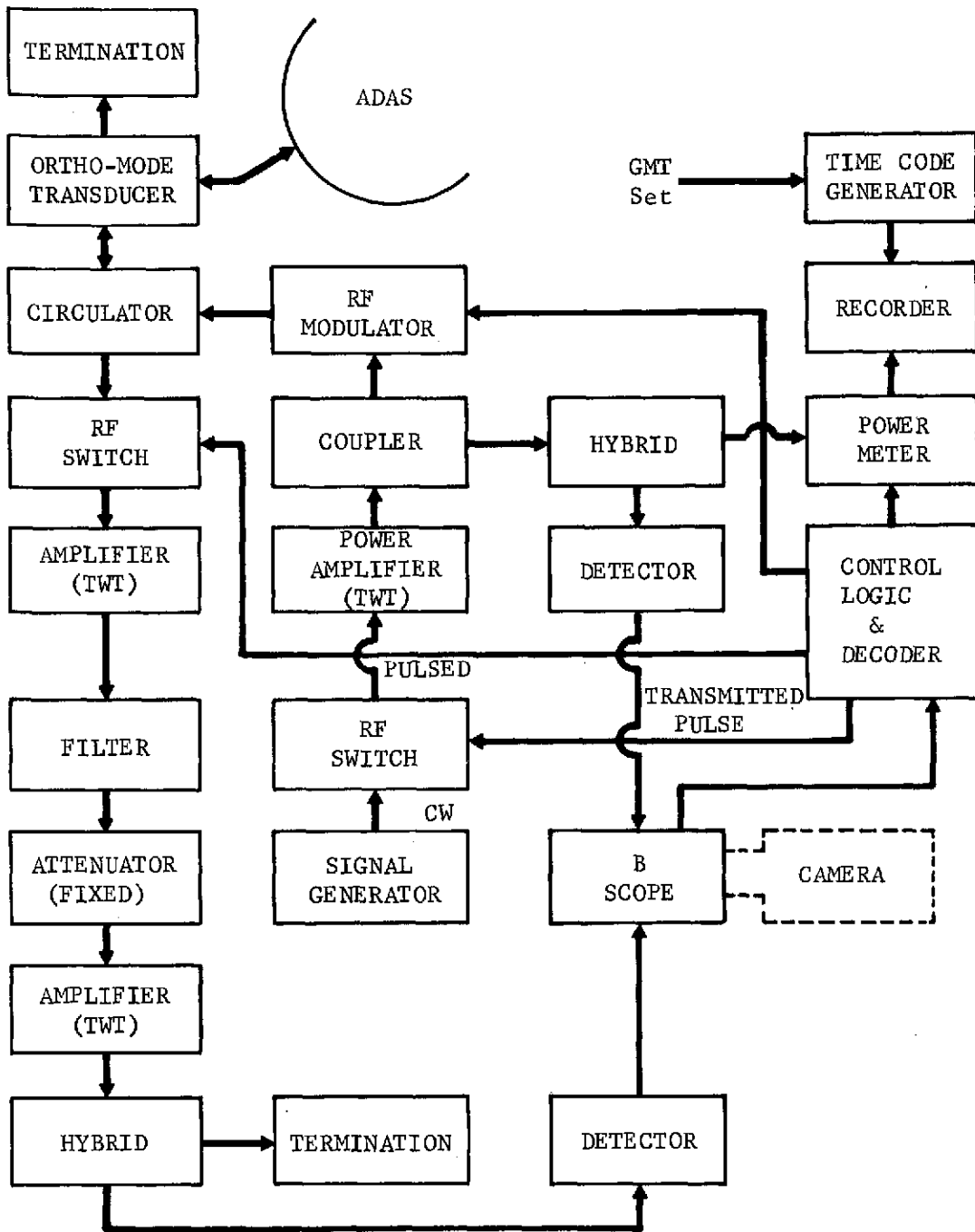
Figure A.I-3   STAPE Test Set Configuration for S193 Altimeter AGC Test
             and Pulse Shape Test

was sampled for each pulse to set the attenuation for the succeeding pulse. The attenuator setting plus a digital readout of the power-meter measurement for each pulse peak power was recorded on magnetic tape. A parallel tape channel recorded an IRIG time code. Thus, both the shape and absolute peak amplitude for each pulse are recorded versus time. Power versus time can be converted to antenna pattern beamwidth by considering Skylab velocity.

The received pulse from S193 was also used for retransmitting to the S193 from the STAPE system. To accomplish this, two setups were used. The first used the received pulse to trigger the transmission of a long fixed-power output pulse, timed for receipt in the S193 AGC gates. The second used an amplifier, delay line, and RF switch to retransmit an amplified encoded pulse received from S193. The encoded pulse retransmitted to S193 was timed to be received in the tracker gates of S193 and provide a calibration pulse to the data acquisition submode using the pulse-compression network. The amplitude of this transmitted pulse thus depended on the received signal amplitude from S193 for received signal levels below the saturation level of the STAPE receiver.

The system was calibrated both before and after data takes and by recorded oscilloscope time ticks. Separate antenna pattern measurements were made before system installation to calibrate the 60-foot dish with the feed specifically designed for use with STAPE.

System-operation design levels and the conceptual goals for STAPE required near-overhead passes of Skylab. Antenna pattern cuts recorded on the ground by STAPE in overhead passes could have been considerably simpler to interpret than those from APEX (See MSC-05546, Appendix A, Section III of this volume) because the S193 antenna was not scanned in the altimeter modes but was used in fixed orientations relative to Skylab. Also, to assist in alignment of the antenna pattern cuts, the S190A camera took time-tagged photos of WFC. Because the location of STAPE was visible in the photos and the S190A mounting alignment was accurately known, vehicle attitude during the S193 pattern-cut measurements could be obtained.

STAPE was used to record pulse shapes and determine that the S193 altimeter transmitter was operating. Orbit changes and failure of the PCN network to operate during SL2 and SL3 caused deletion of many preflight objectives. A pointing problem identified after the first data take was partially avoided by

changing the steering control of the ground antenna from an active radar master control to use of an S-band auto-track built into the STAPE antenna system. The auto-track system tracked the S-band transmitters on Skylab during the data passes. The wider beamwidth of the S-band system (compared to the STAPE K_u band using the same dish) still caused the hunting antenna pointing to modulate the incoming K_u band power levels. STAPE was designed to be mobile and use a wide beamwidth antenna, which would have avoided the pointing and lack of direct overpass problems. However, this option was never used.

B. Goals

STAPE goals included:

1) Measure the pulse shape of the nominal 100-ns altimeter pulse with a wide-band receiver setup;

2) Record a single cut of the S193 antenna power pattern of both vertical and horizontal polarizations as the antenna passed over the receiver site;

3) Provide a pulse-compression-operation calibration pulse by retransmitting, after amplification, the encoded pulse received from S193;

4) Measure the RF using the scatterometer transmitter output;

5) Measure the PRF of the altimeter to indicate proper altimeter timing;

6) Transmit a fixed power level to S193 for a calibration point on the AGC;

7) Assist in diagnosis of failures.

C. Partial Justifications

Justifications included:

1) Provide the incident pulse shape at the earth's surface as an important variable in extracting sea-state information from the reflected pulse shapes and AGC recorded by S193;

2) Provide better pulse shape data because both internal calibration and measurements data were based on widely separated (poor shape resolution) sample and hold gates (i.e. provide analog shape data rather than undersampled digital shape data);

3) Provide antenna pattern shape and beamwidth data for the same reasons as listed for APEX (Appendix A, Section III of Volume IV) for both vertical and horizontal polarizations;

4) RF oscillator frequency had shifted slightly in system tests and though not expected to be of any consequence in flight, a ground measurement capability was still desired because frequency drift could affect scatterometer calibration;

5) Provide a wide-bandwidth ground diagnostic tool that could evaluate both scatterometer and altimeter radiated output characteristics;

6) Provide an external inflight calibration pulse for the PCN (M5DAS2) operation because the internal calibration path suffered some internal EMI or crosstalk distortion (Also see Section III of this appendix);

7) Provide a backup single receiver setup to APEX measurement of scatterometer pulse shape and timing.

D. Successes

STAPE successes included:

1) Recorded pulse shape and width for altimeter mode 1 and mode 5 nominally 100-ns pulses;

2) Assisted in verifying that the altimeter was still operable after the gimbal control failure in SL3;

3) Recorded both horizontally and vertically polarized components of the transmitted pulse power as received on the ground, pulse by pulse;

4) Through a special setup modification, the antenna pointing was shown to be properly aligned after the astronauts pinned the antenna in SL4 (See Appendix A, Section V of MSC-05546, Volume IV).

E. Problems

Problems encountered with this technique included:

1) Changes from the SL2 orbit put the SL3 and SL4 ground tracks off to the side of the STAPE site. The SL2 orbit had directly overflown the WFC site selected. Although designed to be movable to underflight locations, STAPE was not moved because APEX was being moved to underflight locations and there was a high confidence in the success of APEX;

2) Only the large off-boresite angle side-lobe beamwidths of the antenna pattern were measured due to orbit changes;

3) Only power levels of the side-lobe transmitted individual pulses were measured for both vertical and horizontal polarization, due to 1 above. The magnitude of these pulses were not correlatable to the main-beam power output;

4) The contract start date was delayed so that, even though the setup was completed considerably ahead of schedule, STAPE was not available for the SL2 mission and thus lost the beamwidth data-recording opportunity;

5) The film transport plane in the camera used for pulse recording was different for different film speeds, causing the first data recordings to be slightly defocused;

6) The poinging system used with the STAPE receiver was not precise enough to make power-level measurements. Errors generated by the variable calculation and transmission time for parallax-correction pointing commands became significant for the narrow antenna beam used (approximately 0.08-degree half-power beamwidth). The last data takes used auto-tracking on the Skylab S-band transmitter rather than tracking slaved to a radar, which resulted in considerable improvement;

7) Open breadboard layouts used in some of the rack shelves were subject to crosstalk, which partially limited the output power that could be transmitted to S193 from the STAPE location. (However, sufficient power could be transmitted to control the S193 AGC, providing the S193 antenna overflew the STAPE site.)

II. GENERATION OF ALTIMETER SYSTEM SIMULATION BASED ON BENCH
     MEASUREMENTS OF COMPONENT PARAMETERS AND SIMULATED TARGETS
     TO EVALUATE THE EFFECT ON ANTENNA PULSE SHAPE, ANTENNA
     POINTING MEASUREMENTS, RANGE TRACKER, AND S/H GATE WAVEFORM
     RECONSTRUCTION.

An analytical description of the entire altimeter system was
developed by Martin Marietta in two programs for the CDC 6500
FORTRAN IV.* The first of those programs, ALTSYS, simulated
altimeter operation in the calibration data submodes (CDS) in which
the transmitted signal bypassed the antenna system and was coupled
from the transmitter output directly to the receiver input. The
second program, ALTIM, simulated altimeter system operation in the
data acquisition submodes (DAS) in which the transmitter signal was
transmitted through the antenna system, reflected from the ground,
received by the antenna system, and processed through the receiver.
A slightly modified ALTSYS program was used as a subroutine in
ALTIM to simulate the receiver processing in this case. Two other
subroutines included in ALTIM were NORM, which determined the peak
of the average return, simulating the AGC voltage, and TRACK, which
was a static simulation of the tracker system.

A. Altimeter System Description, CDS Submodes (ALTSYS)

The purpose of the ALTSYS program was to convert any input
waveform as a function of time into a sample and hold (S/H) output
waveform as processed by the altimeter. This allowed the receiver
effects on pulse shape data to be evaluated. Figure A.II-1 is a
functional block diagram of the altimeter receiver system. Either
a 10- or 100-MHz IF receiver bandwidth was selected in a particular
submode. The IF filter, square law detector, video amplifier, and
the S/H circuitry were included in the receiver description. The
effects of tracker jitter (S/H gate motion) are discussed in MSC-
05528, Volume V, September 6, 1974, paragraph 11.1, and not included
in program calculations.

Measured data for each of the system components shown in
Figure A.II-1 were used to determine the transfer characteristics
of each block. The data that were implemented as a basis in the
program were obtained from tests of individual components at KSC
before launch.

---

* Additional analytical descriptions for at least major subassemblies
   of the altimeter were also developed by WFC, Applied Science
   Associates, and General Electric (Utica).
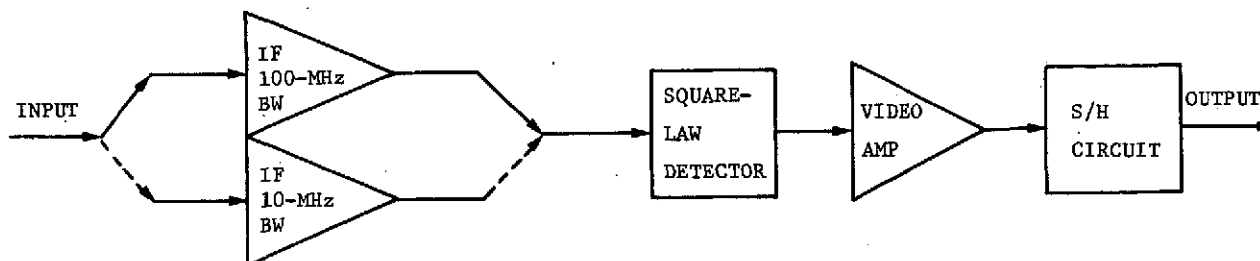
Figure A.II-1   Receiver Block Diagram for Waveform Simulation

1.   Program Description

In the program, the input waveform was transformed into the frequency domain, multiplied by the low-pass equivalent of the selected IF amplifier frequency response characteristic, and then transformed back into the time domain. The waveform was then multiplied by the detector function in the time domain. The resulting waveform was again transformed to the frequency domain, multiplied by the frequency response characteristic of the video amplifier, and transformed back into the time domain. Finally, the resulting time domain waveform was processed by a simulation of the S/H circuitry and the results outputted.

2.   Program Input

Input to the program could be any arbitrary voltage waveform as a function of time. To check out the program and compare with KSC tests, four waveforms were used:

1)   Rectangular with pulse width of 10 ns.

2)   Rectangular with pulse width of 100 ns.

3)   Barker phase coded with pulse width of 130 ns and 13 code bits of 10 ns each.

4)   Sawtooth with rise of 100 and fall of 500 ns.

These waveforms are illustrated in Figure A.II-2.
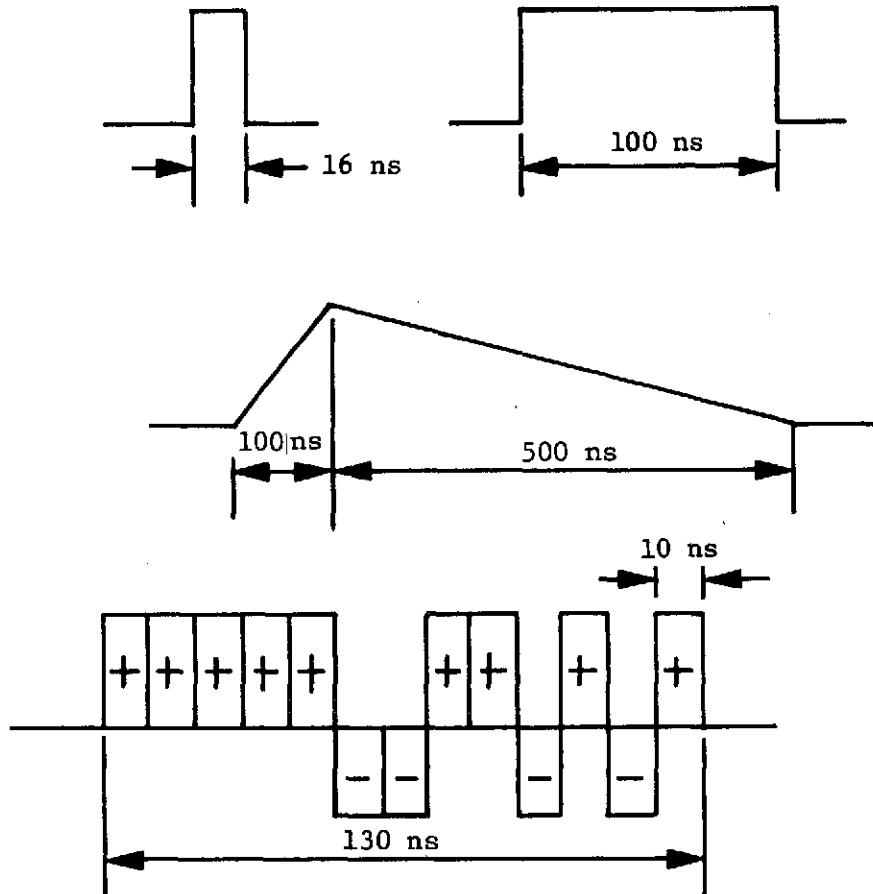
Figure A.II-2   Input Waveforms

3.   Program Outputs

Simulated waveform outputs for various combinations of input
waveforms and IF bandwidths are shown in Figures A.II-3 through
A.II-8.   Both 10- and 25-ns sample gate spacings were used, but
only 10-ns S/H spacings are shown.   The solid curve is the video
amplifier output and the squares indicate the calculated S/H
circuit outputs that are waveform voltage samples.   To show the
effect of sampling resolution on wave shape, the overall pattern
was moved in 2-ns steps and separate plots made with the gates in
positions corresponding to each step.
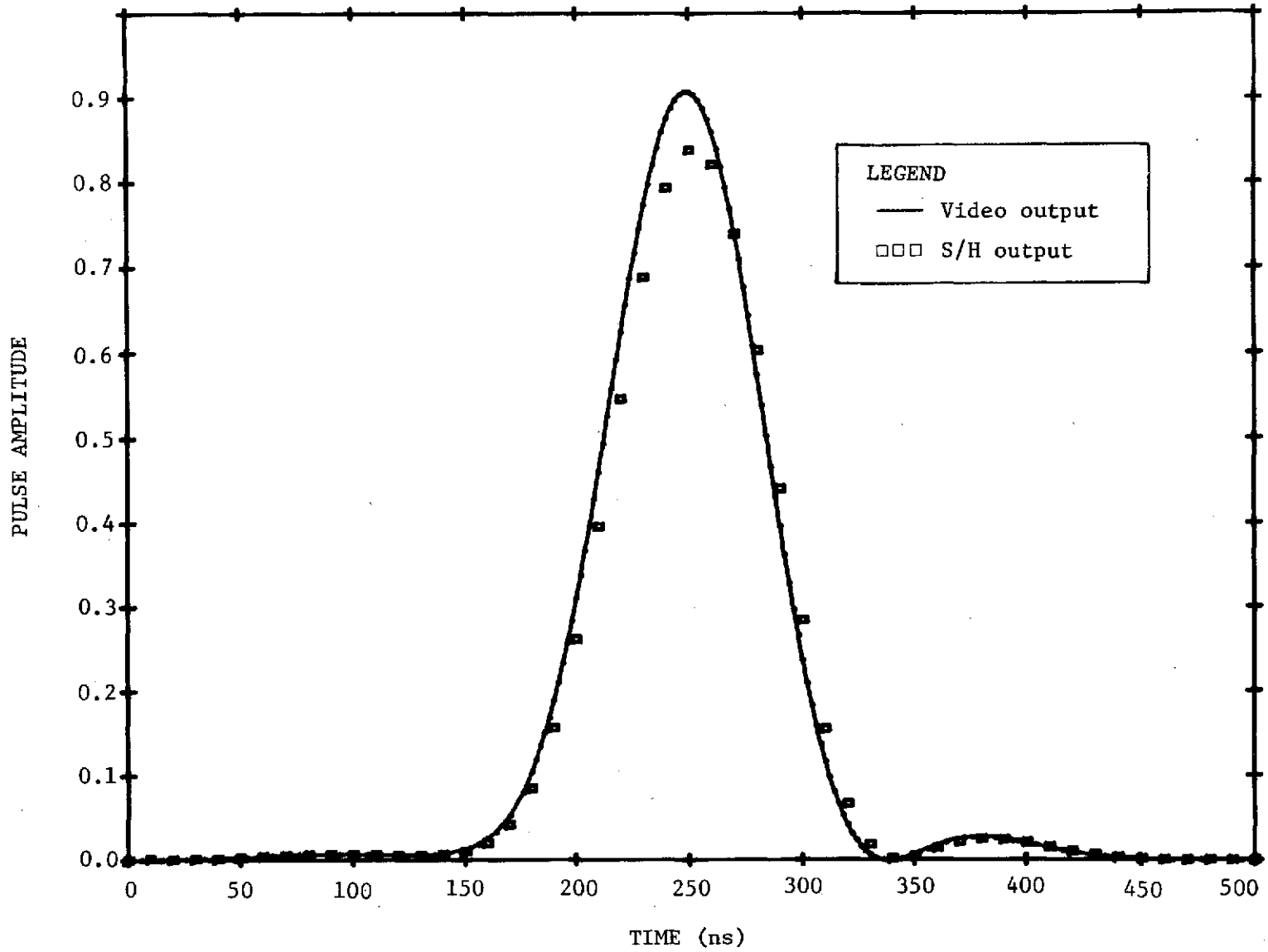
Figure A.II-3   Simulated Rectangular Pulse through Receiver (100-ns Pulse, 10-MHz BW)
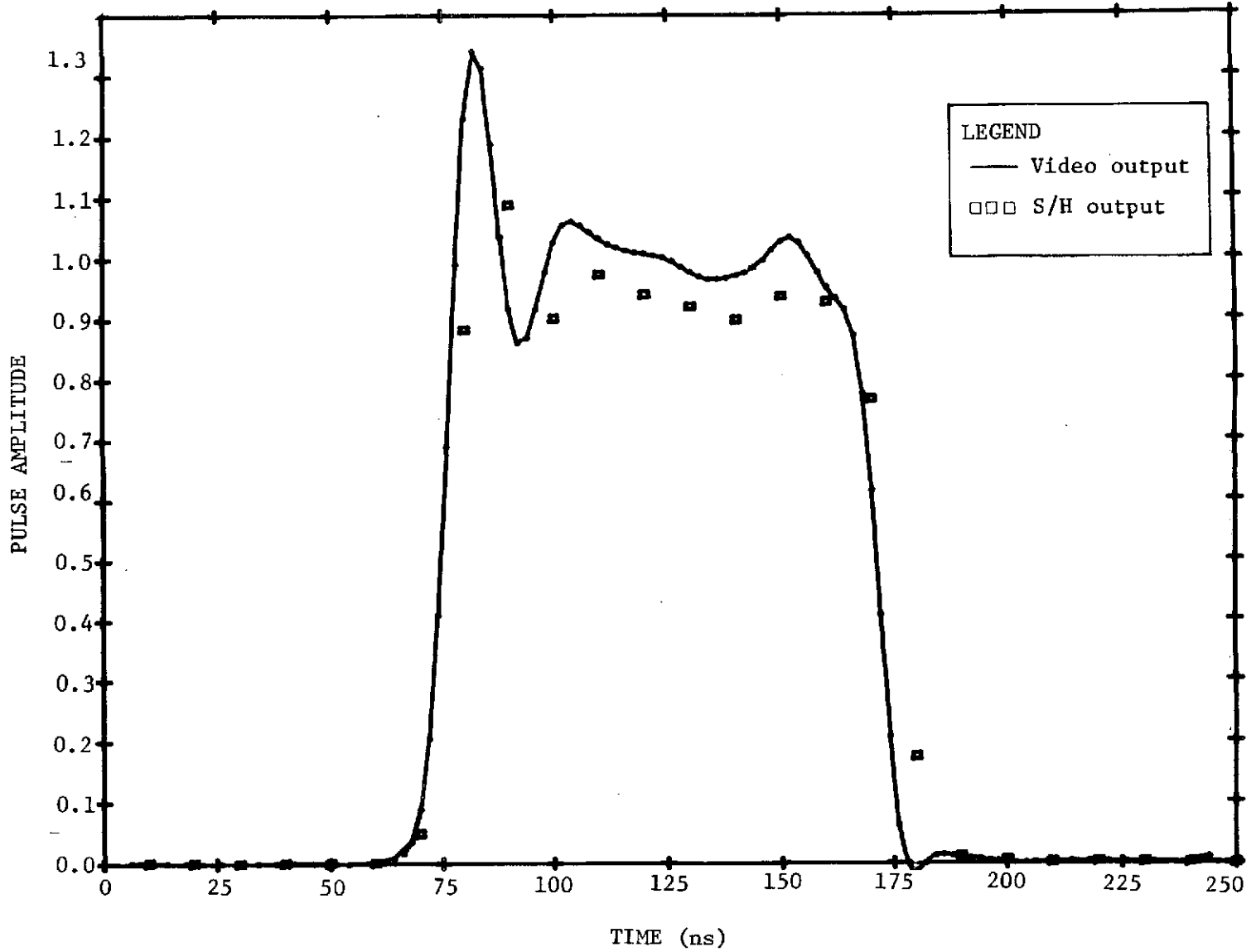
Figure A.II-4   Simulated Rectangular Pulse through Receiver(100-ns Pulse, 100-MHz BW)
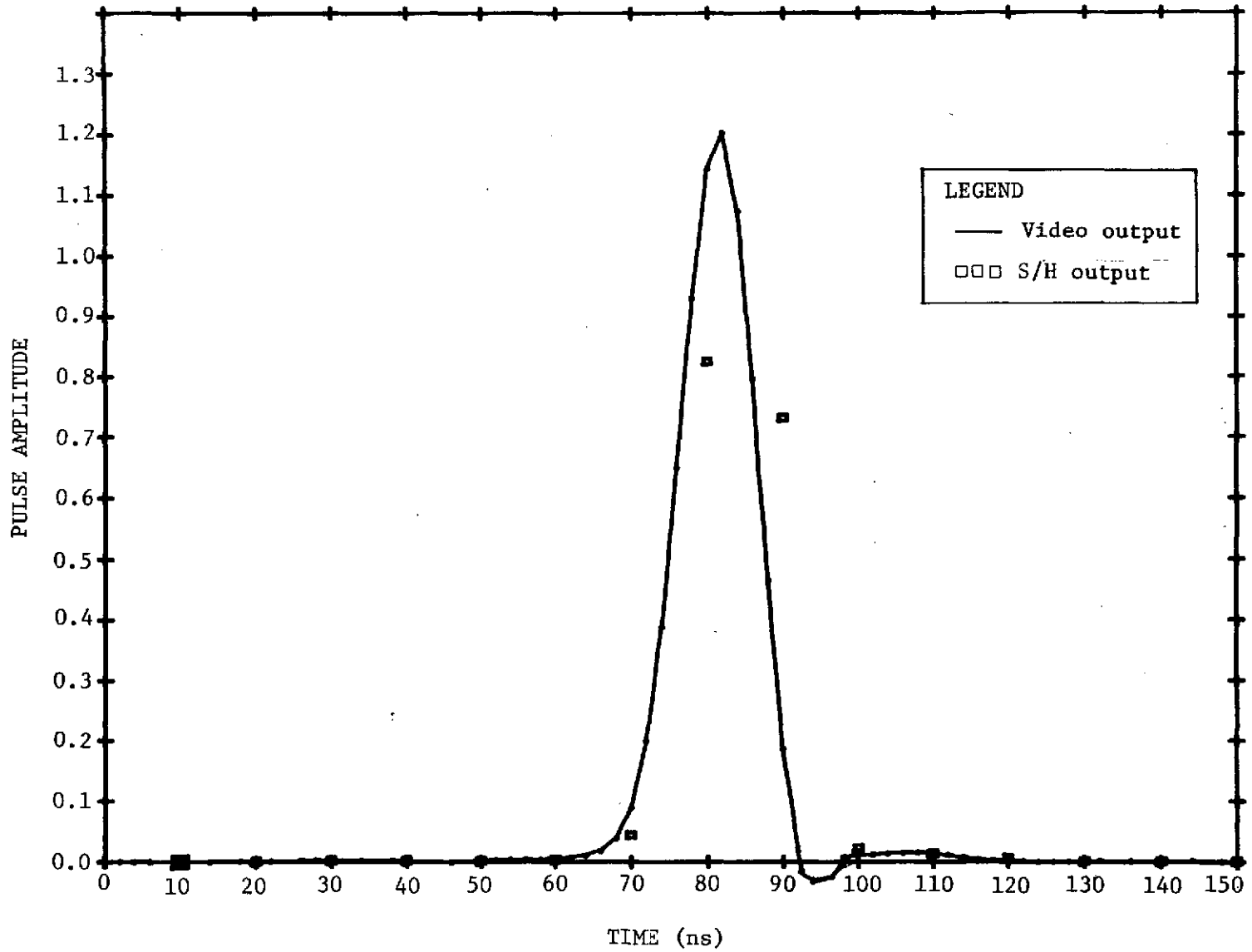
Figure A.II-5 Simulated Rectangular Pulse through Receiver(16-ns Pulse,100-MHz BW)
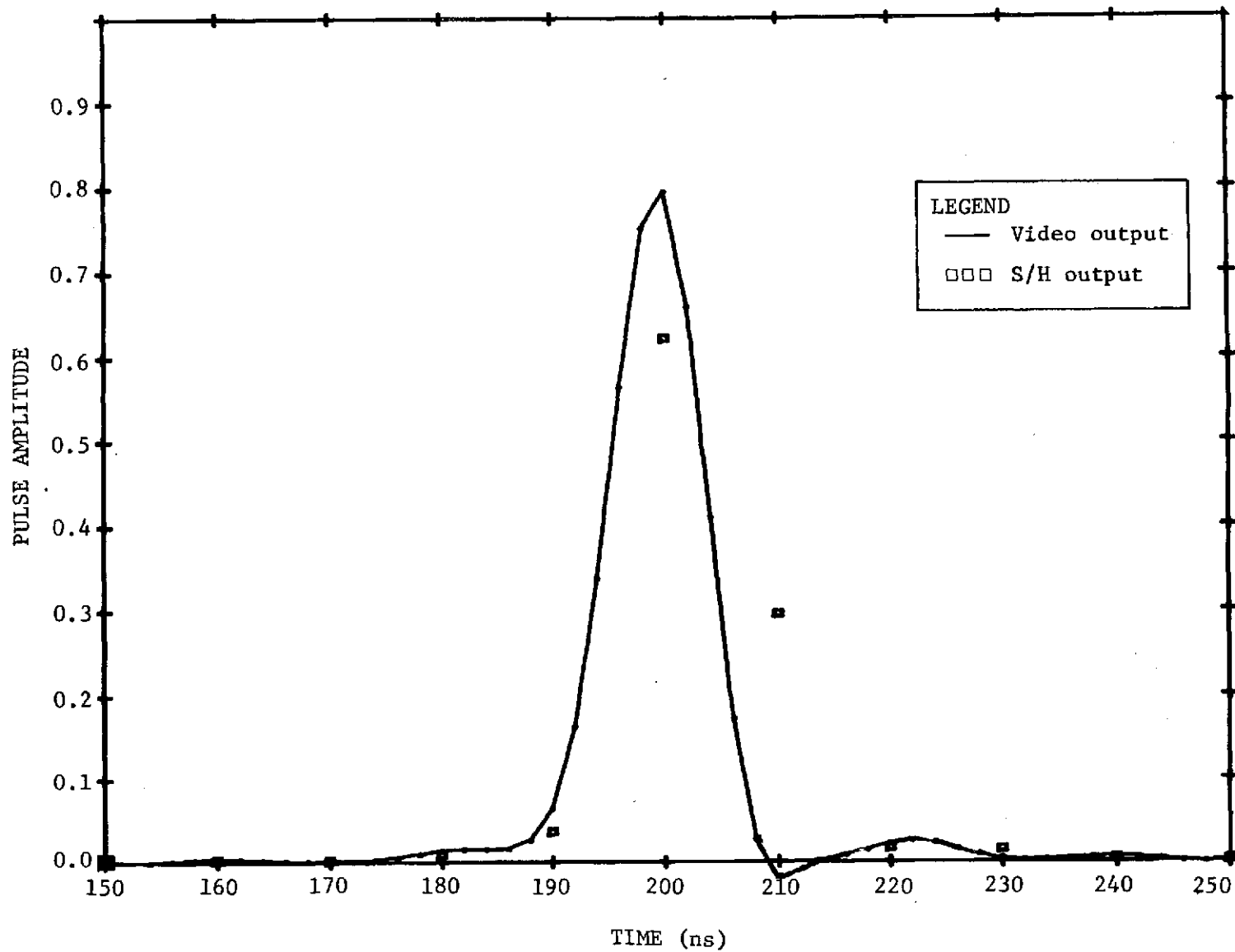
Figure A.II-6   Simulated PCM Pulse through Receiver (130-ns Pulse ,100-MHz BW)
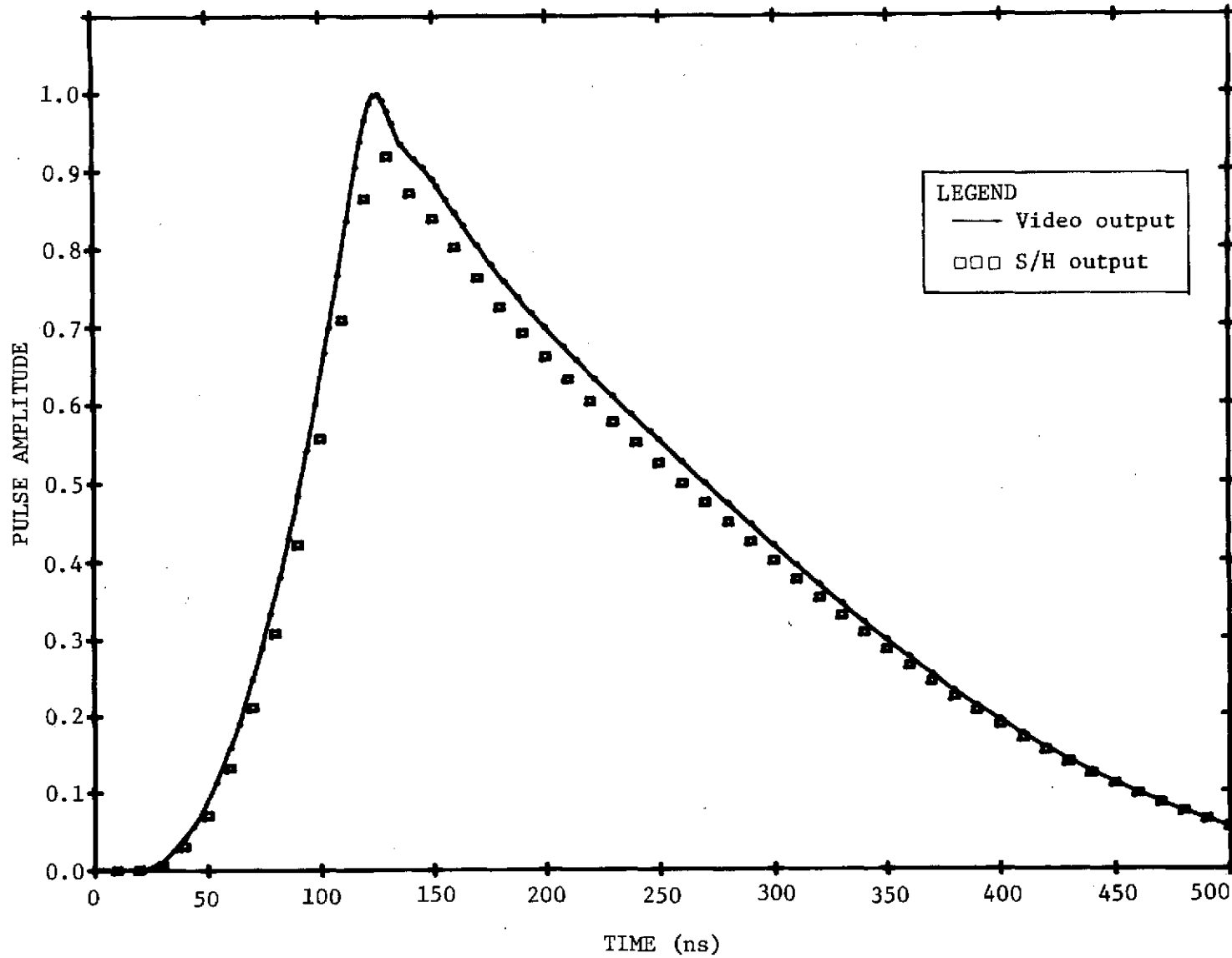
Figure A.II-7   Simulated Sawtooth Pulse through Receiver(600-ns Pulse, 100-MHz BW)
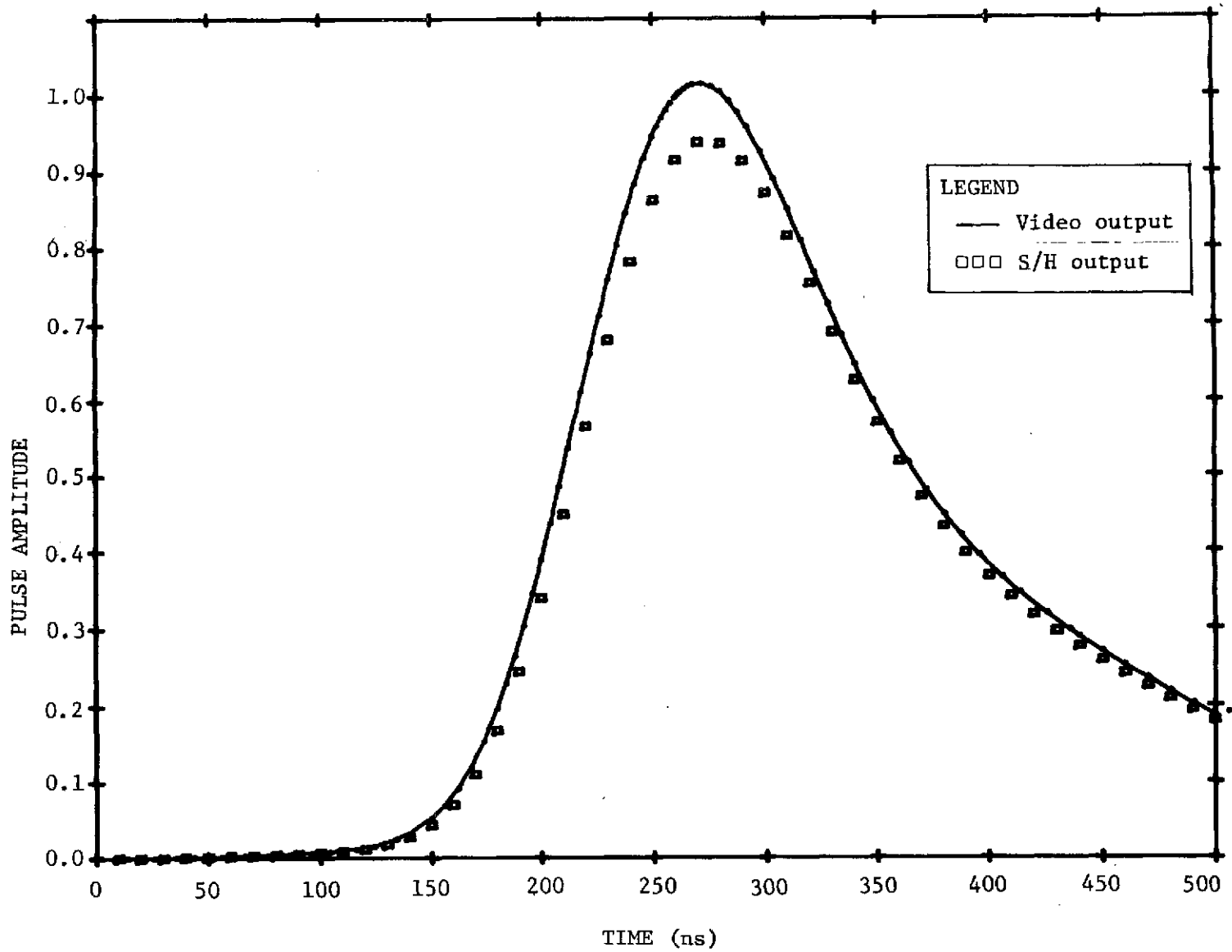
Figure A.II-8 Simulated Sawtooth Pulse through Receiver(600-ns Pulse,10-MHz BW)

Figures A.II-9 through A.II-11 show the S/H output samples for three cases compared to KSC test results. The squares again indicate the program S/H output and the integers 1 and 2 indicate the test results. Test results were multiplied by a constant for amplitude normalization and delayed in time to correspond to the program outputs.

Results of processing the assumed input pulses showed very good agreement with the measured outputs, indicating that the program had properly modeled the receiver. It also indicated that the nonrectangular characteristics of the S/H CDS output were largely derived from receiver characteristics and that the transmitter output pulses were very close to the rectangular pulse assumed. The transmitter output pulse shape was separately verified by the STAPE set-up described in Section I of this appendix.

B. Altimeter System Description, DAS Submodes (ALTIM)

The purpose of the ALTIM program was to simulate parameters that affect altimeter pulse response in the DAS submodes, which were for the most part outside the S193. Added to the ALTSYS program, this then provided a modeling of the entire pulse path from transmitter to S/H and tracker outputs. The ALTIM program thus included antenna pattern, vehicle location and attitude, target characteristics (specific targets only), free-space propagation, tracking of the received pulse, and AGC response for each receiver bandwidth. Processing of the input return (echo) pulse through the receiver was essentially the same as for the CDS simulation previously described, except for added loss/gain terms and the tracker position simulation.

Inputs to the program were:

1) Wind speed converted to sea state to provide a reflectivity model;

2) Spacecraft attitude in degrees*;

3) A selection of one of three transmitted pulse shapes appropriate to the S193 altimeter system, i.e., 100-ns increments;

4) Spacecraft altitude.

---

* Due to the present lack of valid drift rate data, the attitude was estimated from the S/H pulse shape. Thus, the attitude was only estimated over ocean surfaces.
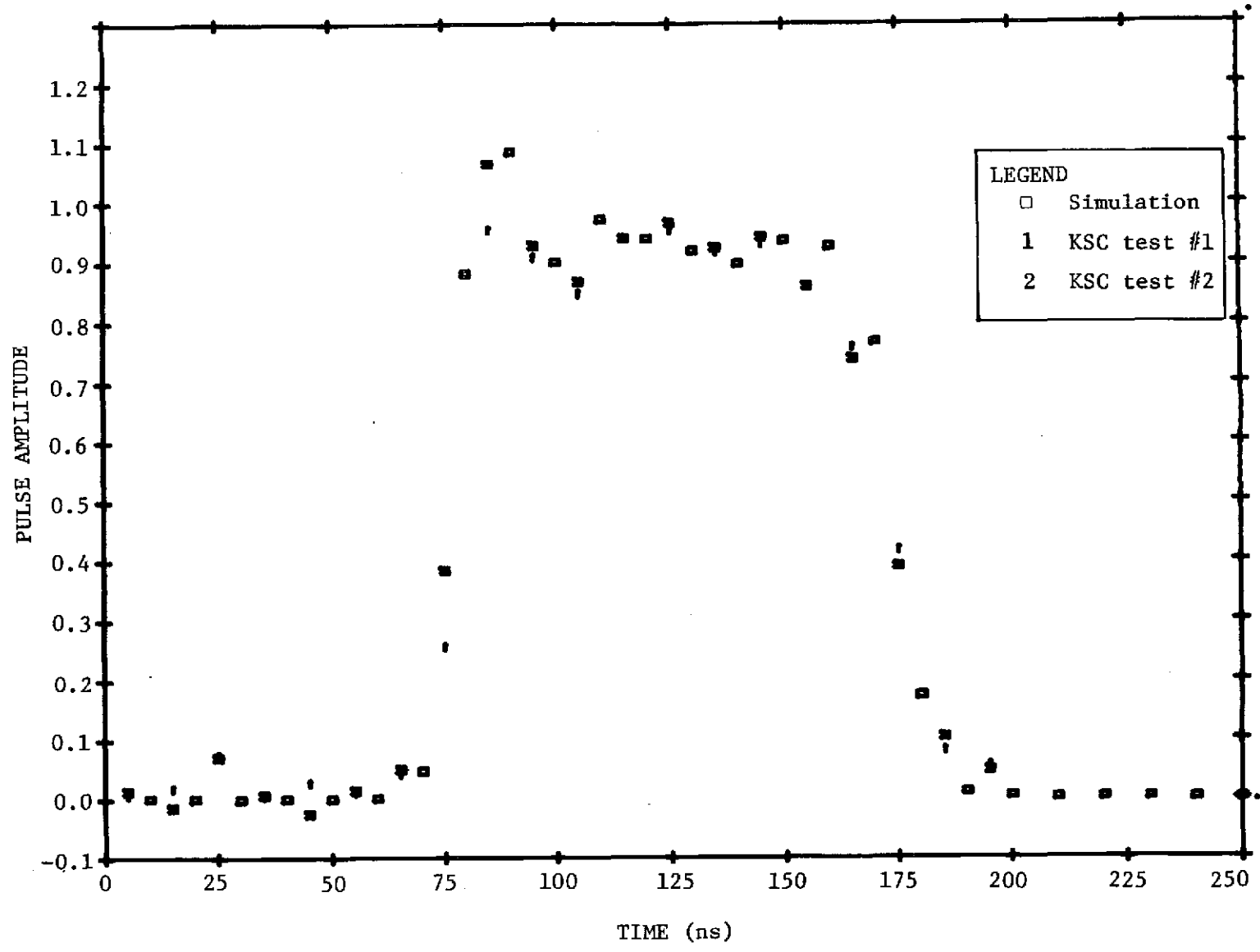
Figure A.II-9 Rectangular Pulse through Receiver 100-ns Pulse 100-MHz BW
S/H Output, Simulation Compared to KSC Tests
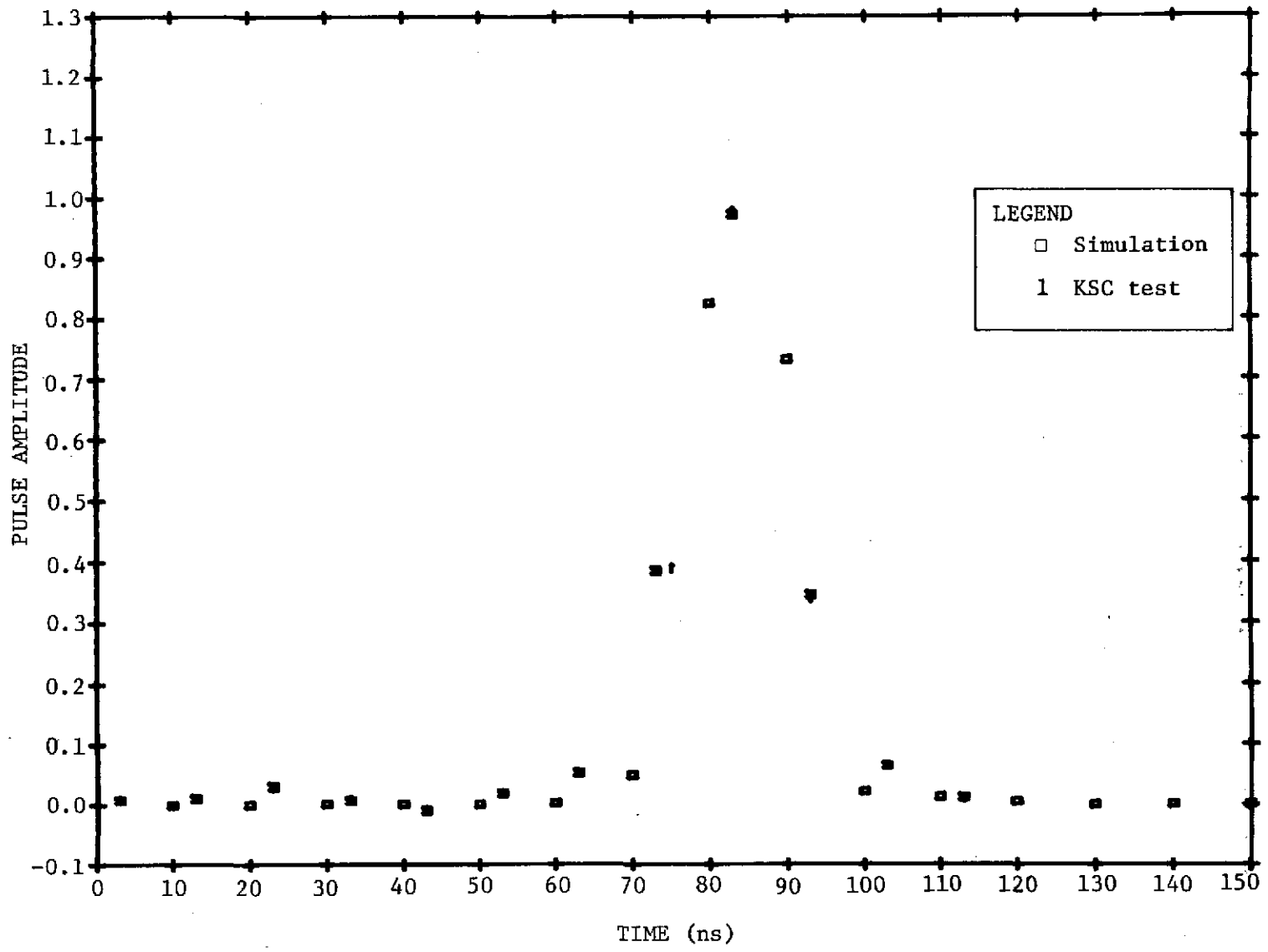
Figure A.II-10   Rectangular Pulse through Receiver 16-ns Pulse 100-MHz BW
S/H Output, Simulation Compared to KSC Tests
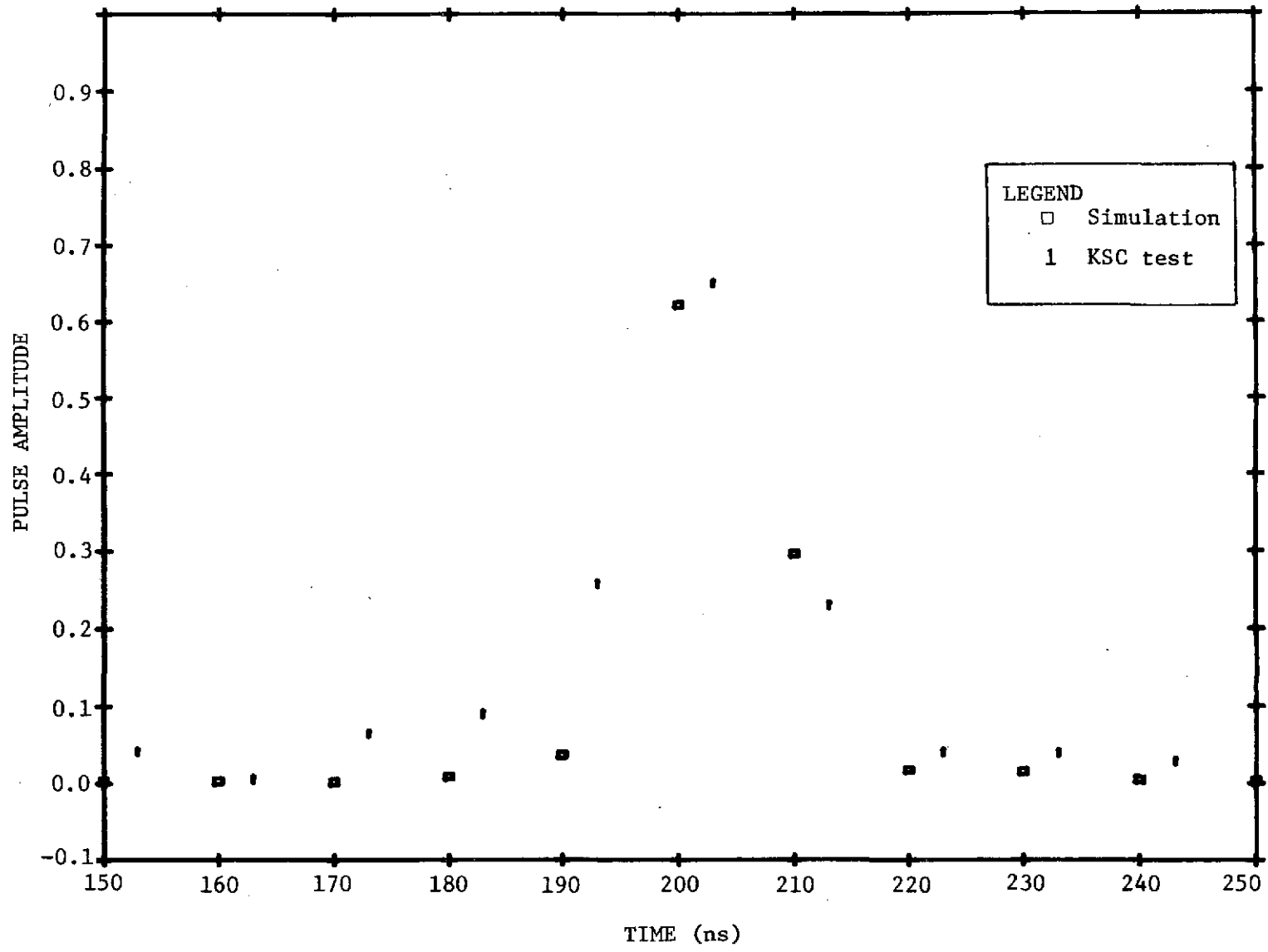
Figure A.II-11   PCM Pulse through Receiver 130-ns Pulse 100 MHz BW
S/H Output, Simulation Compared to KSC Tests

1. Program Description

The program assumed that an impulse (rectangular pulse with unity amplitude, extremely short duration) was transmitted and received after ground reflection. Figure A.II-12 shows the geometry and the parameters used. The general approach was to consider the rectangle on the ground shown in the figure as the illuminated area. This was made large enough so that a ray illuminating a portion of the area outside the rectangle was attenuated by the antenna pattern by at least 50 dB (25 dB in the transmit direction and 25 dB in the receive direction). Each narrow ray in the antenna pattern was considered as reflected from a very small (differential) area with dimensions of DX and DY, as shown in the figure. The round-trip distance from satellite to ground and return (A to B to A) was calculated and divided by propagation velocity to obtain round-trip transmit time in nanoseconds.

The target surface was assumed in order to provide the reflection at the surface. In the specific case of a sea surface, the work of Beckman and Barrick* was used. Figure A.II-13 shows a conversion from wind speed to wave slope. Figures A.II-14 and A.II-15 show a conversion of beam incidence angle to target reflectivity (radar cross-section) for various wave slopes. (The computing process could also be iterated to determine the target σ° values for the measured AGC values.)

The differential power received and corresponding time delay was calculated and stored for each of the differential areas in the rectangle of Figure A.II-12. After this, a series 2-ns time-increment responses from 0 to 3500 ns (1750 increments) was established and sorted into the proper time increments. The incremental responses were added in an individual time increment to determine the total power received in that increment. Plotting the resulting sums against time yielded the power impulse response at the input to the receiver. The square root of this curve was proportional to voltage, assuming that the RF phase of the incoming energy was random.

---

* Beckman, Petr, and Spizzichino, The Scattering of Electromagnetic Waves from Rough Surfaces, Macmillan, 1963.

D. E. Barrick, "Wind Dependence of Quasi-Specular Microwave Sea Scatter," Communications Section of IEEE Transactions on Antennas and Propagation, January 1974, p. 135.

Figure A.II-12 Altimeter Geometry
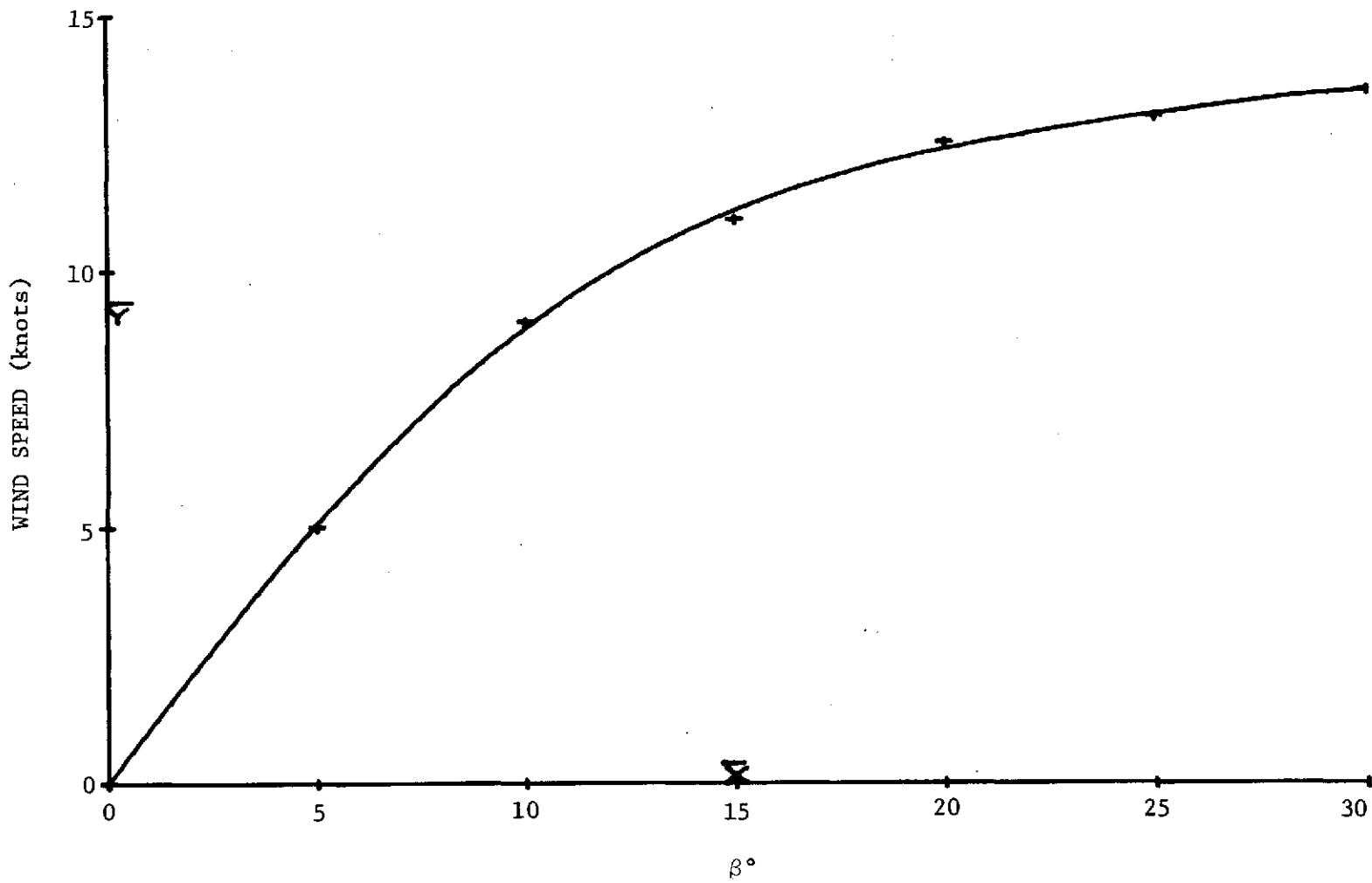
Figure A.II-13   Wind Speed versus β°

RADAR CROSS SECTION, σ_0 (dB)
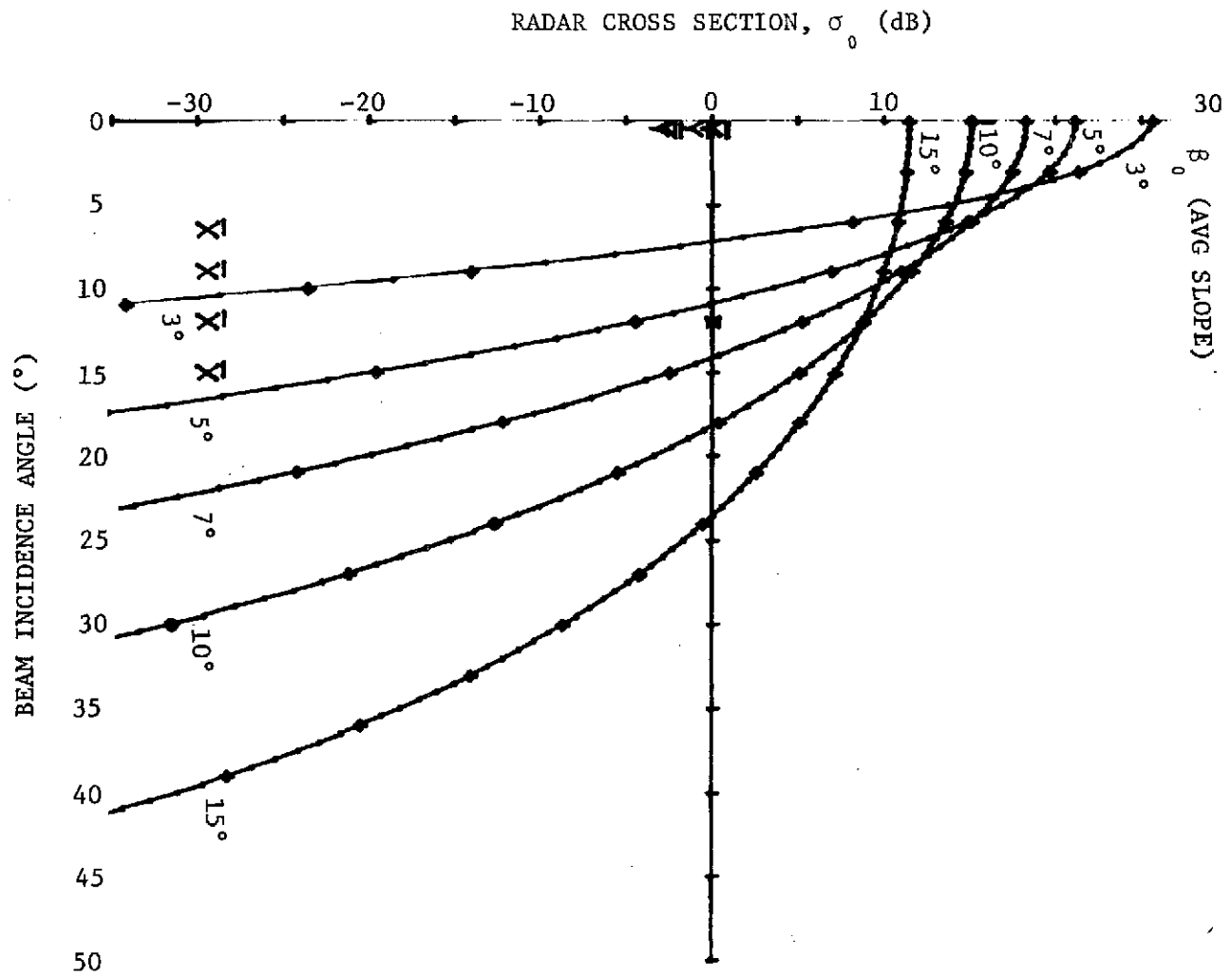
Figure A.II-14   Radar Cross-Section versus Beam Incidence Angle

RADAR CROSS-SECTION, σ_0 (°)
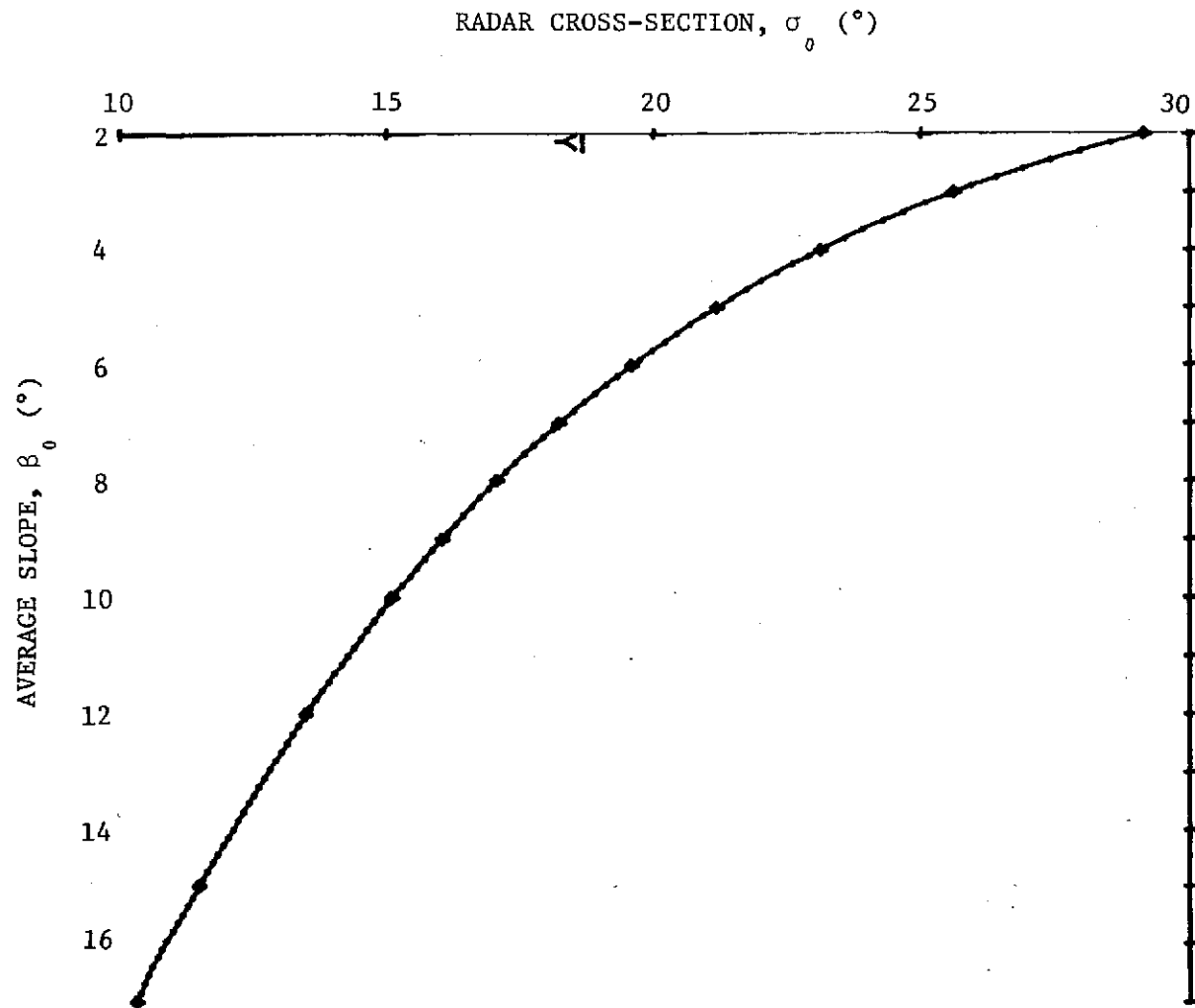
Figure A.II-15   Radar Cross-Section versus Average Slope Beam Incidence Angle = 0.0°

Because the process of transmission both ways through the atmosphere and reflection at the air-ground interface was linear, the convolution of the impulse response with the actual transmitted waveform gave the waveform received at the input to the receiver. This convolution was carried out in the program according to the convolution integral in which the resulting received signal was

$$S_2(t) = \sum_{k=1}^{N} a_k h(t - t_k) \qquad [A.II.1]$$

where

a_k = strength of k-th sample of the transmitted waveform

$h(t)$ = impulse response

t_k = time position of k-th sample in the transmitted waveform

$S_2(t)$ was then normalized so that the resulting maximum of $S_2(t)$ was unity.

This received signal was processed through the receiver in the same manner as ALTSYS (internal calibration signal processing) except that only one sampling position was used, resulting in processing $S_2(t)$ by the IF amplifiers, the video amplifier, the square law detector, and the S/H circuitry to yield one of the program outputs.

Another output produced was the tracker error as a function of tracker gate position. Tracker position was referenced to the return of an impulse traveling a path straight down to nadir (the zero-error position) to yield a relative tracker position. Comparison between the spacecraft altitude, or zero-error position of the tracker, and the computed tracker position based on the return pulse shape yielded the tracker compensation required as a function of spacecraft attitude, beam angle, return pulse shape, etc.

The most significant variable causing errors in calculating the radar cross-section and altitude from Skylab altimeter data was the beam incidence angle. This angle varied primarily as a result of angular deviation of the spacecraft Z axis from the Z local vertical. The deviation was largely caused by rate gyro drift, so that reliable values of this angle could not be obtained from the

attitude control system to the required accuracies*. Fortunately, the magnitude of the beam incidence angle could be obtained directly from the wave shape of the altimeter S/H output. This angle could then be applied to the proper curve and a correction made in radar cross-section and attitude. If this deviation were held to within approximately 0.3 degree, no corrections for beam incidence angle were necessary, but for larger deviations, corrections were necessary and could be successfully applied up to about 1 degree.

The necessary relationships for correcting beam offset from nadir are described in the following paragraphs and figures. Each of the curves shown in the figures has been fitted with a "least squares" technique to a polynomial and the coefficients are given with the curves.

2. Program Results

Several results were derived from operation of the program that were useful in reducing Skylab altimeter data.

a. Beam Incidence Angle as a Function of S/H Waveshapes – Figure A.II-16 is a family of curves relating S/H wave shape to beam incidence angle (θ) for the 100-ns transmitted pulse. It can be seen that the leading edge of the output pulse is nearly independent of θ over the range of interest. Figure A.11-16 is the same scale as the KSC processed flight S/H data, and by drawing the curves of the figure on transparent paper, they can be matched to Skylab data and the proper value of θ determined for any point in the mission where the 100-ns transmitted pulse and 100 MHz were used. Because the simulation was only based on sea-water reflections, approximate results can be expected over land areas.

b. Radar Cross-Section Correction for Beam Incidence Angle – Program ALTIM also calculated the maximum of the averaged input waveform. This corresponded to the AGC output voltage in the altimeter once the effect of the IF filters in the receiver was taken into account. Figure A.II-17 shows the dB change in waveform peak caused by the IF filters and beam angle. This can be used to correct radar cross-section as a function of beam incidence angle. Over the range shown, this corresponds within a few tenths of a dB to the curves developed by GE for the sum of r and f factors in dB.** The correction is within a few tenths of a dB for 10- and 100-MHz receiver bandwidths, so only one curve is shown.

---

* Outputs from the improved rate gyro drift modeling are not available but are expected.

**r- and f factors are variable factors used in the calculation of backscatter cross section. "r" accounts for the difference between the pulse shapes used to obtain preflight calibration data and the actual mean return pulse shapes. "f" is dependent upon pulse shape, pointing error, and altitude.
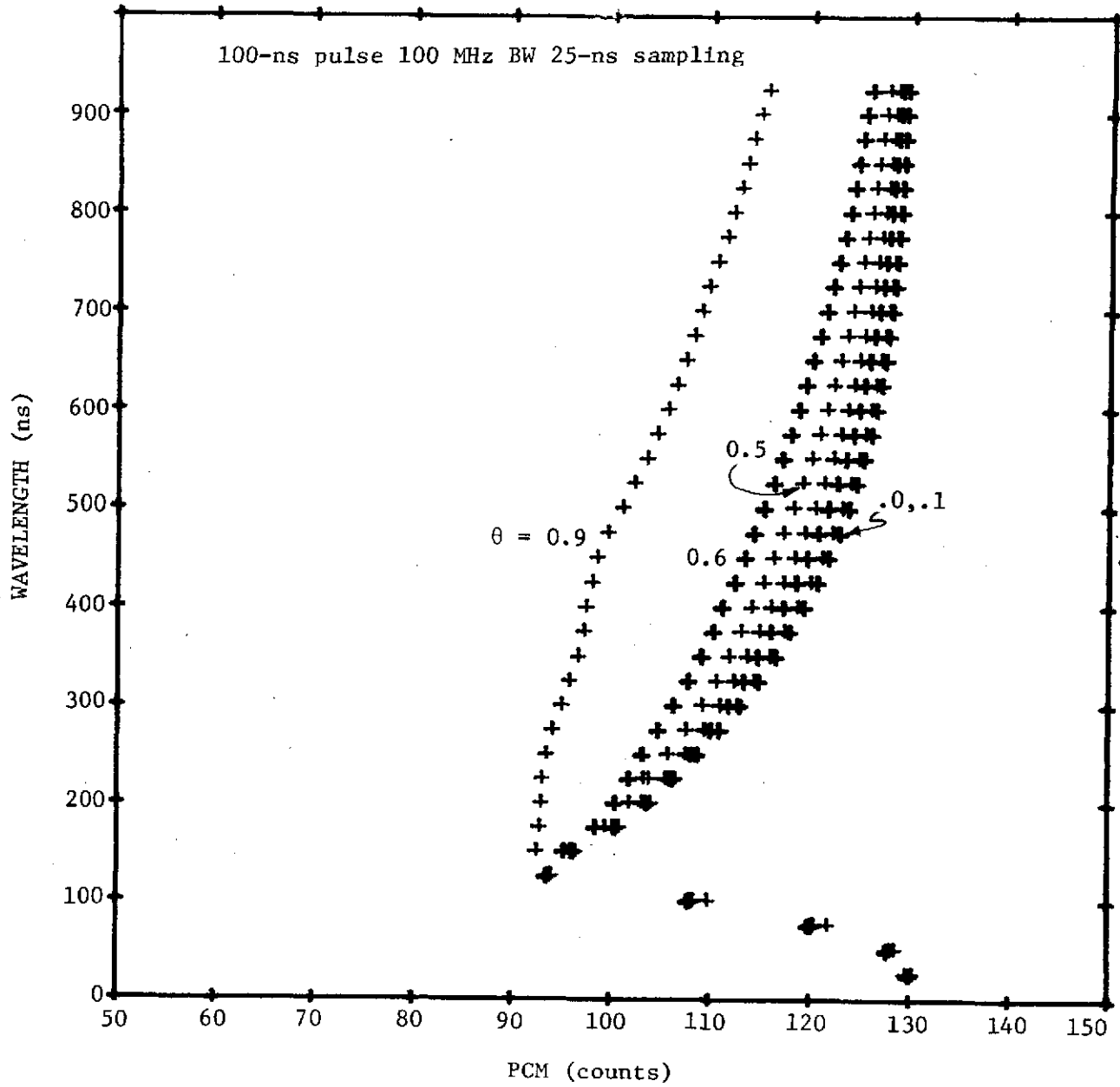
Figure A.II-16   S/H Waveforms for Various Beam Incidence Angles (θ)

CORRECTION (dB)

AO = 0.0
A1 = +1.654665615 E-1
A2 = +1.328377524 E+1
A3 = -6.435823226 E+1
A4 = +1.668985054 E+2
A5 = -1.796613206 E+2
A6 = +8.230715485 E+1
A7 = -1.285168246 E+1

BEAM INCIDENCE ANGLE, θ (°)
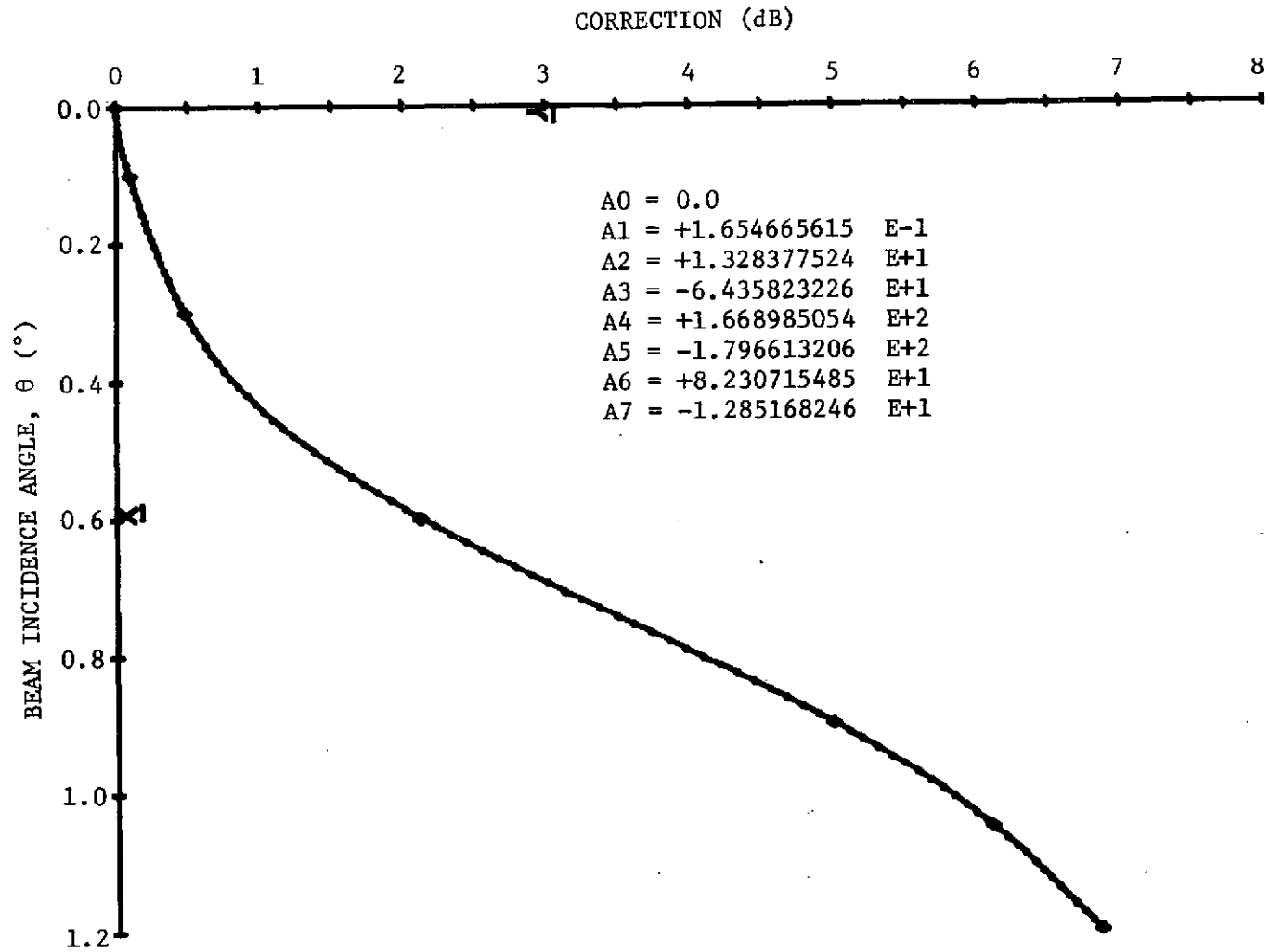
Figure A.II-17 Radar Cross-Section for Beam Incidence Angle (θ)

c.   Correction of Altitude Output for Beam Incidence Angle –
Altitude corrections for beam incidence angle were identical within
the resolution capability of ALTIM (0.3 meters) for the two receiver
bandwidths and for all transmitted pulse shapes. Figure A.II-18
shows the required altitude correction as a function of beam
incidence angle. The correction was less than the program
resolution (0.3 meters) for beam incidence angles of 0.3 degree or
less.

3.   Program Outputs

Outputs from this program were line printer plots and
tabulations and DD280 plots. A description of these outputs with
examples calculated for a given set of input conditions is given
below.

1)   Input to the receiver in arbitrary units proportional to
the voltage of a theoretical transmitted impulse
(rectangular pulse of nearly zero duration), Figure A.II-19.

2)   Input waveform (envelope) to receiver in arbitrary units
proportional to voltage and power for selected transmitted
waveforms, Figure A.II-20.

3)   Waveform to input of tracker (through tracker filter) for
wide and narrow IF filters, Figure A.II-21.

4)   Output waveform from S/H circuitry at the output of the
receiver in normalized units proportional to S/H data
output volts. The waveforms are output from before
sampling, after 10- and 25-ns sampling and from both
bandwidths, Figures A.II-22 through A.II-27.

5)   Output tracker error as a function of tracking gate
position to permit determination of tracker offset as a
function of transmitted waveform, sea state, and space-
craft attitude. These are shown in Figures A.II-28 and
A.II-29 for the narrow and wide bandwidths respectively.

These examples were given for a normal beam incidence angle
and 10-knot wind speed for a fully risen sea. If conditions
changed, the shapes of the curves change, and this permits
comparisons under controlled conditions. For instance, if the zero
crossing point were taken on the tracker error curve for beam
incidence angles, a correction curve could be constructed for the
altitude word as a function of beam incidence angle. (Of course the
time delay derived must be converted to a one-way distance.)

ALTITUDE CORRECTION (m)

BEAM INCIDENCE ANGLE, θ (°)

$A0 = +6.308708812$ E-2
$A1 = -2.895746711$ E+0
$A2 = +8.982005981$ E-1
$A3 = +6.106607792$ E+1
$A4 = -5.848051756$ E+1
$A5 = +2.646982061$ E+1
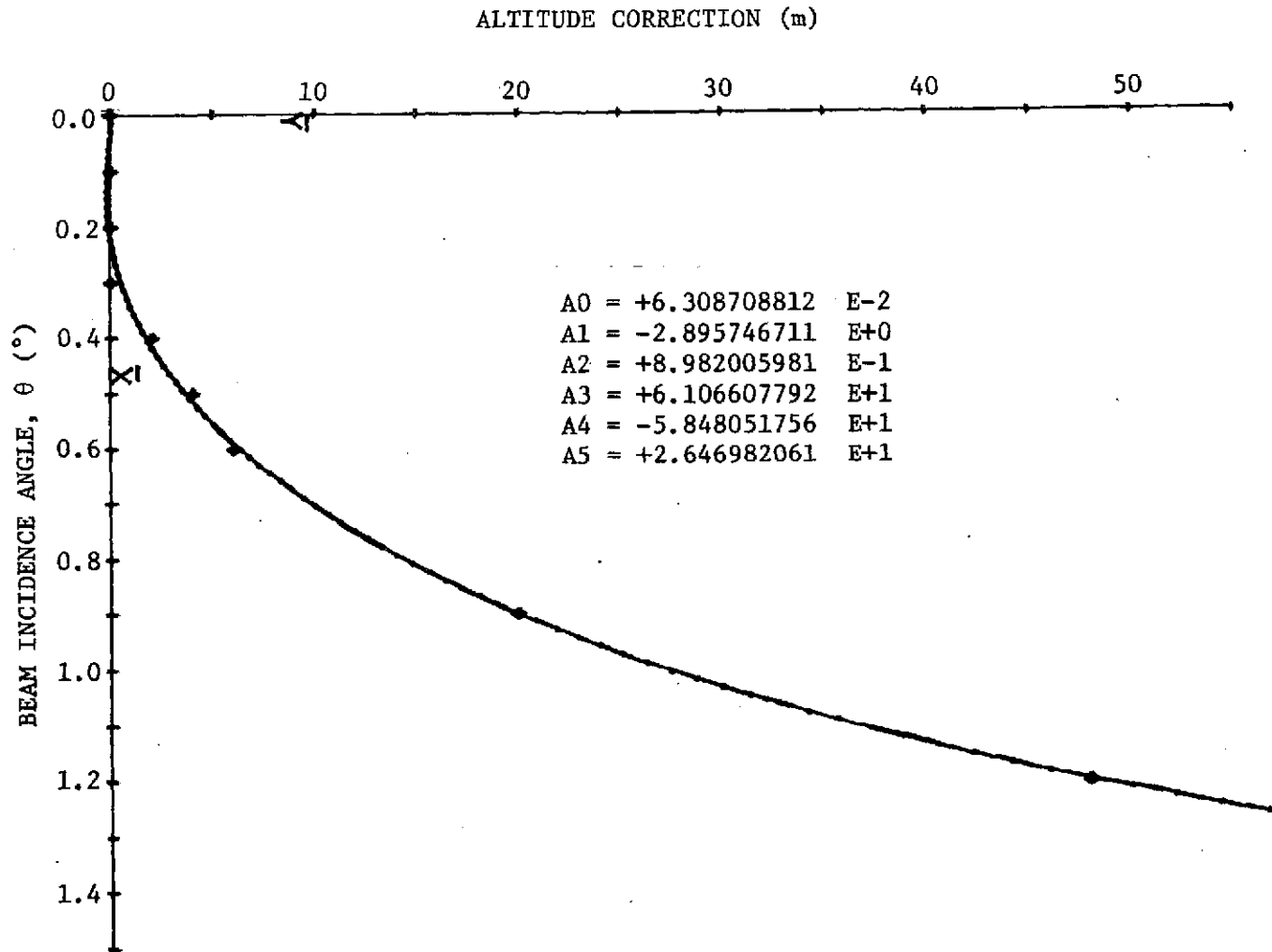
Figure A.II-18   Altitude Correction for Beam Incidence Angle
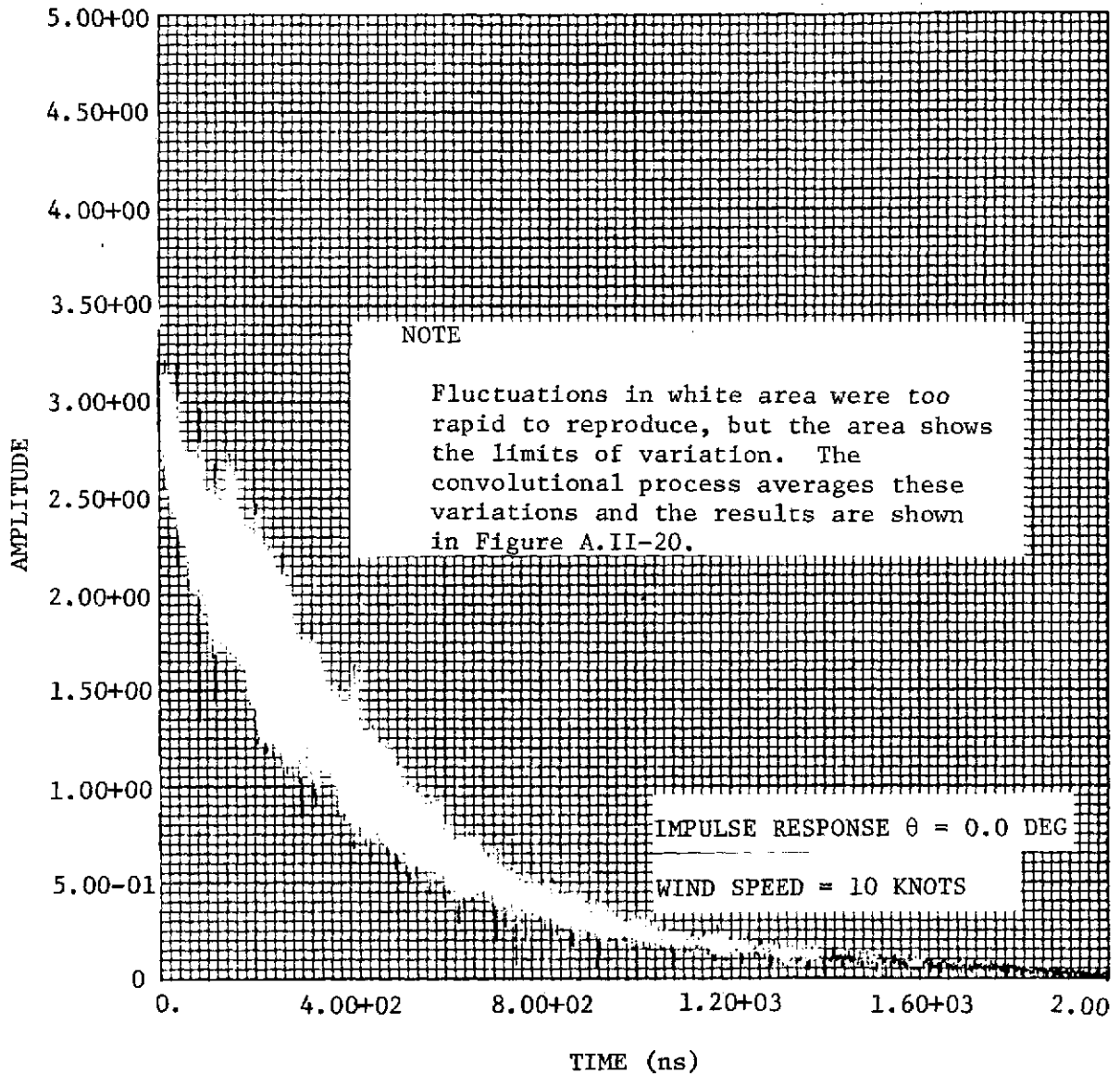
Figure A.II-19   Input to Receiver in Arbitrary Units Proportional
to Voltage of Theoretical Transmitted Wave
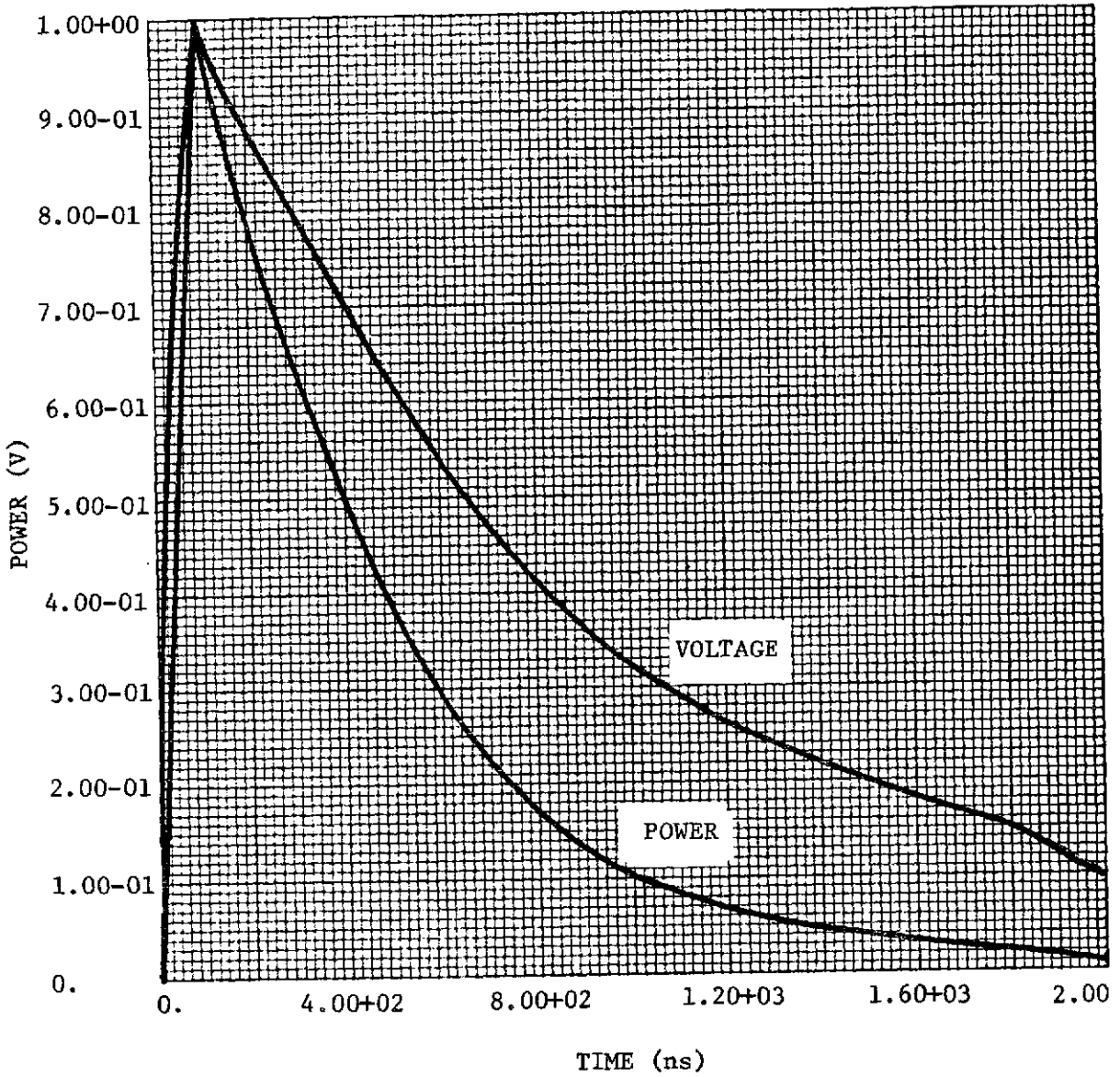
Figure A.II-20   Input Waveform to Receiver in Arbitrary Units
Proportional to Voltage and Power
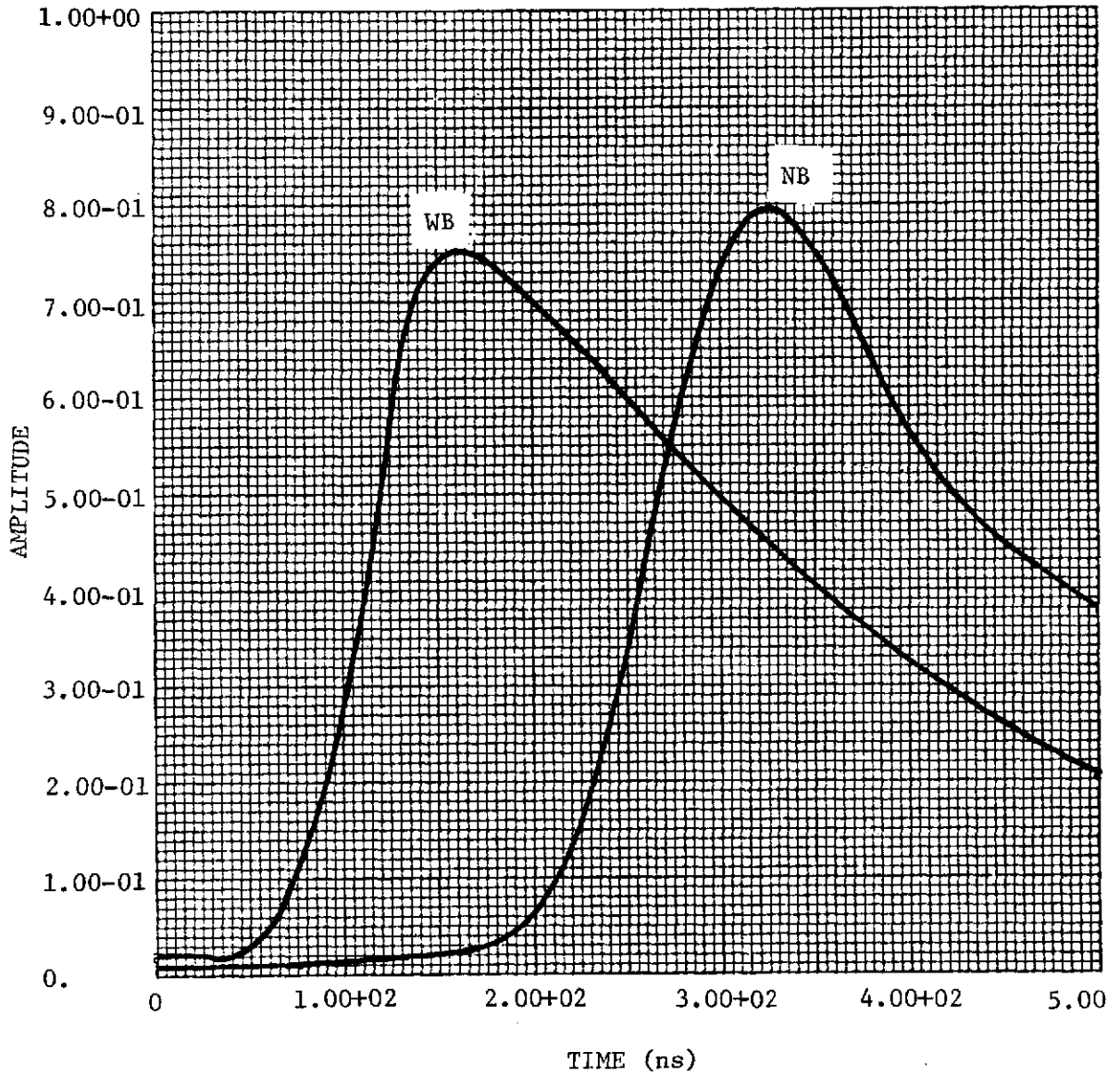
Figure A.II-21 Waveforms to Input of Tracker for Wide and Narrow Filters
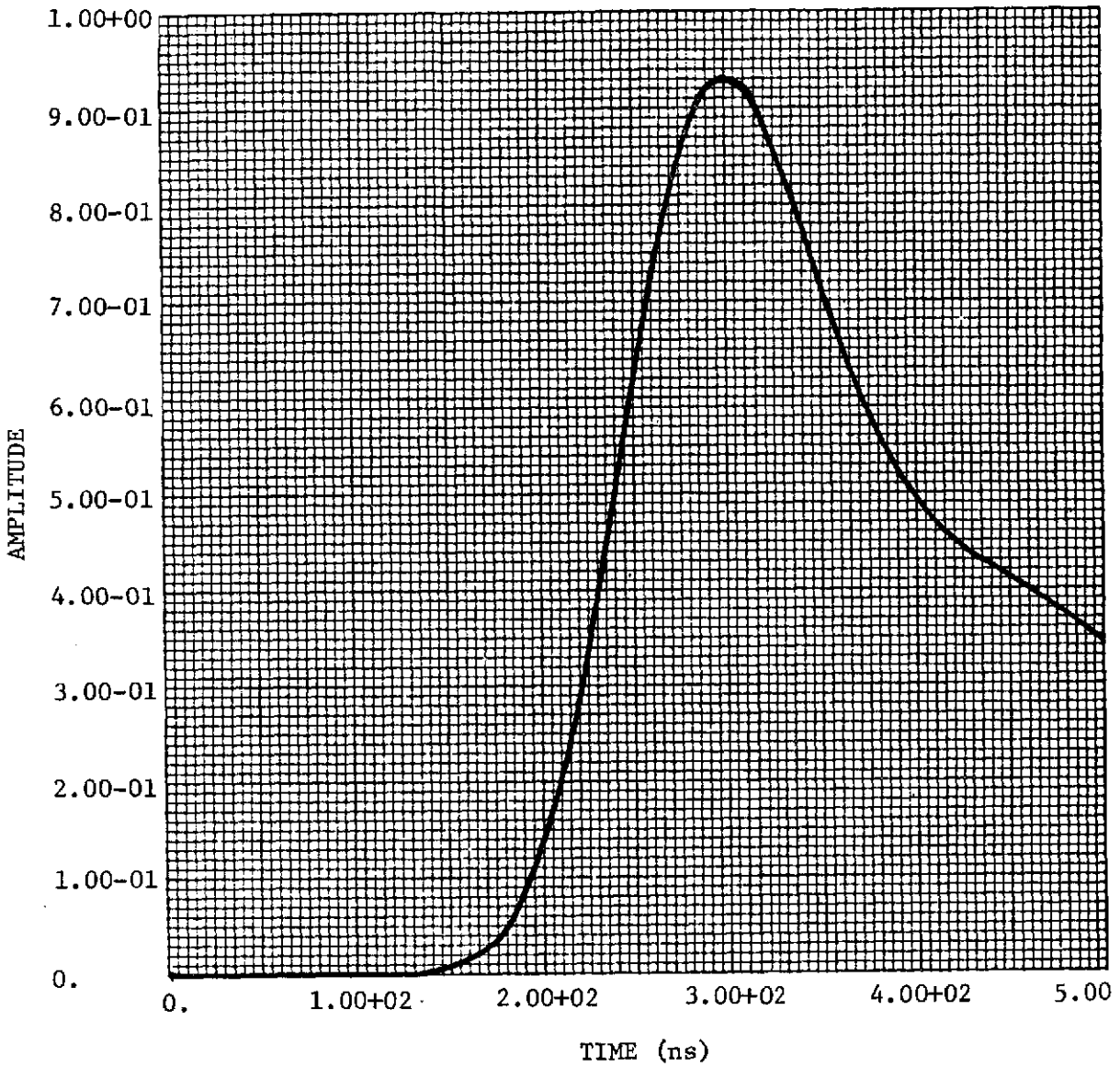
Figure A.II-22   Output Waveform, Presampling, 100-ns Pulse, 10-MHz BW
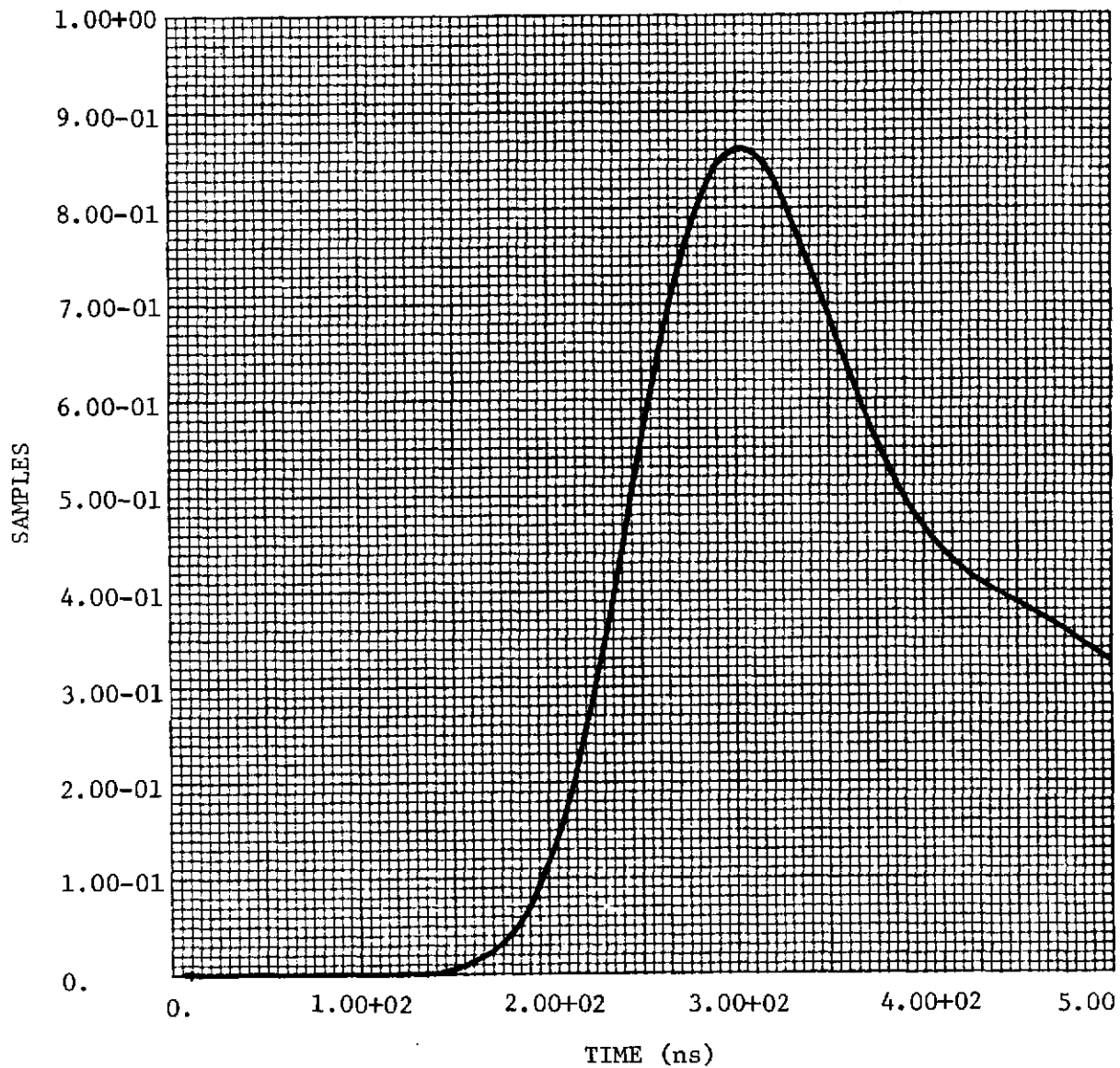
Figure A.II-23   Output Waveform, 10-ns Sampling, 100-ns Pulse, 10-MHz BW
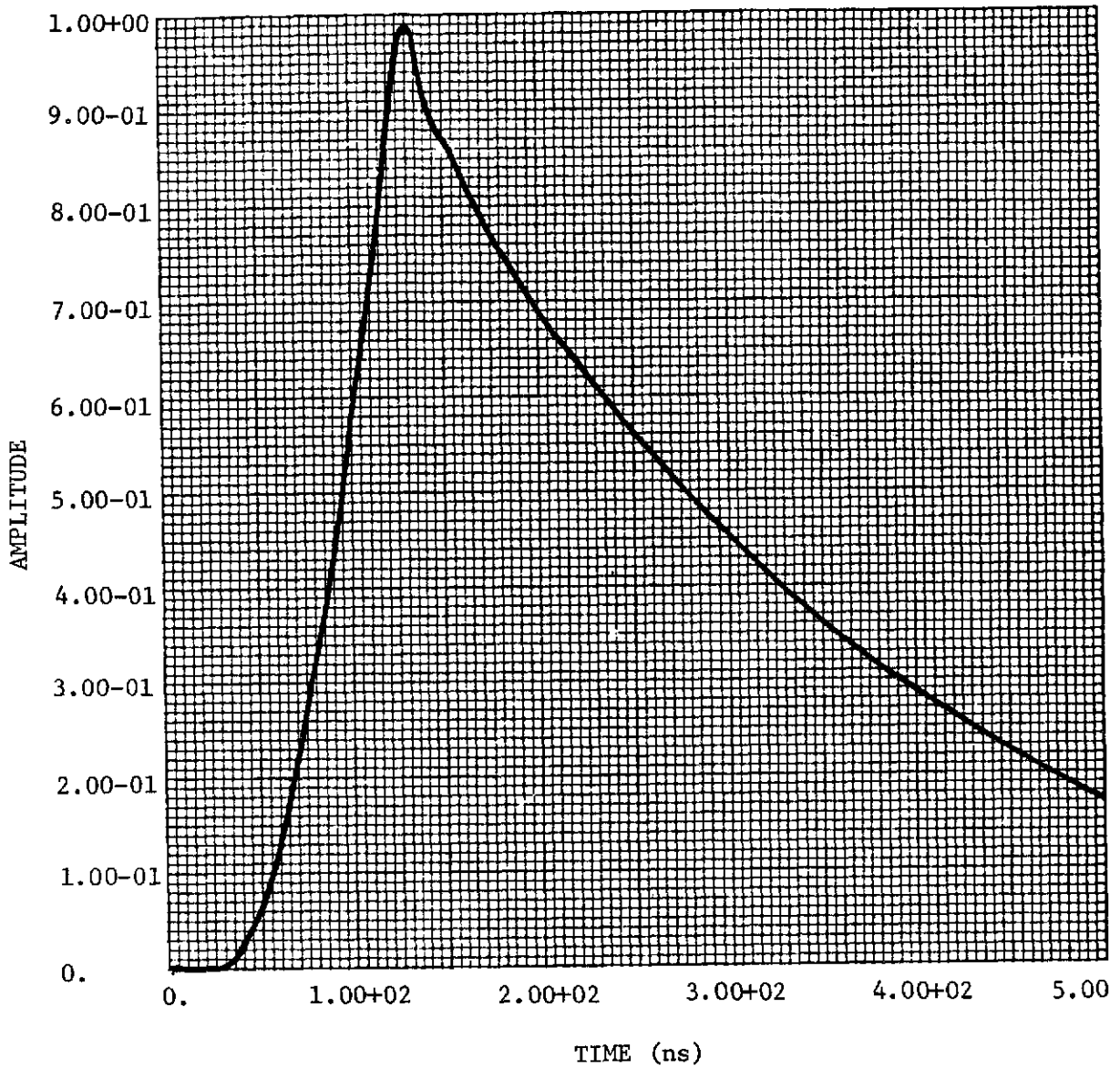
Figure A.II-24 Output Waveform, Presampling, 100-ns Pulse, 100-MHz BW

MSC-05546
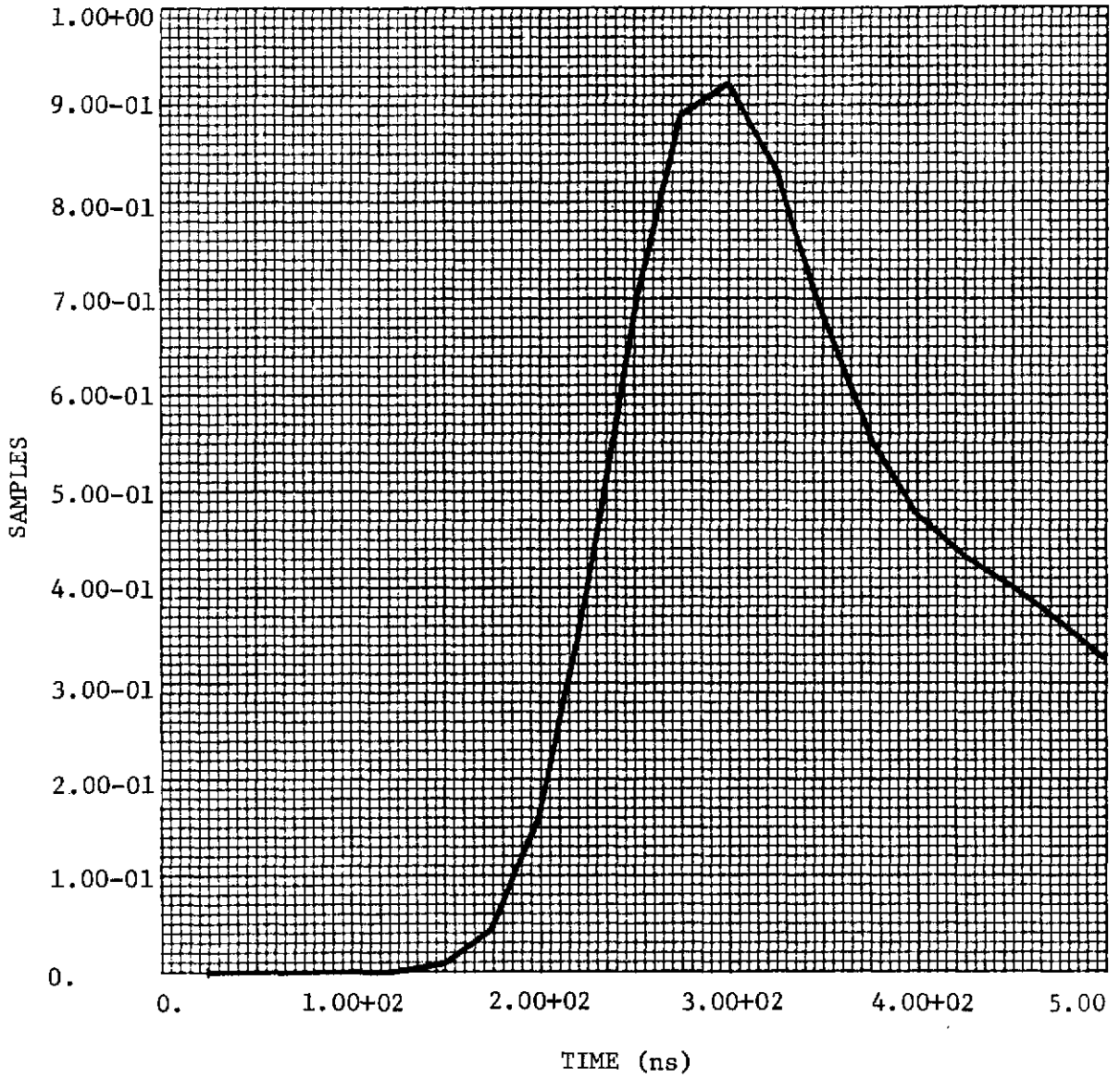
Figure A.II-25 Output Waveform, 25-ns Sampling, 100-ns Pulse, 10-MHz BW

V-106
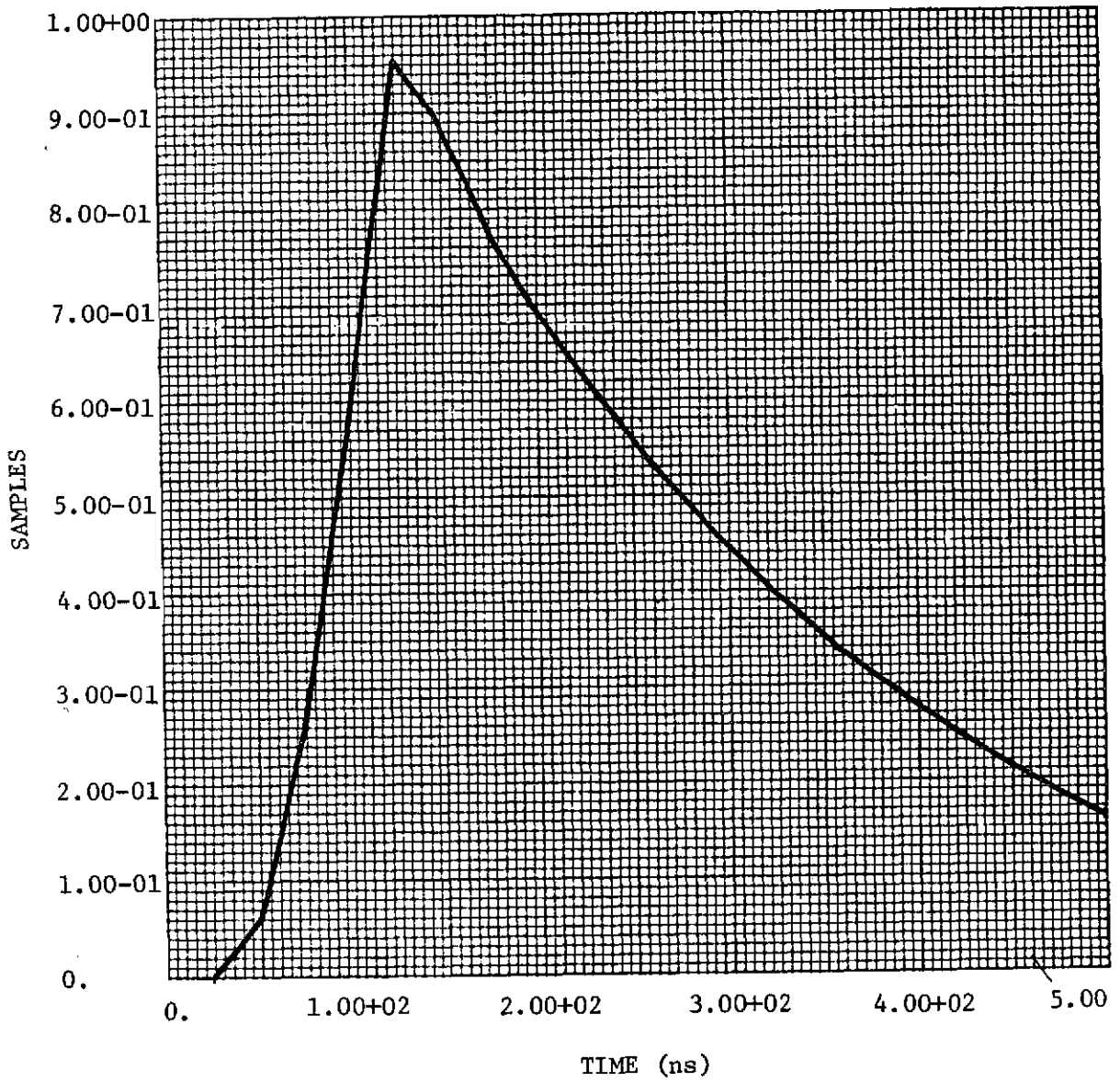
Figure A.II-26   Output Waveform, 10-ns Sampling, 100-ns Pulse, 100-MHz BW
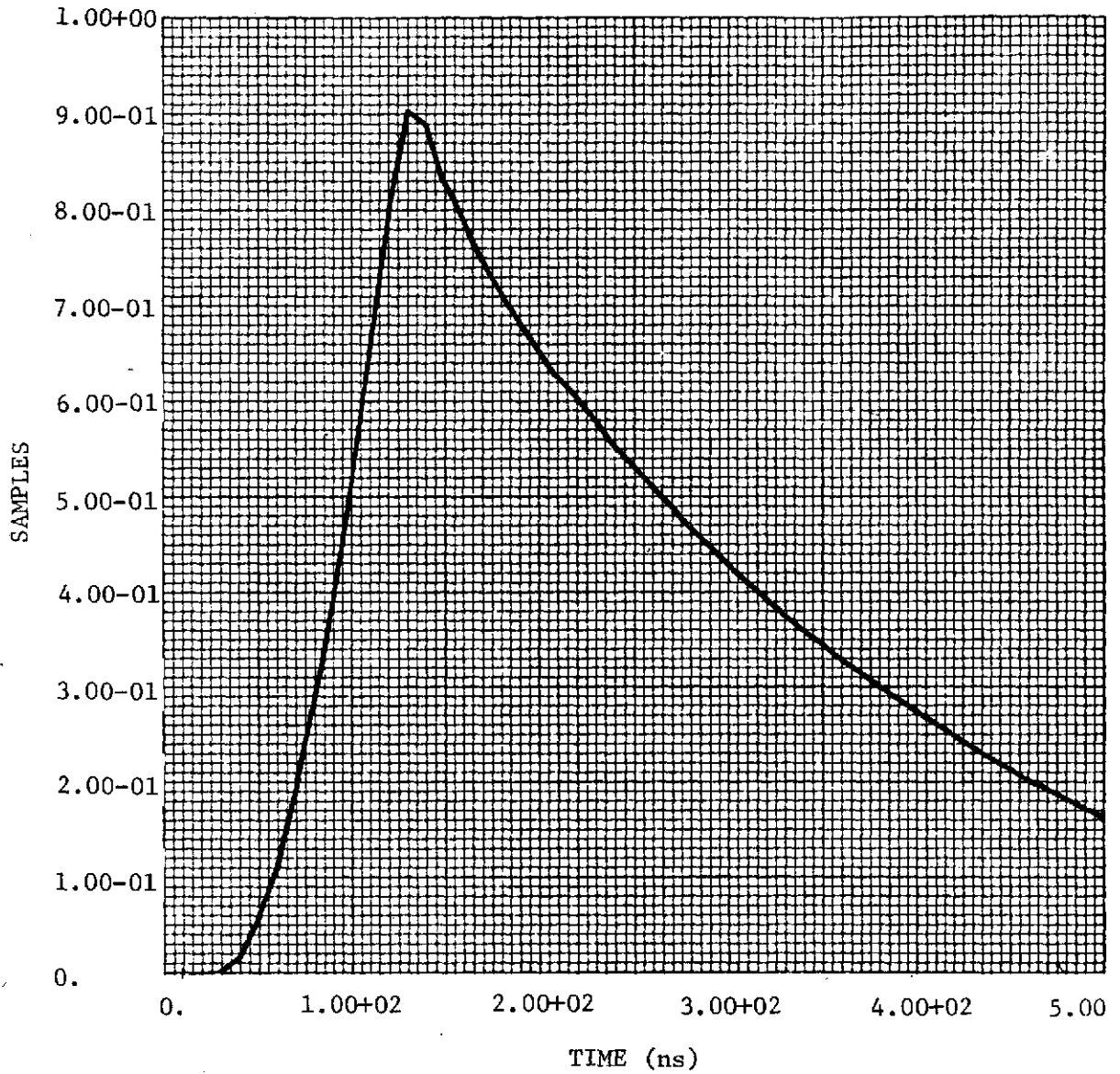
Figure A.II-27   Output Waveform, 25-ns Sampling, 100-ns Pulse, 100-MHz BW
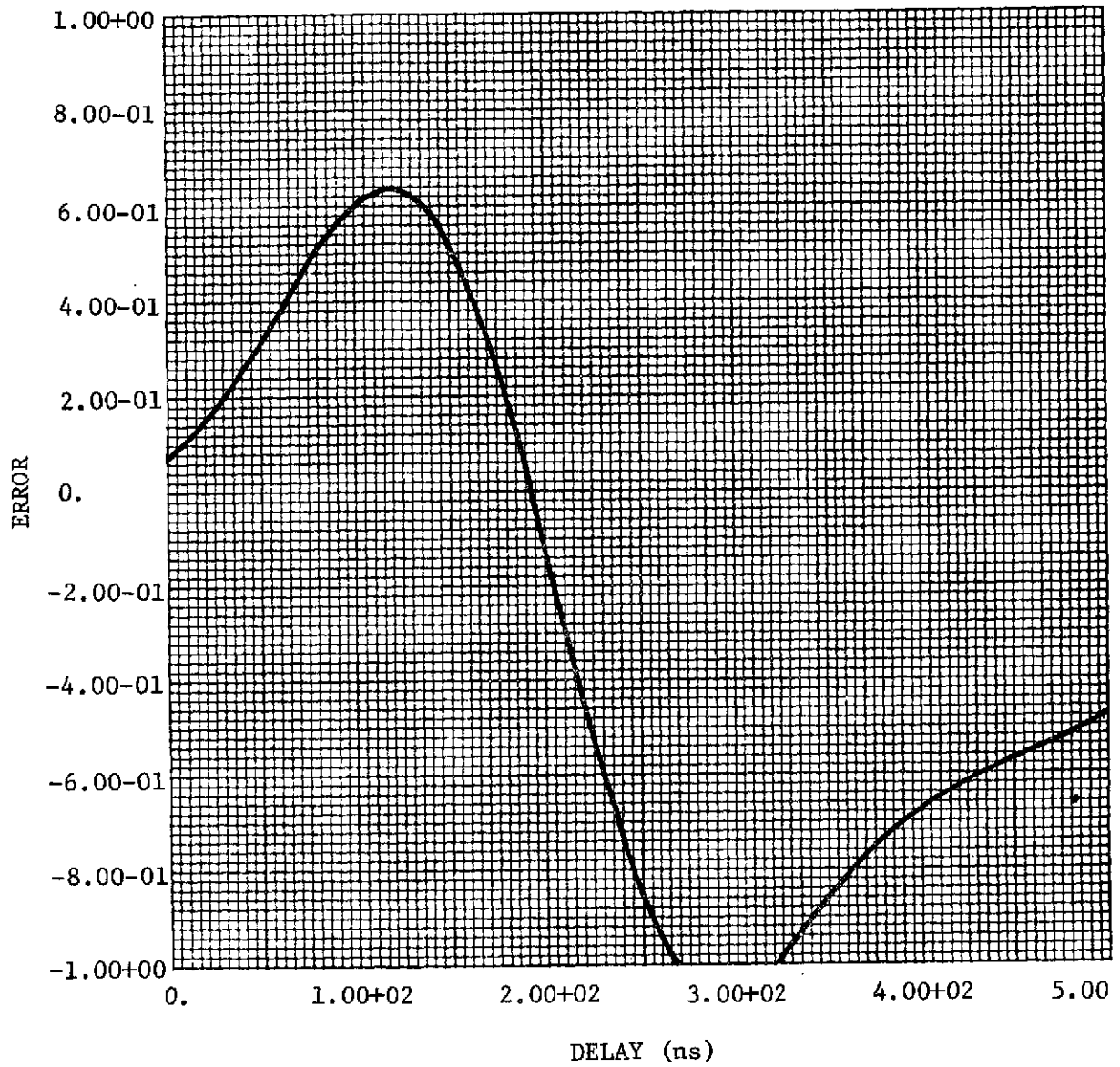
Figure A.II-28 Tracking Error versus Delay, Narrow BW
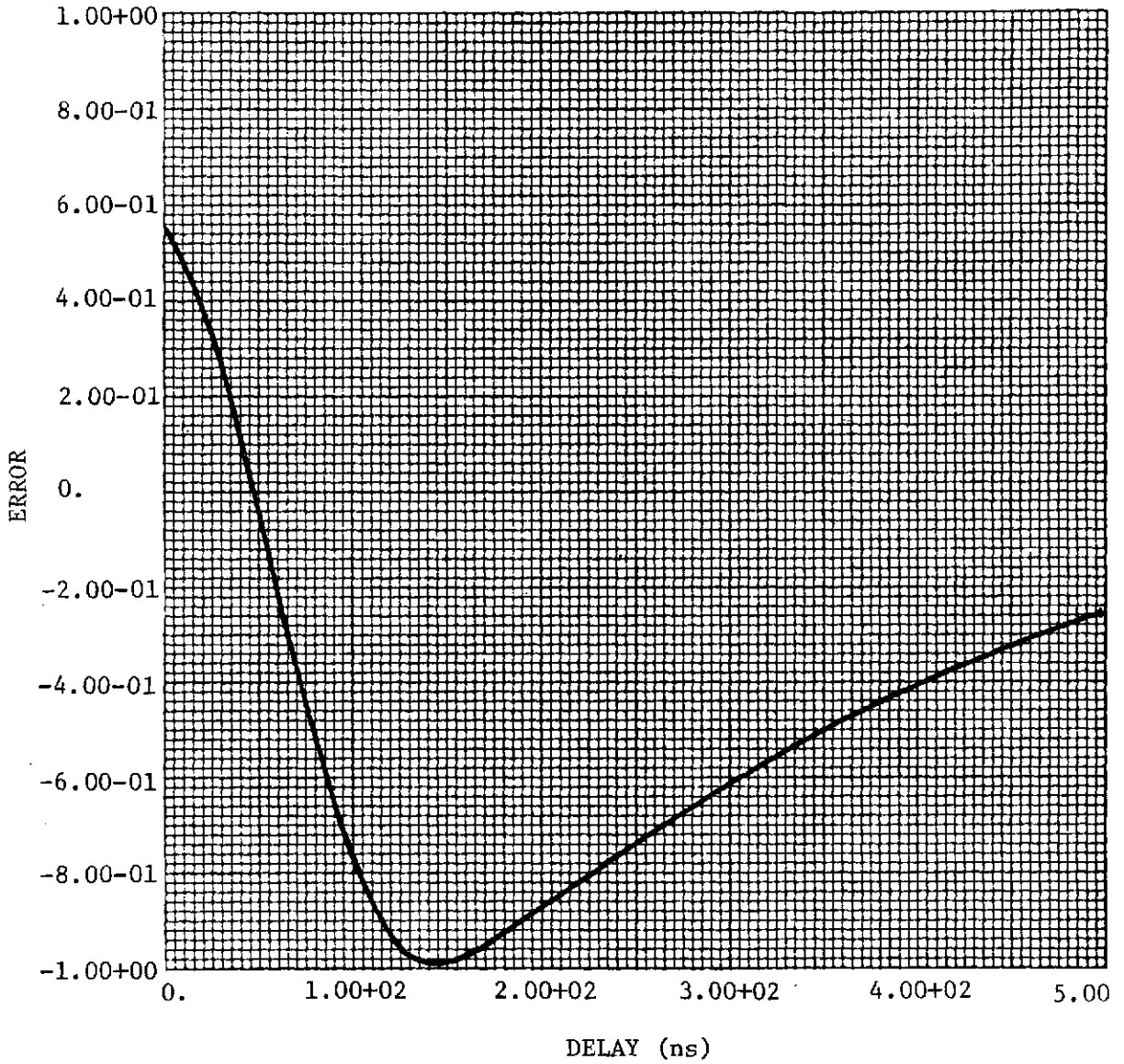
Figure A.II-29   Tracking Error versus Delay, Wide BW

III. USE OF GROUND-BASED TRANSPONDER TO EVALUATE PULSE ENCODING/
COMPRESSION SUBSYSTEMS

The S193 altimeter mode 5 data acquisition submode 2 (M5DAS2
or M5SM1) used a binary phase-modulated 13-bit Barker-coded pulse
for use with a delay-line pulse compression network (PCN) to
evaluate the usefulness of pulse-compression techniques for
evaluating sea state from space. The 130-ns pulse was modulated
in 10-ns increments. In the postflight scientific evaluation, the
resulting pulse shape of the compressed received pulse was to be
compared to the results of the so-called "brute force" single
transmitted narrow pulse of 10-ns used in a succeeding submode,
M5DAS3. To calibrate in-flight operation of both the transmitter
with the encoding modulator and the receiver with the pulse
compression network, an internal calibration submode (CDS2) coupled
the transmitter output pulse to the receiver through attenuators,
while recording the same sample and hold data as in DAS2.

Both encoder and PCN were operational during ground tests.
However, the resulting pulse shape data from the internal
calibration (CDS2) did not match "ideal" design expectations.
This created some concern that there was significant internal
crosstalk with undetermined delay times from the transmitter
affecting the directly connected and attenuated signal to the
receiver. Because this crosstalk would be range gated out of the
actual data-taking submodes due to the long space path delay time
in actual flight, the internal (undelayed) calibration was
questioned as a valid indication of the system performance.
However, it is still obviously a valid indication of system
operation. During ground systems test, it was impossible to
provide a long enough time delay while retaining the integrity of
the transmitted pulse for a baseline of the actual DAS2 operation.
Thus, an in-flight test setup was designed to provide clean echos
of the transmitter pulse to the receiver with the space path
effects included. An alternative approach was to use the "specular"
return from a "smooth" sea as the baseline of DAS2 operation. While
this alternative approach is usable and now required due to the
final results of the mode 5 operations, it suffers from using the
sea to calibrate the system supposed to measure the sea.

The test setup approach to providing the clean echo is
described below. Unfortunately, for programatic reasons and the
fact that the pulse compression network would not switch in until
SL4, the test setup capability was not verified with S193. However,
the setup was verified in ground checkout tests and was used near
the end of SL3 to assist in determining that S193 was still

operational. At that time, the STAPE system recorded received
pulse shapes and retransmitted properly to the S193, but the S193
tracker gate was not captured due to insufficient received power
resulting from misalignment of the S193 antenna existing at the
time.

The test setup was one configuration of the STAPE setup (see
MSC-05528, Volume V, paragraph 8.2.1, and Section I of this
appendix.) A block diagram is shown in Figure A.I-2. Though
simple in concept, the timing and system power-level constraints
posed a problem, and bandwidth and component matching could not
be ignored. The ground system used a 60-foot steerable dish
antenna to receive the encoded pulse from the S193 and retransmit
the same pulse, amplified, back to the S193 receiver. To maintain
isolation of the STAPE system receive and transmit paths, RF
switches and a delay line were used. To record the received and
retransmitted pulses, both were detected and the video pulse
displayed on an oscilloscope for recording by a high-speed
"framing" camera.

Additional constraints were applied to the relative vehicle
and STAPE locations due to internal S193 internal timing, both mode
sequence timing and tracker gate width (in time). These resulted
from the requirements:

1) That the S193 mode be started sufficiently ahead of the
STAPE site overpass to have sequenced to the DAS2 submode
and desired subsubmode over the test setup;

2) That the overflight be sufficiently close to directly
overhead;

3) That the STAPE pulse turnaround be sufficiently short so
the tracker gate (time interval) that would be locked to
the terrain at the PCA (point of closest approach) time
would also contain the return pulse generated by STAPE.

Because the AGC gate width during tracking was 600-ns wide, this
imposed tight constraints on the STAPE setup for it to capture the
tracker gate. Another aspect of this attempt to capture the tracker
gate and override the ground return at the PCA time of capture was
a requirement to provide enough return pulse amplitude to control
the AGC during the capture process. Once the tracker gate was
captured at PCA, the range-related timing constraints indicated the
ability of the S193 to hold the gate for up to approximately 15 seconds.
Then the S193 was expected to lose lock on the STAPE pulse, attempt

reacquisition of the ground, and abort because the range separation
by that time was too great for relock to the ground before abort
sequence time out. Thus, during the tracker gate lock on STAPE,
the ground return was also separated enough in range from the STAPE
return that it would not interfere or contaminate the clean
calibration return from STAPE. Data reduction would then be
required to select the time interval at which STAPE was providing
the calibration signal to the S193.

IV. COMPARISONS OF ALTIMETER ALTITUDE DATA WITH TOPOGRAPHIC
MAPS AND GEOID CALCULATIONS FOR EVALUATION OF RELATIVE
AND ABSOLUTE ALTIMETER ACCURACIES

One technique for evaluating the integrity of the S193
altimeter for altitude contour plotting was to plot the
elevation derived from S193 altimeter data and compare it to
the actual elevation shown on a detailed contour map. S193
altimeter elevation was calculated using SKYBET altitude data
and S193 altimeter altitude data. SKYBET altitude was the
radial distance between the surface of an earth reference
ellipsoid and the Skylab orbital altitude calculated from
earth-based tracking data by the SKYBET program. S193 altimeter
altitude data output was the measured distance between Skylab
and the actual earth terrain.

SKYBET altitude data for a particular period was interpolated
by using the Hewlett-Packard 9810A calculator programed for a
least-squares fifth-order polynomial curve fit to the periodic
SKYBET altitude parameter for the same general period to obtain
the fifth-order coefficients for describing the altitude. These
coefficients were programed in the Martin Marietta, CDC 6500
computer in FORTRAN IV, along with the altimeter measured data
outputs. The program used the coefficients for the fifth-order
polynomial equation with the proper time expression to calculate
the appropriate SKYBET-derived altitude data. The time expression
set the proper start time and calculation period for the SKYBET
data. To derive the earth elevation data, S193 altitude data were
subtracted from the SKYBET data for each period.

A. Contour Plotting over Land and Water

Altitude contour plots were made from altimeter data taken
during several passes by plotting the elevation data in feet
versus time in seconds. The elevation data was smoothed by
averaging each S193 measured data point with two points before
and two points after. (i.e., five-point running averages were
calculated and plotted every 0.13 seconds.) This smoothing
reduced the noise and altitude jitter. Figure A.IV-1 shows plots
of EREP pass 14 (217:15:04:02.26) over the Chesapeake Bay and
Atlantic Ocean area.

Terrain elevation was also plotted for each contour plot
with a dotted line to give a composite picture of altimeter
accuracy. Elevations were taken from detailed contour maps and
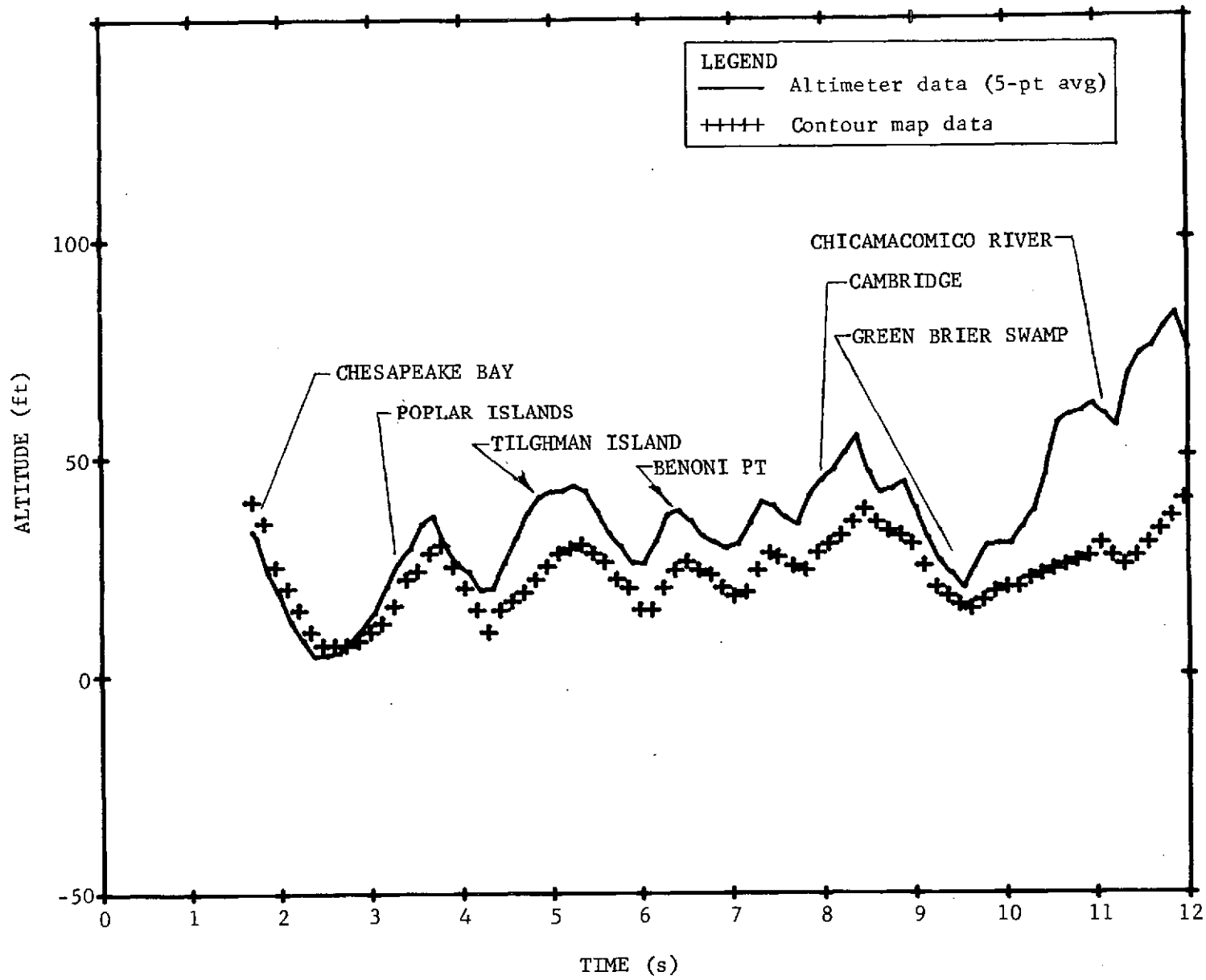
Figure A.IV-1 Altitude Contour Plot of Chesapeake Bay and Atlantic Ocean Area
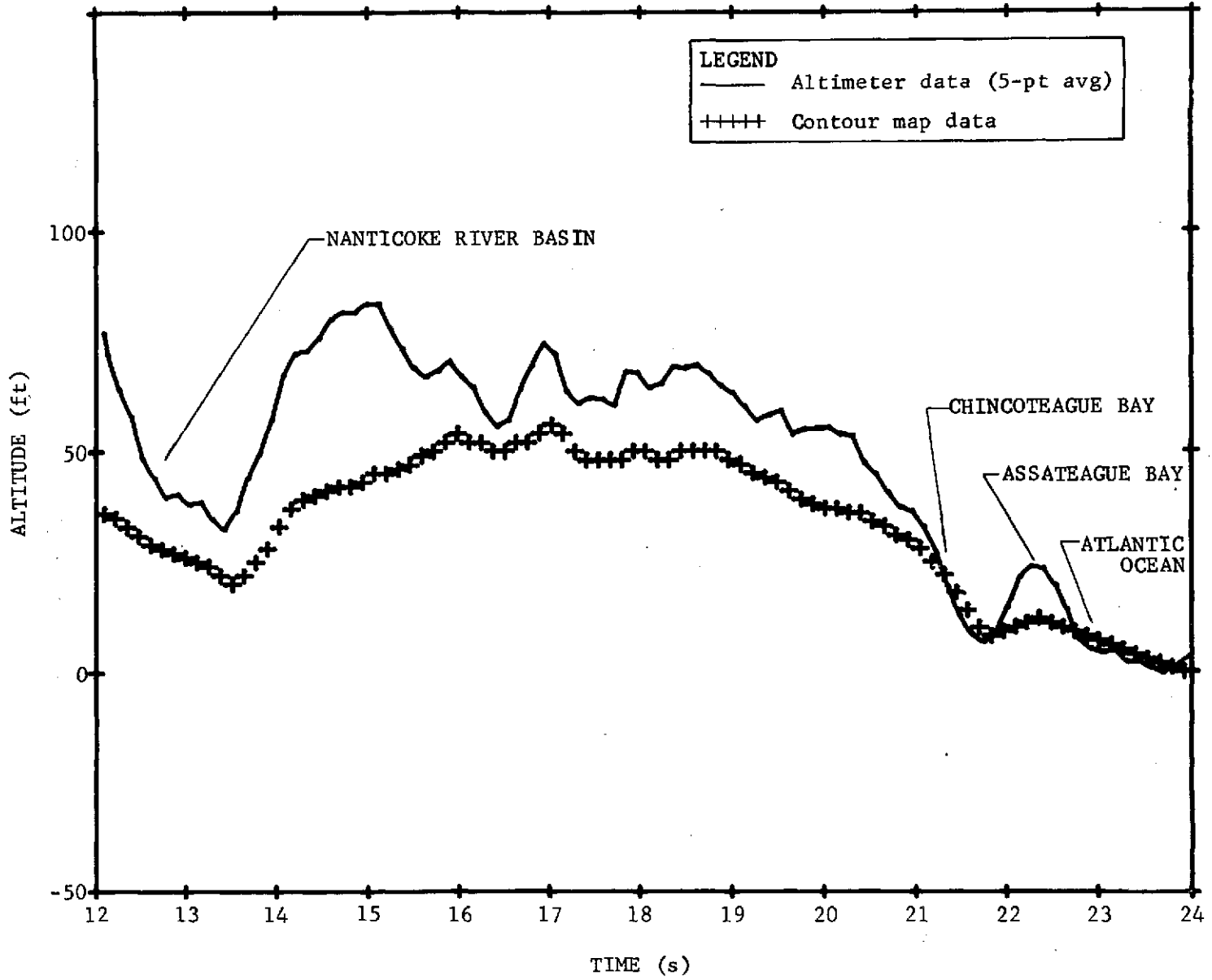
Figure A.IV-1 (continued)
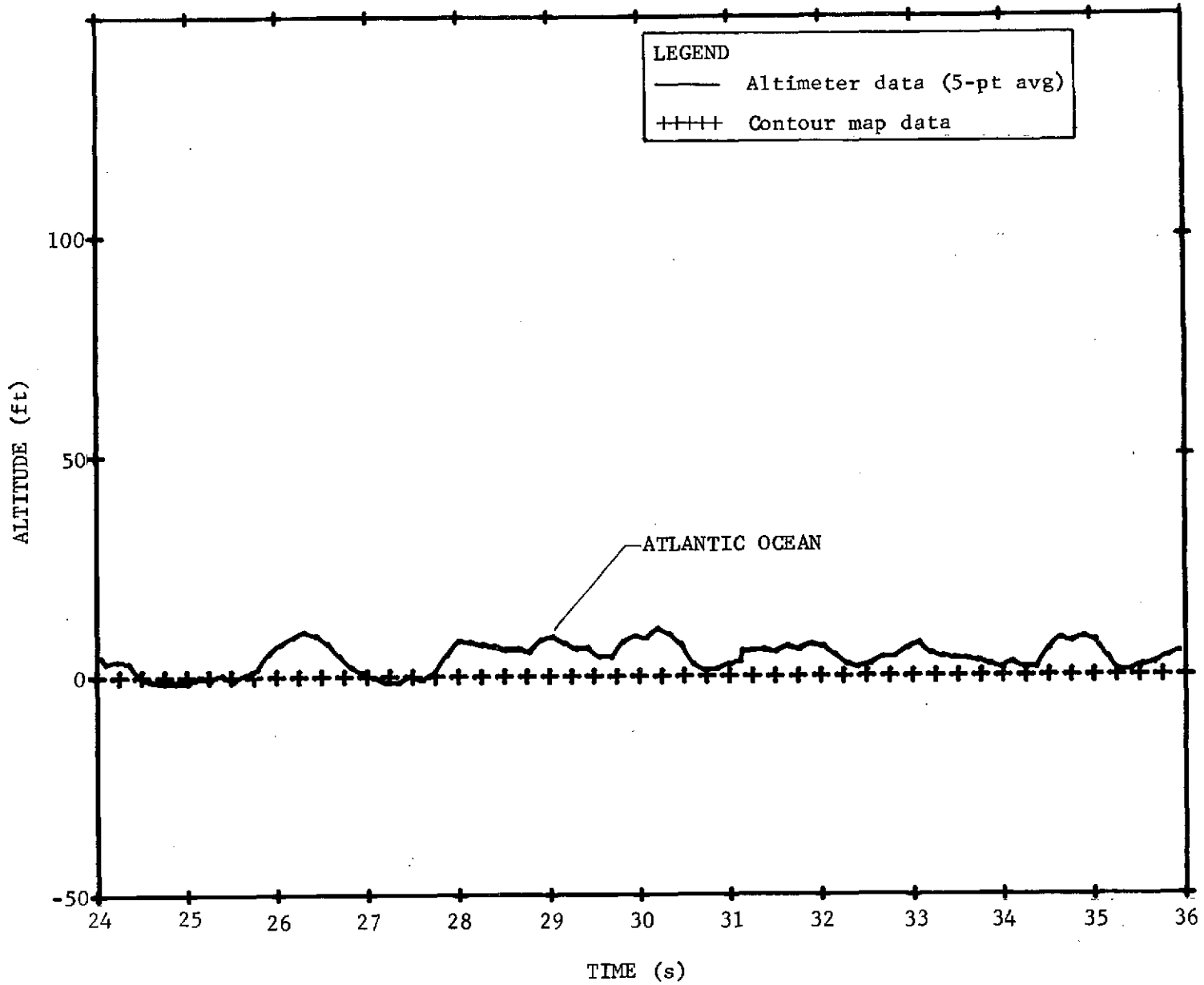
Figure A.IV⬛ (continued)
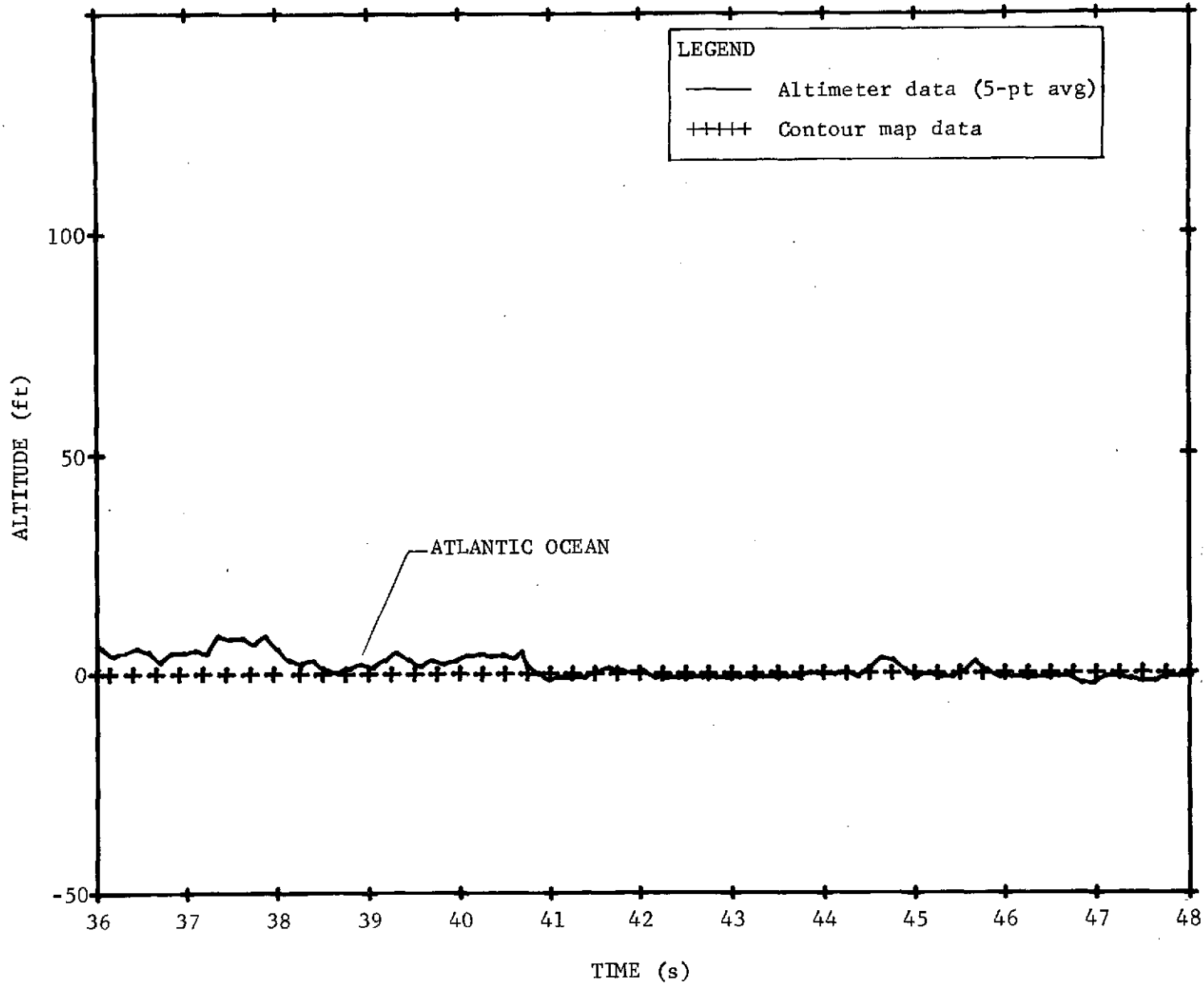
Figure A.IV-1 (continued)
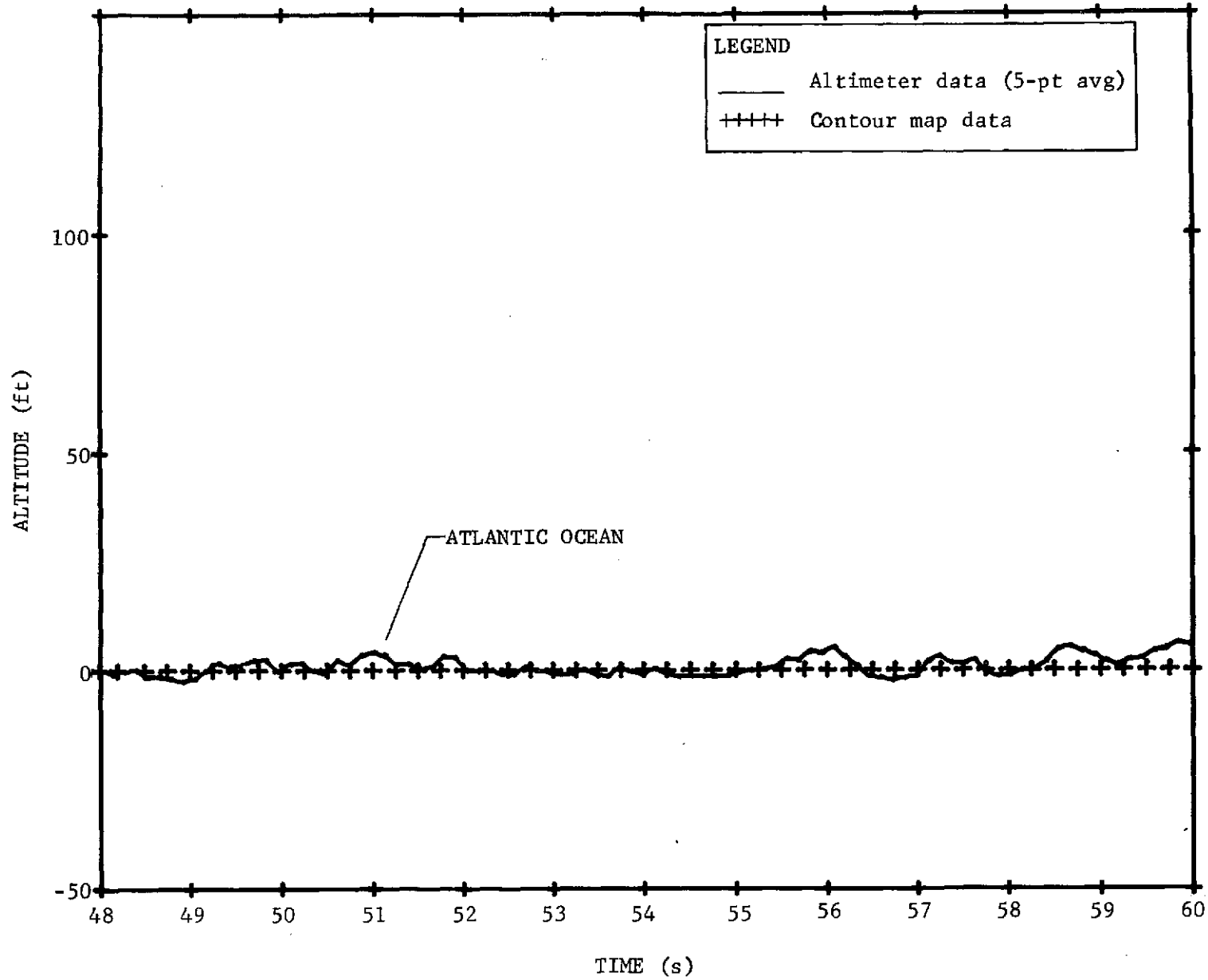
Figure A.IV-1 (concluded)

were approximately the average value of a 6-nautical-mile-diameter area because the S193 in-flight transmitted pulse was reflected from a circular area approximately 6 nautical miles in diameter, assuming vertical beam incidence and a beam-width limited system. Because, in most cases, only the relative altitude variation was being evaluated, the ground contour plots and S193 altitude plots were often adjusted to coincide at one end of the data take.

Significant geographical features that were easily identified were also pointed out on the S193 contour plots. One possible source of error in this particular example (Figure A.III-1) is that the spacecraft had an attitude error of more than 1 degree, which caused the beam illumination area to be elongated, and degradated the altitude data.

S193 elevation compared quite favorably with actual elevation in areas where S193 tracker lock was consistently maintained. The differences in absolute elevation were roughly comparable to expected SKYBET error because the accuracy requirements of the SKYBET program for altitude were not nearly as stringent as those for the altitude outputs from the S193 altimeter nor as uniform as spacecraft altitude.

In general, S193 altitude acquisition and contour plotting was very good over smooth areas like oceans and relatively flat or moderately rolling terrain. Over mountainous areas, unlocks were more frequent, which caused interruption of valid data during the unlock. At reflectivity discontinuities such as transition between water and land or between sparse vegetation and forests, an unlock frequently occurred, but reacquisition was generally obtained without serious effects on data quality.

B. Contour Plotting of the Sea Floor

Altitude contour plots were made over water to evaluate the ability of the S193 altimeter to perform gross contour plotting of the sea floor. The technique used was to plot sea surface contours derived from S193 altimeter data and compare them to the known contours of the sea floor. Altitude contour plots were made over the Atlantic Ocean off the coast of Argentina, using altimeter data from EREP Pass 22 (245:14:37:40.56). The measured sea surface contour was plotted in meters versus time in seconds. These S193 elevation data were smoothed by using the five-point moving-window averaging technique. The plots are shown in Figure A.IV-2.
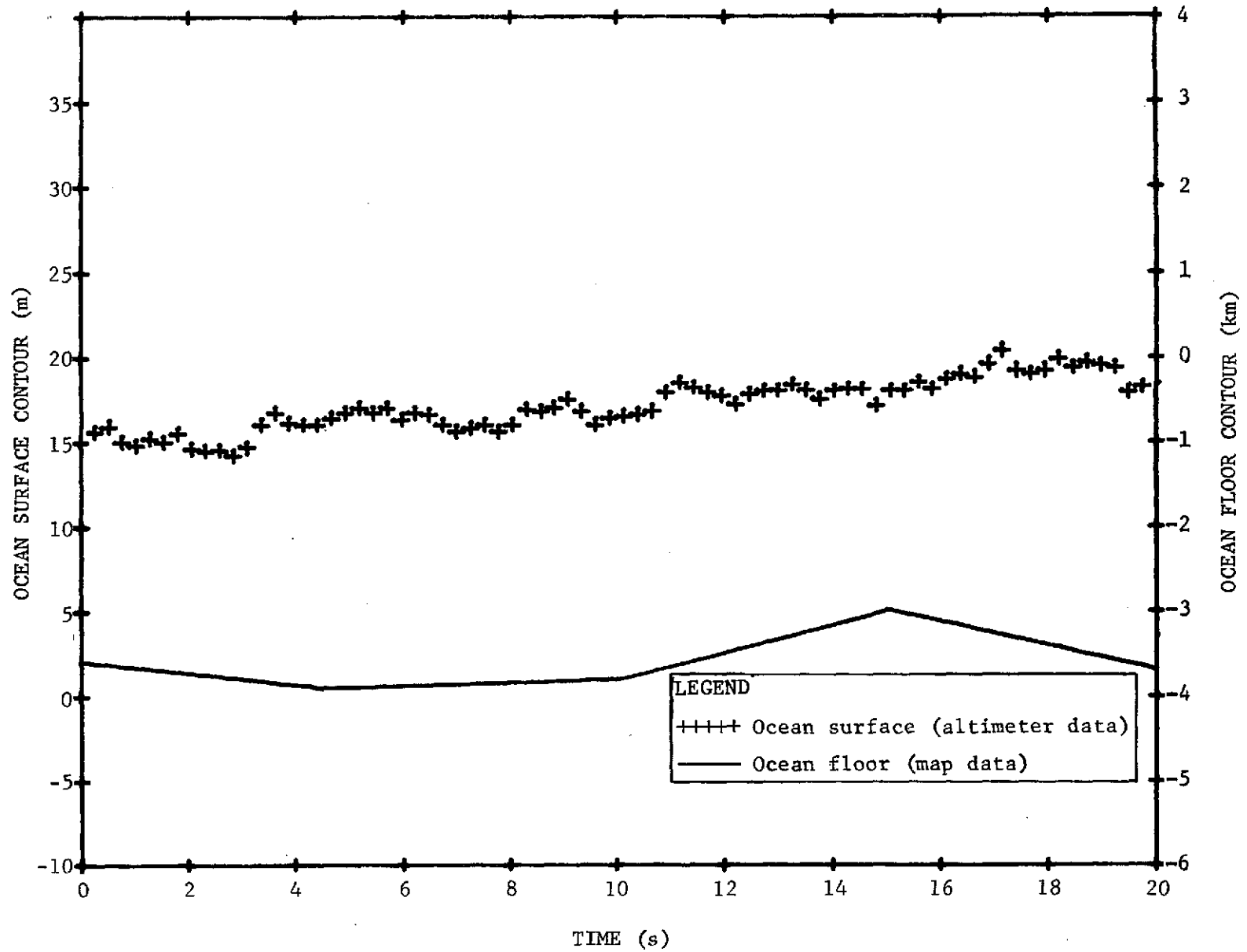
Figure A.IV-2 Altitude Comparison of Atlantic Ocean Surface and Sea-Floor Contours
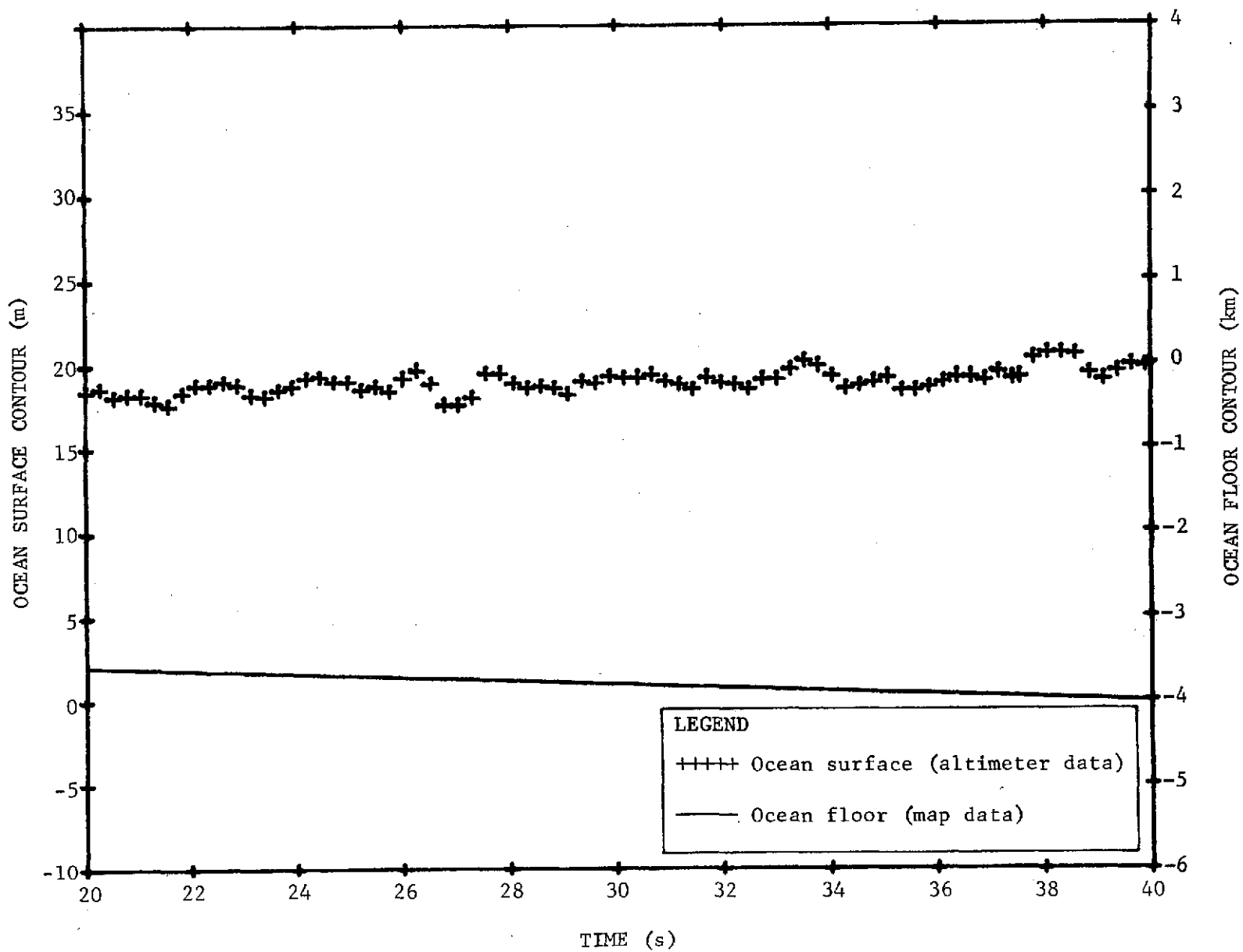
Figure A.IV-2 (continued)
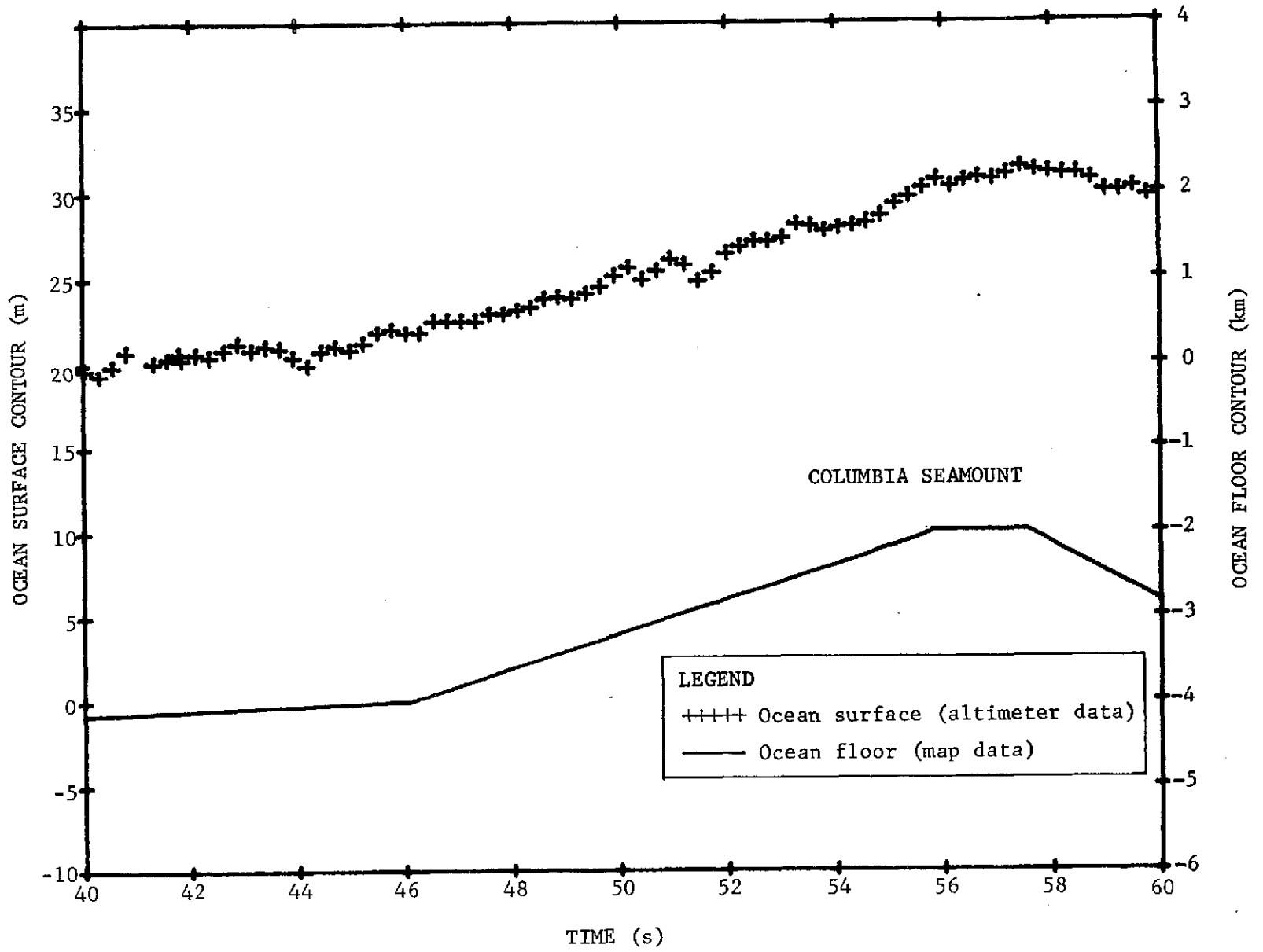
Figure A.IV-2 (continued)
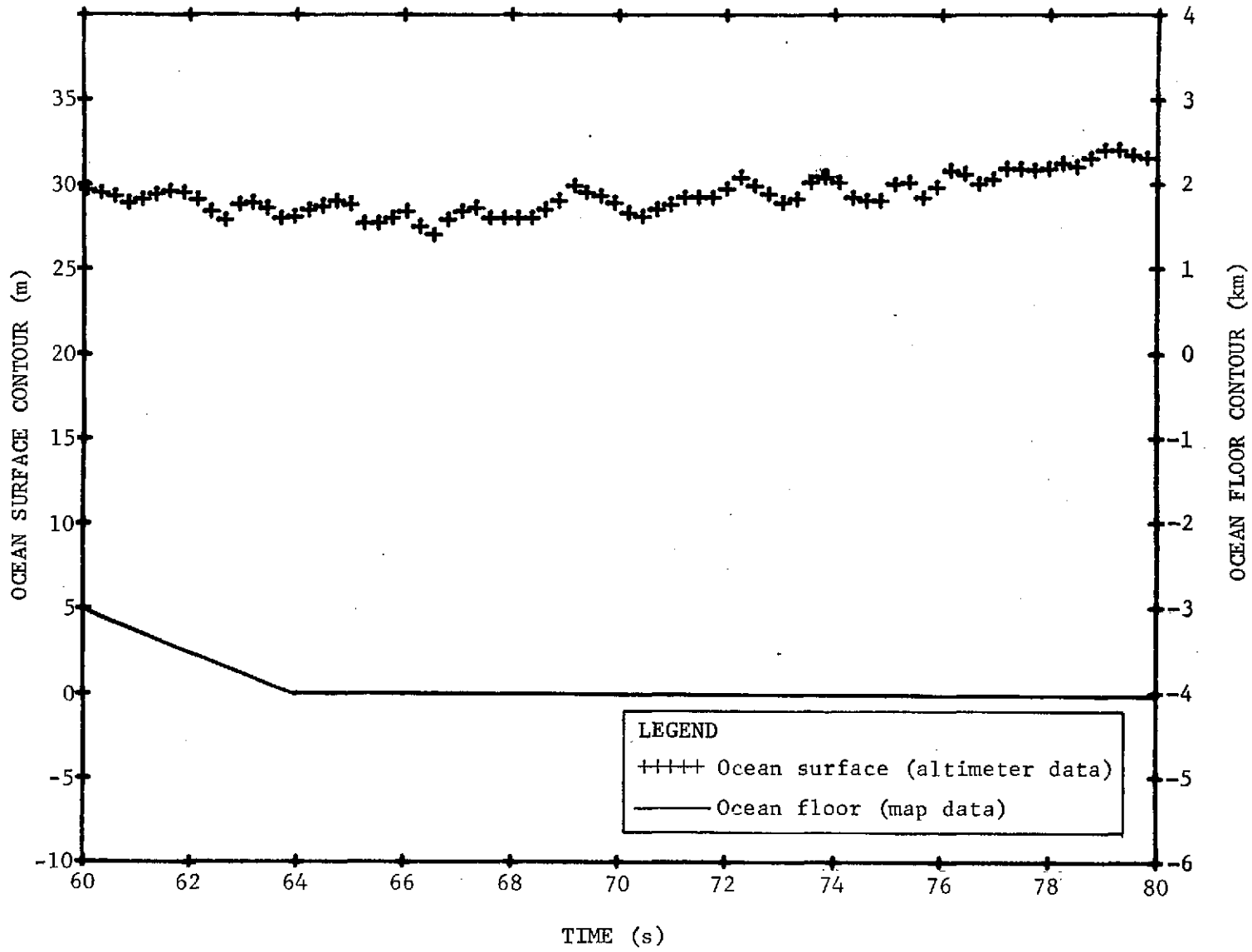
Figure A.IV-2   (concluded)

The actual terrain contour of the sea floor was also plotted with a solid line in kilometers versus time in seconds for each contour plot to give a composite picture of the measured relationship of the surface to the sea floor. Actual sea-floor elevations were taken from detailed bathymetric charts, and are the approximate average value of an area 6 nautical miles in diameter because the S193 in-flight transmitted pulse was reflected from a circular area approximately 6 nautical miles in diameter. EREP Pass 22 had good spacecraft attitude stability and vertical beam incidence, and therefore orientation caused no serious effects on data quality.

The Columbia Seamount, the most significant geographical feature that is easily identified, is pointed out on the contour plots. In comparing these two plots, it is easily recognizable that the S193 sea surface contour correlates with the known sea floor contours in this area.

Figure A.IV-3 is another example of the use of altitude contour plots over water to evaluate the relationship of the sea surface to the sea floor. The Columbia Seamount area was again chosen for the test because of its significant geographical features. S193 altimeter elevation was plotted directly from the residual altitude obtained from the JSC TR524 production data products* (S072-7). The plots were made in meters versus time in seconds once every 1.04 seconds using the symbol X. Each point is the mean of an eight-point data frame. The actual contour of the sea floor and the surface contour calculated using the least-squar curve-fit technique with SKYBET altitude data and S193 altimeter data were also plotted again for reference. In comparing these plots, it is obvious that there is a problem with the residual altitude from the TR524 data product. Investigation showed that the problem is in the residual altitude data and not in the S193 altimeter altitude data. Further study of the TR524 SKYBET processing techniques in deriving the residual altitude will be required to determine the source of the problem. However, when the same SKYBET orbital data were used and smoothed as done for comparison in both Figures A.IV-1 and A.IV-2, the correlation with surface expectations was very good.

---

* Earth Resources Production Processing Requirements for EREP Electronic Sensors, Document PHO-TR524 Rev A, Ch 2, JSC, 18 October 1974.
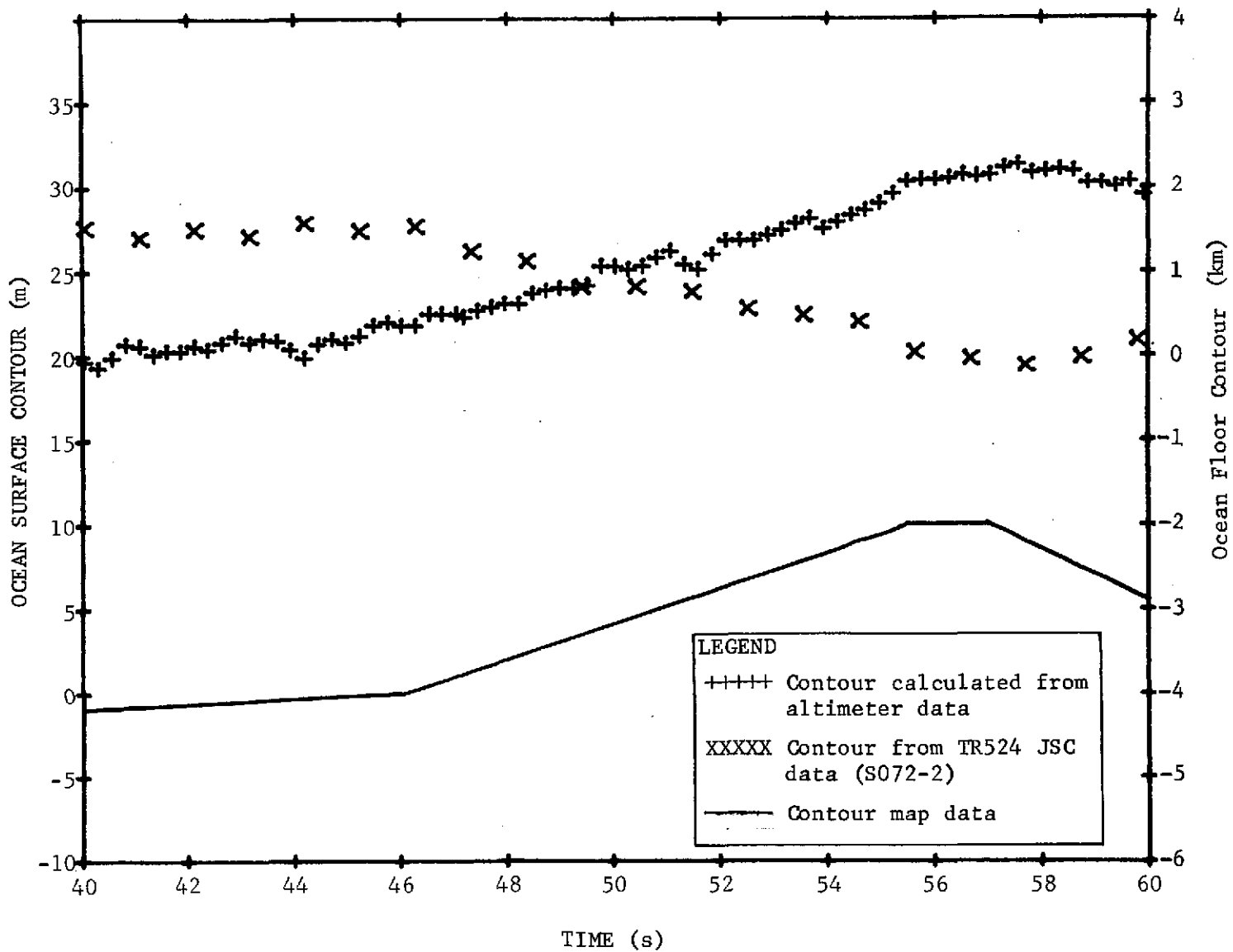
Figure A.IV-3 Sea-Floor Topography Compared with JSC Altitude Data

MSC-05546

V.   CALCULATION OF RADAR CORRECTION FROM JSC COMPUTER-COMPATIBLE
     TAPES AND OTHER USER INPUTS

The S193 altimeter sensor measured the strength of the return
pulse received from the surface by providing a readout of the
internal AGC voltage. Converting this voltage to a backscatter
value that can be associated with the sampled terrain involves
many variables and is quite complicated. Some calculations of
these backscatter values are being done by JSC. However, to
evaluate the usability of AGC data for computing backscatter values,
a less stringent approach was taken by Martin Marietta. While
believed to be correct, no accuracy estimates have been evaluated
and the results may suffer from some oversimplifications. The
technique is presented here, along with some results that
illustrate the ability of S193 to provide backscatter measurements
and comparative data for those who pursue this type of calculation
further.

The Martin Marietta computer program (S193 ALT) was developed
to calculate target radar cross-section (RCS) using AGC values
from tapes (S071-1) prepared by JSC as inputs. A plot of RCS
in decibels versus time in seconds was produced. A tabulation of
RCS, time, mode status, latitude, and longitude was also prepared.

A.   Program Inputs

The following inputs were required:

1)   S071-1 tape inputs

     a)   Received power in decibels above or below 1 milliwatt;

     b)   Time (GMT in hours, minutes, and seconds);

     c)   Range in meters;

     d)   Tracker lock status;

     e)   Latitude in degrees;

     f)   Longitude in degrees;

     g)   Mode number;

     h)   Submode number;

i)   Sub^2 mode number;

j)   Sub^3 mode number;

k)   Frame number.

2) User inputs

a)   A (SMCORR) matrix (10 x 6) to correct for radar cross-section calibration changes caused by mode and submode switching. These are due to pulse shape and bandwidth switching and minor errors in calibration and processing of raw data;

b)   Polynomial coefficients for beam incidence angle correction;

c)   Beam incidence angle, which can be obtained from matching returned waveforms to WFC and Martin Marietta models. SKYBET angles were not accurate enough for this purpose because of the result of rate gyro drifts during the mission, but a reworking of the drift data promised to provide angles that might be accurate enough.

B. Program Description

The program added a number in decibel units to the received power in decibels above or below 1 millivolt at the receiver AGC output point. This additive number was made up of several values, which include:

1)   Correction for translating the reference from the AGC output point to the antenna terminals;

2)   Antenna gain and free-space loss at altitude;

3)   Received pulse shape correction for the 100-ns transmitted pulse with the beam at normal incidence;

4)   Transmitted output power;

5)   Correction for beam incidence angle off normal. This correction was derived from program ALTIM discussed in paragraph A.II.B.3);

6) Altitude range in kilometers (See paragraph 7.5.4 of MSC-05528, Volume V.);

7) Correction for decibel conversion as a function of mode status.

The approximate formula (See paragraph 7.5.4 of MSC-05528, Volume I.) gives:

$$\sigma_{o_{dB}} = P_r + 74.7 \quad \text{(100-ns transmitted pulse)} \qquad \text{[A.V.1]}$$

$$\sigma_{o_{dB}} = P_r + 82.7 \quad \text{(16-ns transmitted pulse)} \qquad \text{[A.V.2]}$$

Due to the point where the telemetry measures the AGC, 33.0 dB must be subtracted because of the existence of 33.0-dB gain between the antenna terminals and the measurement point.

This gives the approximate normalized radar cross-section as:

$$\sigma_{o_{dB}} = P_r + 41.7 \quad \text{(100-ns pulse) (based on paragraph} \qquad \text{[A.V.3]}$$
$$\text{7.5.4 of MSC-0-528, Volume V)}$$

and $\sigma_{o_{dB}} = P_r + 49.7 \quad \text{(16-ns pulse)}$ [A.V.4]

The WFC backscatter formula (See paragraph 7.3 of MSC-05528, Volume V) is:

$$\sigma_{o_{dB}} = P_r + L_P + L_s + r - \left(P_{cal} + L_{cal} + F \right) \qquad \text{[A.V.5]}$$

where

$P_{cal} = -35.1$ dB nominal

$F = -135.5$ dB at zero beam incidence angle

$r = 0.748$ for 100-ns pulse 10 MHz IF BW = -1.3 dB (See paragraph 11.2.7 of MSC-05528, Volume V.)

$L_p \cong 0.2$ dB = propagation loss

$L_s \cong 1.1$ dB = losses between transmitter and integrated receiver input (See paragraph 7.1.3 of MSC-05528, Volume V.)

which gives

$$\sigma_{o_{dB}} = 41.5 \text{ dB} + P_r \quad \text{(based on paragraph 7.3 of MSC-05528, Volume V)}$$

Thus both formulas for evaluating the normalized radar cross-section agree within 0.2 dB, which is less than the readability of the preflight AGC calibration curves.

C. Program Output

A sample of a program output tabulation is shown in Table A.V-1. Figures A.V-1 and A.V-2 are sample plots of radar cross-section versus time in seconds. (Zero seconds is the beginning of a GMT day.)

Table A.V-1 Sample σ° Tabulation

HR.	MIN.	SEC.	DBM	SECT	FC	S3M	S2M	S1M	M	LAT	LONG	ALT M
15	22	45.36	-33.6	8.2	2	0	0	0	5	-16.7191	-37.3134	428616.7
15	22	45.62	-31.1	10.6								
15	22	45.88	-30.4	11.4								
15	22	46.14	-31.1	10.6								
15	22	46.40	-31.9	9.9	3	0	0	0	5	-16.6579	-37.2713	428598.6
15	22	46.66	-31.9	9.9								
15	22	46.92	-31.9	9.9								
15	22	47.18	-31.9	9.9								
15	22	47.44	-32.7	9.1	4	0	0	0	5	-16.6136	-37.2342	428581.4
15	22	47.70	-31.1	10.6								
15	22	47.96	-31.9	9.9								
15	22	48.22	-31.1	10.6								
15	22	48.48	-31.9	9.9	5	0	0	0	5	-16.5524	-37.1921	428563.1
15	22	48.74	-31.1	10.6								
15	22	49.00	-31.1	10.6								
15	22	49.26	-31.9	9.9								
15	22	49.52	-32.7	9.1	6	0	0	0	5	-16.5134	-37.1490	428545.5
15	22	49.78	-31.9	9.9								
15	22	50.04	-31.1	10.6								
15	22	50.30	-31.9	9.9								
15	22	50.56	-31.9	9.9	1	0	1	0	5	-16.4597	-37.1105	428527.9
15	22	50.82	-31.1	10.6								
15	22	51.08	-31.9	9.9								
15	22	51.34	-32.7	9.1								
15	22	51.60	-32.7	9.1	2	0	1	0	5	-16.4095	-37.0679	428510.4
15	22	51.86	-32.7	9.1								
15	22	52.12	-31.9	9.9								
15	22	52.38	-31.9	9.9								
15	22	52.64	-31.9	9.9	3	0	1	0	5	-16.3629	-37.0212	428492.0
15	22	52.90	-32.7	9.1								
15	22	53.16	-31.9	9.9								
15	22	53.42	-31.1	10.6								
15	22	53.68	-32.7	9.1	4	0	1	0	5	-16.3121	-36.9672	428473.7
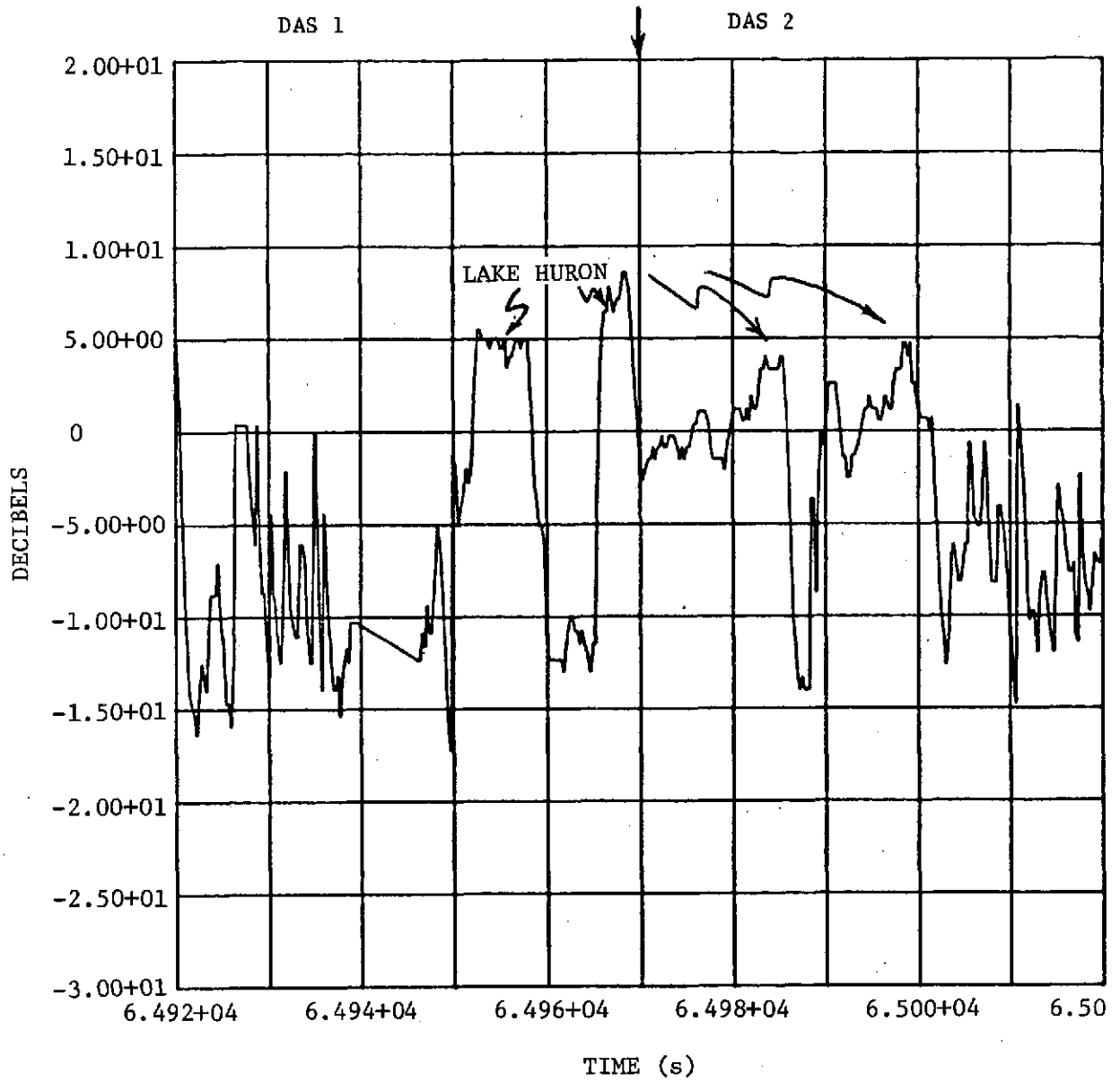
Figure A.V-1 Radar Cross-Section, Mode 1, EREP Pass 38
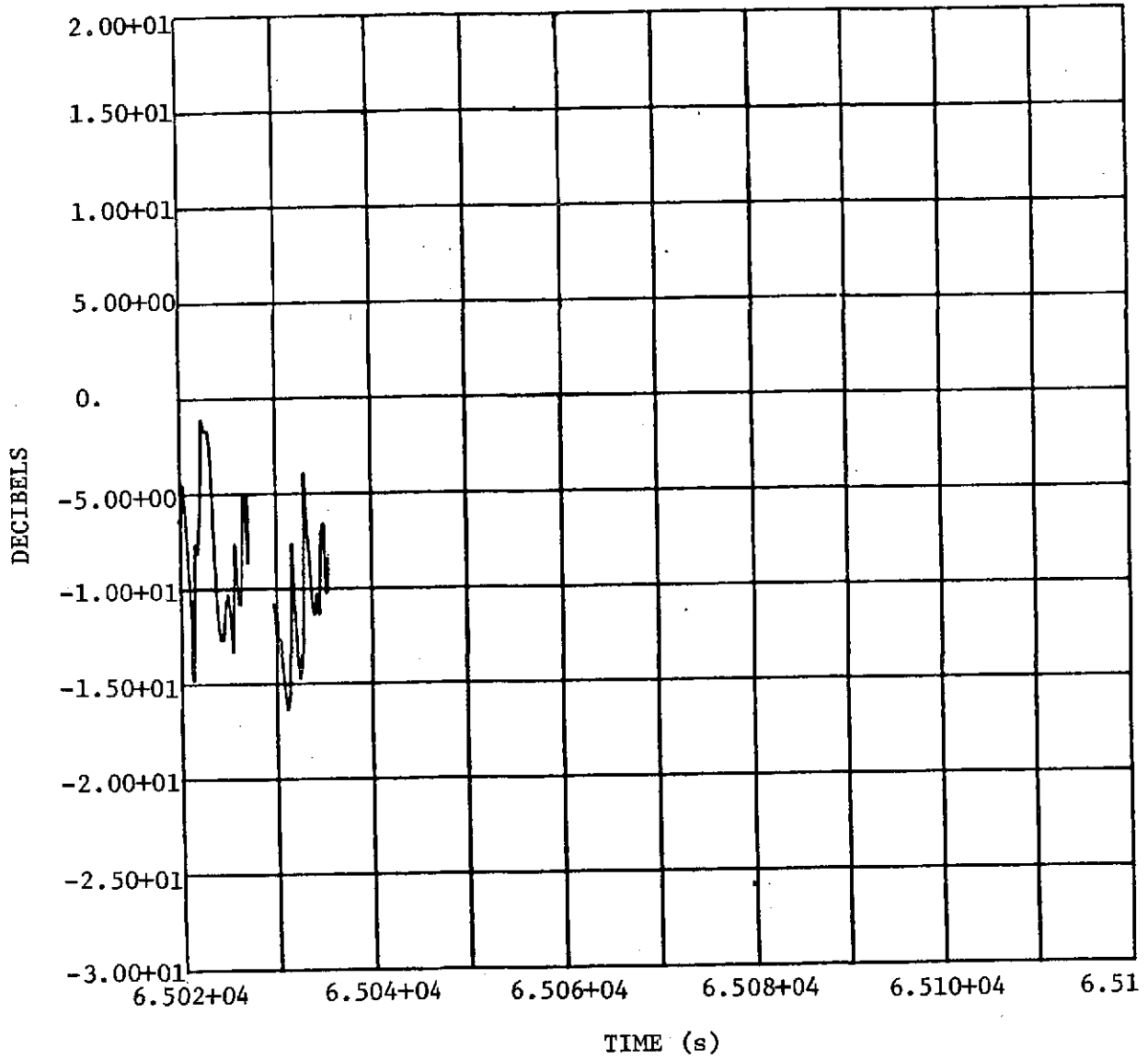
Figure A.V-1 (concluded)
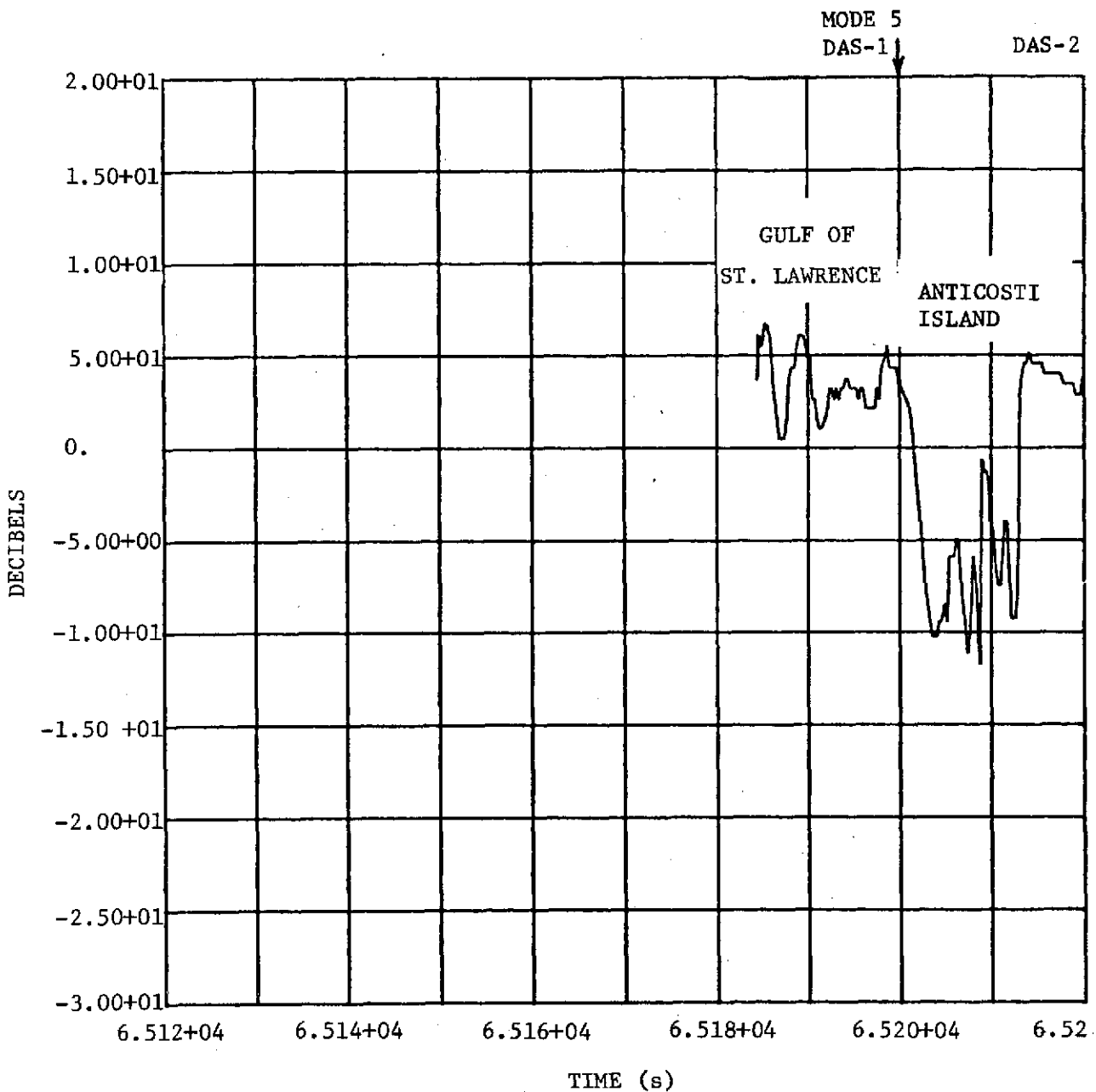
Figure A.V-2 Radar Cross-Section, Mode 5, EREP Pass 38

Figure A.V-2 (continued)

Figure A.V-2   (continued)

Figure A.V-2 (continued)

TIME (s)

Figure A.V-2 (concluded)